FORSCHUNGSZENTRUM ROSSENDORF FZR

FZR-215

Institute of Nuclear and Hadron Physics

Annual Report 1997

Cover Picture:
The cover picture displays the heavy ion tumour treatment site at the Gesellschaft für Schwerionenforschung Darmstadt with the positron emission tomograph that has been developed in Rossendorf (cf. page 67).

The use of the cover picture was permitted by GSI.
Photograph: Achim Zschau

Forschungszentrum Rossendorf e. V.

Postfach 51 01 19
D-01314 Dresden
Bundesrepublik Deutschland

Telefon +49 (3 51) 2 60 22 70
Telefax +49 (3 51) 2 60 37 00
E-Mail E. Grosse@fz-rossendorf.de
Internet http://www.fz-rossendorf.de/FWK/

Als Manuskript gedruckt

FZR - 215
March 1998

ANNUAL REPORT 1997

Institute of Nuclear and Hadron Physics

Editors:
H.W. Barz, F. Dönau, W. Enghardt, E. Grosse,
B. Kämpfer, H. Prade, M. Schlett, R. Wünsch

Explanation of special symbols:

The letters given in brackets in the following text and used as appendix in the title of the scientific contributions do express our grateful acknowledgement to the funding, sponsoring or grants provided by several institutions.

Research projects were funded by the Federal Ministry of Education, Science, Research and Technology BMBF (B), by the German Research Community DFG (D), by the GSI Darmstadt (G), by the KFA Jülich (K) and by the special program HSP III (H) or were sponsored within Scientific agreements with eastern European countries (W).

CONTENTS

Preface

The Forschungszentrum Rossendorf (FZR) on the outskirts of Dresden is the largest research center in the Wissenschaftsgemeinschaft Gottfried Wilhelm Leibniz (WGL), one of several national organizations in charge of extra-university scientific research and development. Among the five institutes of the FZR the Institute of Nuclear and Hadron Physics (IKH) is one which is rather strongly devoted to fundamental research in subatomic systems, but it also investigates and exploits the possibilities for the transfer of experimental and theoretical techniques and methods from nuclear physics to other sciences and to non-nuclear technology.
This Annual Report 1997 of the IKH presents last years achievements in the four main domains of activity of the institute. In each of them it combines reports about theoretical, experimental and technical developments - in accordance to the institutes aim to connect the physics experiments in each of the adressed fields to related theoretical and technical expertise.
The first chapter of this report is devoted to the projected Radiation Source ELBE, which is the most remarkable example of the transfer of technology mentioned above. Centered around a superconducting accelerator, which will produce up to 40 MeV electron beams of 1 mA at 100% duty cycle, this new facility will deliver secondary beams of different kind:

- *High-brilliance infrared radiation in the wavelength range 5 μm - 150 μm coming from two different free-electron-laser (FEL) undulators.*
- *X-radiation in the keV range produced from electrons channelled through a single crystal or by Compton-scattering laser light.*
- *Intensive bremsstrahlung to investigate resonance fluorescence in nuclei up to high excitation - with the potential of polarization studies.*
- *The high energy photons can again be used to produce neutrons in the 0.1 - 10 MeV range as well as high intensity positron beams.*

Hadron Physics at the FZR - as described in the second chapter - is dealing with hadronic interactions as such and also within the hadronic medium formed in collisions between nuclei. Experiments were performed at the COSY proton cooler synchrotron at the Forschungszentrum Jülich (KFA) and at the heavy ion synchrotron SIS at GSI Darmstadt. Theoretical studies performed at the IKH refer to these experiments and to data obtained at higher energy accelerators.
The third chapter combines experimental and theoretical research in Nuclear Physics. Here collective excitations of nuclei as well as their interplay to single nucleon degrees of freedom play an important role. Most of the work reported deals with electromagnetic processes in nuclei, but other studies of nuclear collision dynamics have been performed as well. Attention is also given to the similarity between nuclei and molecular clusters as mesoscopic systems composed of Fermions.
Last but not least this Annual Report contains a chapter on Biomedical Research performed using nuclear technology. The main contribution of the Institute to this field comes from Positron Emission Tomography (PET) and the outstanding achievement here is the successful operation of a PET scanner simultaneous to the tumour treatment with heavy ion beams when the first patients were treated at GSI in December.

On the long term biomedical research will also be performed with the beams coming from ELBE. In a two-days workshop held in December 1997 the use of intensive infrared light with freely adjustable wavelength - as the ELBE-FEL-facility will deliver - as discussed with possible future users from outside of the FZR. Here projects from the areas of medicine, biochemistry, biophysics and physical chemistry have played the main role during one of the days, whereas the applications in condensed matter physics and materials research were the theme of the other.

The scientific activities of the institute have benefitted from generous support from various institutions. First of all, we gratefully acknowledge the close and fruitful collaboration with the colleagues from the Technical University (TU) Dresden and many other scientific institutions in Germany and abroad; such contacts are of vital importance for our institute. Specific projects were financially supported by the Federal Ministry for Education, Science, Research and Technology (BMBF), the German Research Community (DFG), the Saxon State Ministry for Science and Art (SMWK), KFA Jülich and GSI Darmstadt. We express our gratitude to all these as well as to the Executive Board of the Forschungszentrum Rossendorf for its essential support of the ELBE project.

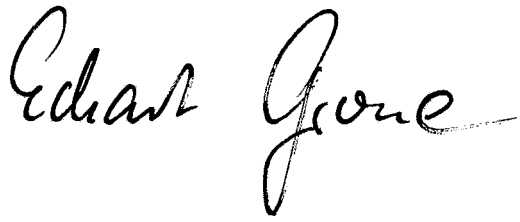

The Radiation Source ELBE

During the year 1997 intensive design work was performed in preparation for the research to be tackled with the new Radiation Source ELBE after its installation at the FZR in the end of 1999. Project leader is Dr. F. Gabriel and his department (Experimental Facilities & Information Technology) is planning and setting up the accelerator, the equipment associated to it including the building and also a free-electron-laser (FEL) for the far infrared (IR) beyond 25 μm; support is coming from other Departments of the FZR (New Accelerators, Technical Infrastructure) and from outside (TU Dresden, Refrigeration and Cryo-Engineering; Stanford University, HEPL ; DESY and others). A schematic plan of ELBE is shown below; the construction work will start in May 1998 on the basis of this plan.

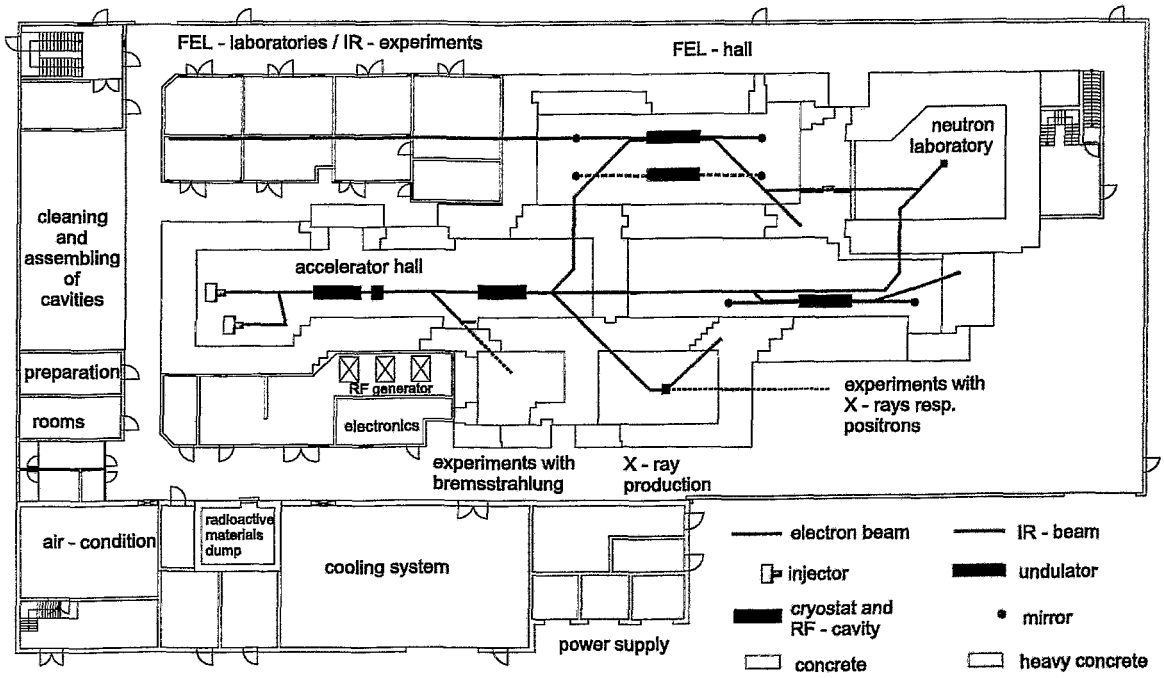

In the following some of the design work as performed by the Institute of Nuclear and Hadron Physics in 1997 will be described - together with several contributions from other institutions. Work on two RF injectors (H. Büttig et al., A. Bushuev et al.) is reported on in the first two reports. A third, thermionic injector with a separate RF-buncher will very likely be the one to start FEL operation, which requires a high bunch charge; the design values are 85 pC at 11.8 MHz corresponding to an average current of 1 mA. The beam transport system (P. Gippner et al.) is designed such that the charge density does not become too large to avoid an unwanted Coulomb blow up of the bunches; in longitudinal direction a pulse compression may be achieved by appropriate adjustment of accelerator RF and quadrupole settings.

Short pulses together with a properly adapted tranverse phase space are important for sufficient energy transfer in the FEL-undulator and for obtaining laser action in the optical resonator (M. Wenzel et al.). Whereas for the mid-IR a short period permanent magnet undulator is under consideration, the far-IR will better be produced with a set-up consisting of electro-magnets; here also the energy dissipation due to ohmic losses has to be considered for the optimisation (A. Wolf). For both cases the undulator length has to be chosen long enough for sufficient gain (R. Wünsch), but also short enough to

reduce diffraction losses. Experiments as the FEL annealing of SiC (M. Wenzel et al.) will certainly profit from the higher radiation intensity of ELBE - possible due to the superconducting accelerator structures - as compared to FELIX, where these first studies were performed.
ELBE will be a source not only for IR-FEL-radiation but also for X-rays, which can be produced from channeling in a single crystal; besides "ordinary" channeling radiation (cf. Annual Report 1996) more sophisticated processes may become important (U. Nething et al.). Compton backscattering when used for X-ray generation requires a very good electron-beam quality to assure sufficient intensity (H.W. Barz et al.); this process should produce very low background and it should preserve the polarization of the input radiation. As ELBE will also be a strong source for positrons (cf. Annual Report 1996) and neutrons (K. Seidel et al.) a large variety of research in a number of fields will become possible; a special advantage here is that in the same laboratory different radiation is available simultaneously - eventually even correlated in time properly.

Measurement of the Bunchlengths and the Average Current at the Gun-Testfacility

H. BUETTIG[2], M. FREITAG, W.GLAESER[1], H. GURATSCH[2], H. HAUCK[1], H. KRUG[1], D. JANSSEN[2], A. NOWAK[1], R. SCHLENK[1], P. VOM STEIN[2], J. VOIGTLAENDER [1], B. WUSTMANN[1]

A new cw thermionic RF gun for the ELBE - project[1] has been built and successfully tested in a special test-facility. After excellent results for the emittance and the energy distribution [2] we have been measured the bunchlenghts by means of a combination of dipolmagnet and kicker-cavity. In agreement with the corresponding calculations [3] we have obtained a bunchlengths of 8 ps FWHM (see Fig. 1).

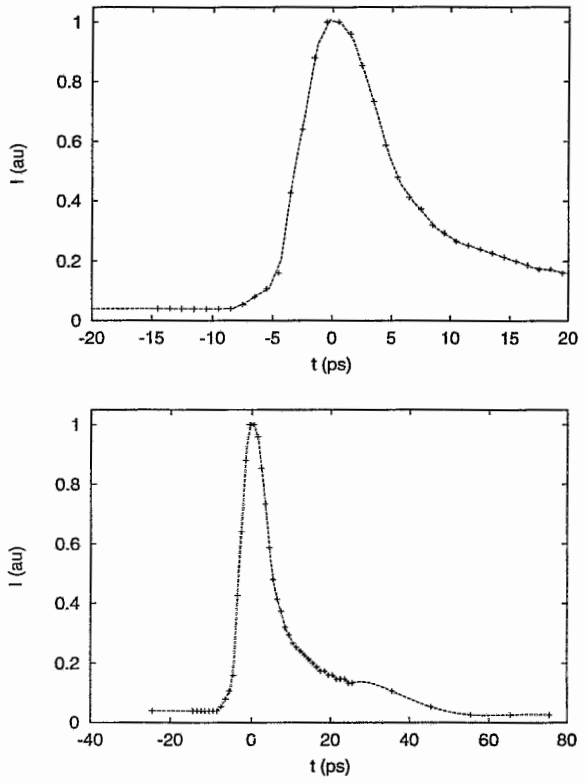

Fig. 1 *Minimal bunchlenghts of the cw thermionic RF gun*

If we reduce the electron energy from 300 keV to 100 keV in order to meet the radiation limits permitted outside the test-facility shielding, 400 μA is obtained for a cathode diameter of 150 μm

[1] *Zentralabteilung Forschungs- und Informationstechnik, FZR*
[2] *Zentralabteilung Neue Beschleuniger, FZR*

References

[1] F. Gabriel ed.,FZR Internal Design Report (1995)
[2] D. Janssen, P. vom Stein , Nuclear and Hadron Physics and Project ELBE, Annual Report 1996, p. 5
[3] D. Janssen, P. vom Stein, Nucl. Instr. & Meth. A 380(1996) 497-504

Status of the Development of a Superconducting RF Gun

A. BUSHUEV[1], D. JANSSEN[2], M. KARLINER1[1], S. KONSTANTINOV1[1] J. KRUCHKOV[1], V. PETROV[1], I. SEDLYAROV1[1], P. VOM STEIN[2], A. TRIBENDIS[1], V. VOLKOV[1]

In the beginning of 1996 the Drossel collaboration was established between the FZR and the BINP Nowosibirsk for the development of a new electron injector. The injector combines the principle of a photocathode rf gun [1] with the use of superconducting (sc) accelerating cavities. The result of this development should be a sc rf gun, which delivers a bunched electron beam with excellent beam properties in a continuous wave (cw) mode.The design of this gun was finished in 1996. Beam dynamics simulations (PARMELA [2]) show a transverse emittance of 1.7 π mm mrad for 200 pC bunch charge and a gradient of 20 MV/m at the cathode [3].
In 1997 the manufactoring of the niob - cavity including the rf - filter and the cooling insert is completed in Nowosibirsk. First tests at room temperature show the expected behaviour of the rf - filter and the tuning system.The design of the preparation chamber for the photocathode is finished. The production of the chamber at the BINP and in Rossendorf is under way. For the design of the cryogenic- and the lasersystem we are in contact with the TU Dresden, the VIK Dubna and the Max Born Institut Berlin.

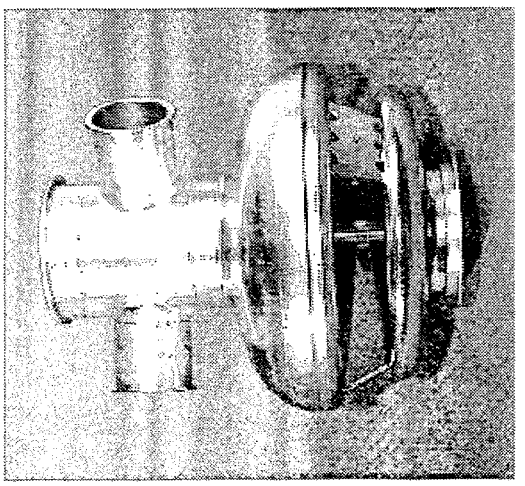

Fig. 1 *Gun cavity with rf- filter*

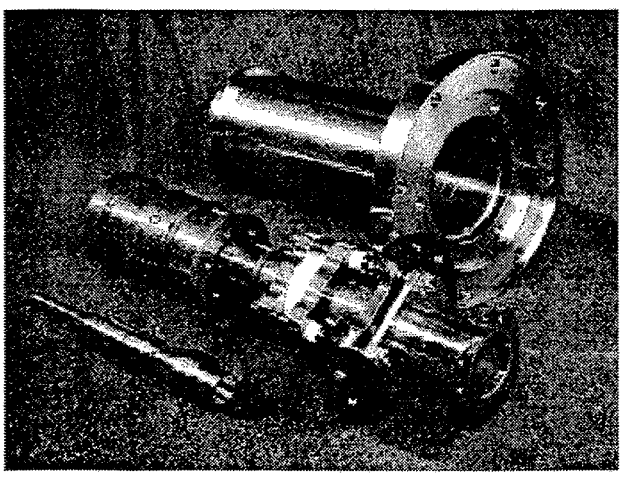

Fig. 2 *Cooling insert with the cathode stem*

[1] *BINP Nowosibirsk* [2] *Zentralabteilung neue Beschleuniger*

References

[1] C. Travier, Nucl. Instr. & Meth. A 304 (1991) 285-296
[2] J. Billen, L. Young, Proc. of the 1993 PAC, Vol.2 790-792
[3] D. Janssen, P.vom Stein, Proc. of the 1997 PAC, in print

The Status of the Beam Transport System for the ELBE Project

P. GIPPNER AND B. FRANCZAK[1]

The beam transport system, which guides the electrons from the accelerator into the cave of the free electron laser (FEL) should be (i) achromatic and isochronous or (ii) achromatic and able to compress the length of the beam bunches within a certain interval. The proposed system is shown in Fig.1.

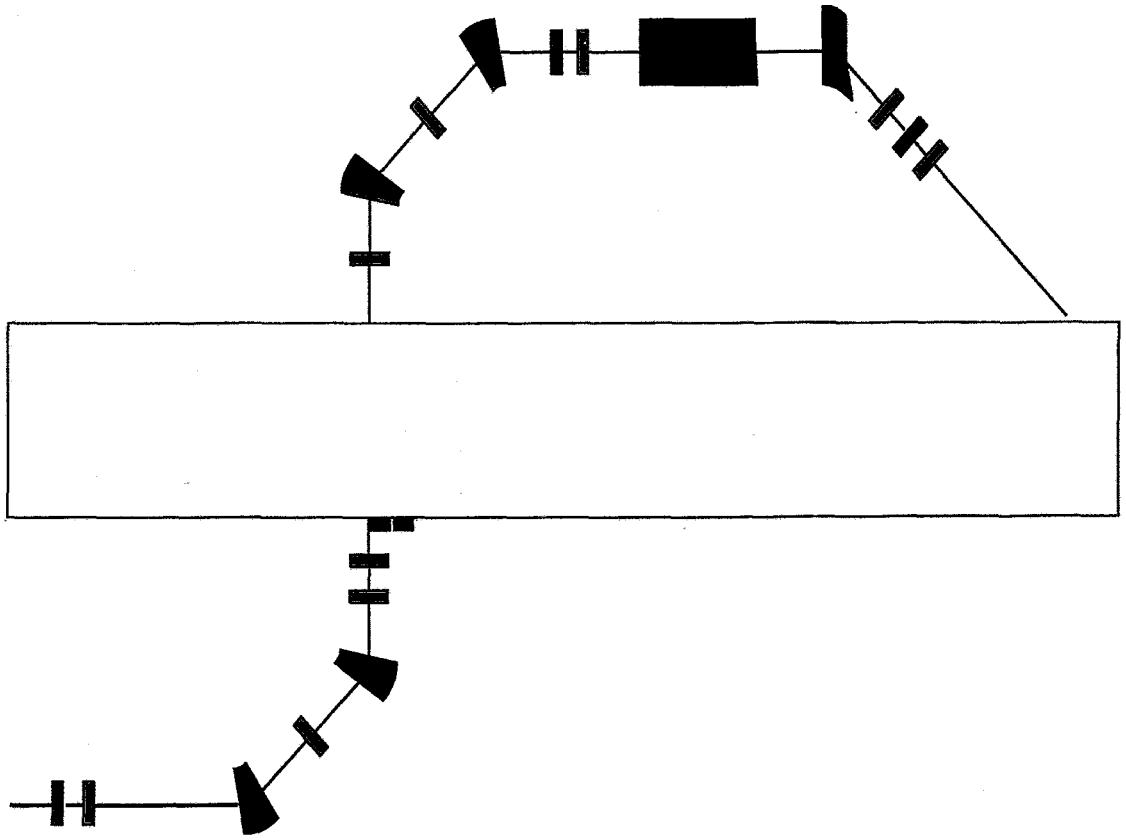

Fig. 1 *The bending system of the ELBE project. The green trapezoids represent the dipole magnets, the blue and red boxes indicate the vertically and horizontally focusing quadrupoles, respectively. The black rectangle shows the position of the FEL.*

The calculations were performed with the computer codes MIRKO [1] and TRANSPORT [2] for an electron energy of 20 MeV. By use of the GKS graphics package MIRKO allows an interactive work. It is well suited for getting the field parameters of the quadrupoles, which can easily be introduced into TRANSPORT for calculations to higher order. The FEL was simulated as a linear arrangement of dipoles with alternating polarity. By this way the beam properties were calculated, starting at the exit of the accelerator up to the beam dump. With the code PARMELA [3] the space charge effects were studied for a micropulse charge of 85 pC. We found that these effects can be compensated without additional quadrupoles.

[1] *GSI Darmstadt*

References

[1] B.Franczak, GSI Darmstadt, MIRKO, Version 5.13, 1989
[2] D.C. Carey, K.L. Brown, F. Rothacker, SLAC-R-95-462
[3] L.M. Young, J.H. Billen, Los Alamos National Laboratory, LA-UR-96-1835

Particle Tracing in a Mid-Infrared FEL at the ELBE accelerator

M. Wenzel, R. Wünsch, W. Seidel, E. Grosse

The General Particle Tracer (GPT) [1] was used to study the electron motion (Fig. 1), the micro bunching (Fig. 2), the light amplification (Fig. 3) and the saturation (Fig. 4) in a proposed mid-infrared free electron laser. Longitudinal and transversal emittance effects have been taken into account. The electron beam and undulator parameters of the simulations were the following: electron energy 37 MeV, bunch length 3 ps, geometrical emittance 0.44 mm mrad, energy spread 9.6 keV, undulator period 2.7 cm, number of undulator periods 40, undulator parameter 1.0. An electromagnetic wave of an appropriate resonant wavelength is superimposed. Its amplitude is treated as a free parameter. It is assumed to be constant along the undulator.

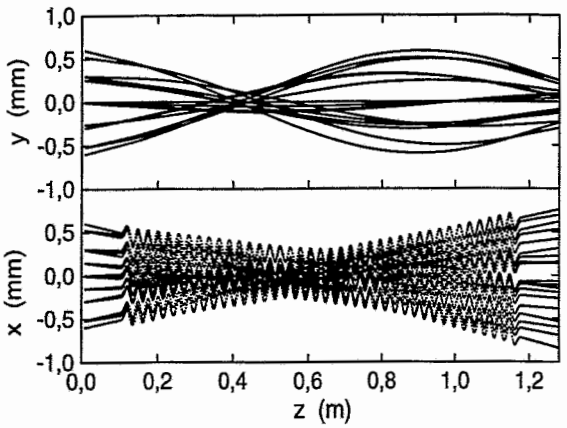

Fig. 1 bottom: *motion of the electron beam in the wiggle plane (xz).*
top: *Betatron oscillation in the magnet field plane (yz).*

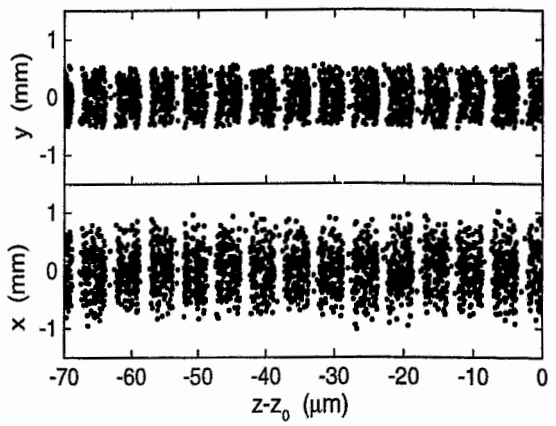

Fig. 2 *Electron bunching at a given time, one period before the end of the undulator (z_0). The electric field amplitude is 90 MV/m. Bunching in z-direction can be observed on a micrometer scale in the x- and y-projections.*

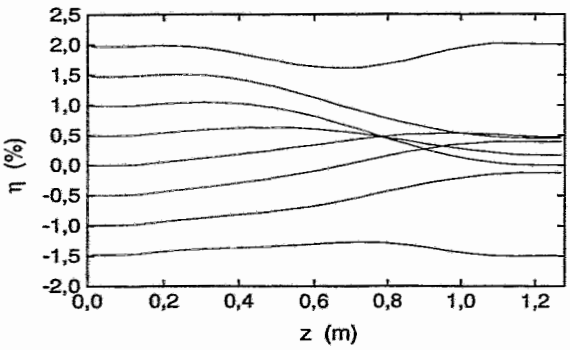

Fig. 3 *Relative deviation $\eta=(E-E_R)/E_R$ of the electron energy E from the resonance energy E_R as a function of z. The maximum of the energy loss occurs at $\eta=1.3\%$. Note that the energy transfer starts after passing half of the undulator.*

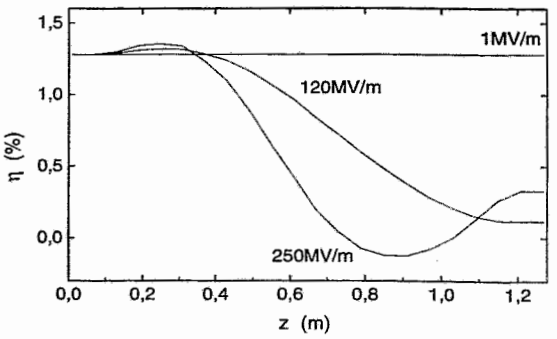

Fig. 4 *Relative deviation η along the undulator at different radiation field amplitudes. At about 120 MV/m the saturation of the energy transfer occurs at the end of the undulator. The curve at 250 MV/m is above the saturation.*

These simulations show that the proposed FEL with the designed beam parameters should allow lasing in the mid-infrared region.

References

[1] Bas van der Geer, Marieke de Loos, Pulsar Physics, Utrecht

Design studies for (the far-infrared) FIR-FEL at ELBE

A. WOLF[1]

For the production of far-infrared radiation width $\lambda > 25\,\mu$m the ELBE electron beam will be injected in an electromagnetic undulator. Such a device has the advantage of allowing a fast change of magnetic field strength and thus optical wavelength. Because of the high electric energy dissipation in the copper coil such an undulator is better suited for undulator periods above 50 mm and consequently for longer wavelengths. For long wavelengths diffraction losses at entrance and exit of the undulator have to be reduced by using a sufficiently large undulator gap; if this gap is at least 3 times larger than the 1σ-width of the optical beam, its Gaussian shape is not significantly deformed by diffraction effects.

With this condition taken into account an optimization was performed for a constant undulator period of 90 mm and constant energy dissipation per unit length: On the basis of a modified one dimensional model of linear free electron lasers [1],[2] the single pass gain was calculated in dependence of the undulator total length for different wavelengths (Fig. 1). To keep diffraction effects small the gap width was increased with increasing length (cf. Fig. 2) - leading to a reduction in the magnetic field strength factor K_{rms} as shown in Fig. 3. As seen from Fig. 1., saturation in single pass gain (9%) is nearly reached for λ=150 μm at an undulator length of 2 m. This value will be used for FIR-FEL; for shorter wavelengths of 20-100 μm it results in a single pass gain of about 10%, which is a good value for lasing to occur.

Further details of the ELBE project design will be published in a forthcoming laboratory report.

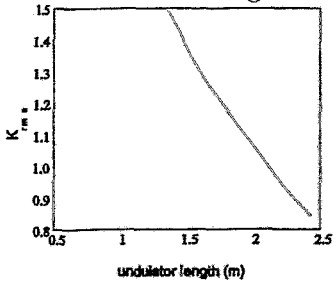

Fig. 3 *K_{rms} in dependence of the undulator length, when the gap is varied.*

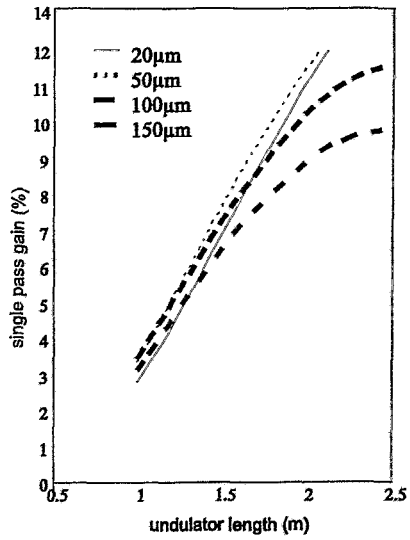

Fig. 1 *Single pass gain calculated versus undulator length.*

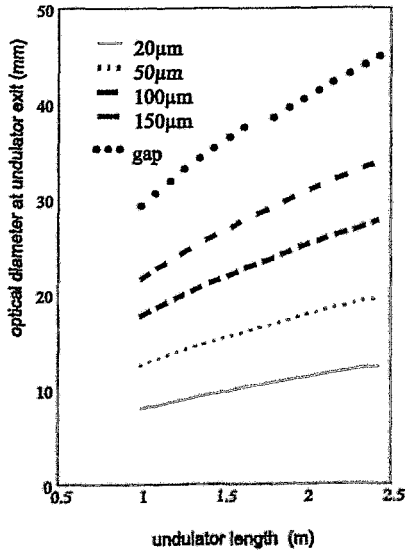

Fig. 2 *Diameter of the optical mode for rising from 20 to 150 µm. The gap was varied with the undulator length.*

[1] *Scientific Department of Experimental Facilities and Information Technology*

References

[1] K. W. Berryman, "Design, operation and applications of far-infrared free electron lasers", Dissertation 1995 Department of Physics of Stanford University

[2] P.W. van Amersfoort e. a. "The FELIX project status report April 1988", Rijnhuizen Report 88-176

Numerical Simulations of the Infrared Free Electron Laser at ELBE

R. WÜNSCH

We have performed one-dimensional numerical simulations [1] for the free electron laser (FEL) at ELBE with the following beam and undulator parameters:
Electron beam: energy: 20 (40) MeV, energy spread: 0.2%, norm. emittance: 20 mm mrad, (micro) bunch charge: 85 pC, bunch length: 3 ps, average cross-section: 3.14 mm^2;
Undulator: period: 8 (2.7) cm, total length: 2 (1.62) m, peak field on axis: 0.3 T
Filling factor, slippage and finite emittance have approximately been taken into account by means of a modified FEL parameter ρ.

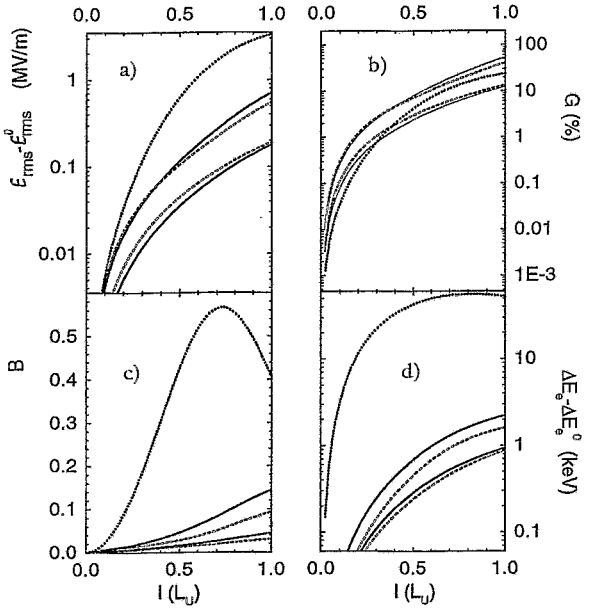

Fig. 1 *Growth of optical field strength $\mathcal{E}_{rms}$ (a), gain factor G (b), bunching factor B (c) and energy spread of the electron beam ΔE_e (d) as a function of the path length in the undulator in units of its total length L_U. The two lower curves belong to the undulator period λ_U=8cm, the upper curves to λ_U=2.7 cm. (Full lines: E_e=20 MeV, broken lines: E_e=40 MeV.) The initial electric field strength $\mathcal{E}^0_{rms}$ for the full and broken lines is 3 MV/m. The dotted lines represent the results for a stronger optical field $\mathcal{E}^0_{rms}$=30 MV/m (λ_U=2.7 cm, E_e=40 MeV).*

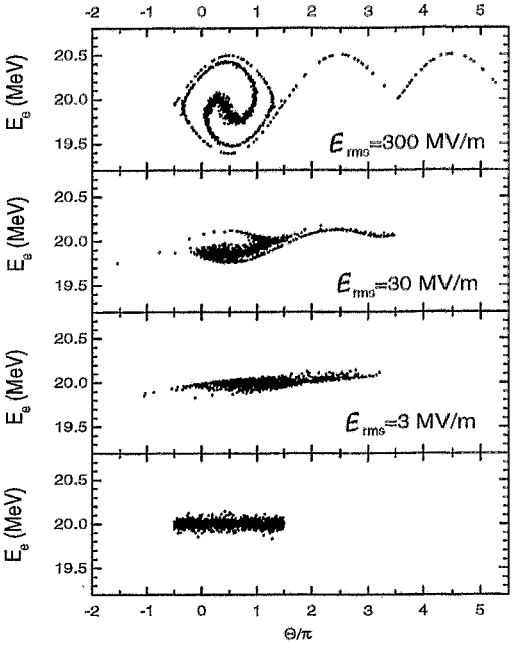

Fig. 2 *Longitudinal distribution (energy versus ponderomotive phase) for 1000 test electrons at beginning and end of the undulator (λ_U=2.7 cm). The initial distribution (lowest figure) is uniform in phase and Gaussian in energy with a width Γ=40 keV (0.2 %).*
The upper figures show the distributions at the end of the undulator for 3 values of the initial electromagnetic field.

The figures illustrate the behavior of the FEL for moderate optical fields ($\mathcal{E}^0_{rms}$=3 MV/m), where the gain of optical energy is well described by the small-signal gain G_0 of ref. [1] when the corrections used in ref. [2] are included. For strong fields ($\mathcal{E}^0_{rms}$=30 MV/m), where saturation and over-bunching are to be expected, the gain is reduced by about 40%.

References

[1] J. B. Murphy and C. Pellegrini in *Laser Handbook, Vol. 6, Free Electron Lasers*, eds. W. B. Colson, C. Pellegrini and A. Renieri (North Holland, New York, 1990), p. 9
[2] P. W. van Amersfoort et al., *The FELIX Project Status Report April 1988*, Rijnhuizen Report 88-176

Considerations on Bragg-Reflected Channeling Radiation and on Coherent Bremsstrahlung [B]

U. NETHING, R. ZAHN, W. ENGHARDT, H. PRADE

On the one hand parametric X-rays (PXR) [1] are generated when a relativistic charged particle traverses the periodic structure of a crystal and the associated virtual phonon field is Bragg reflected. On the other hand channeling radiation [2] is emitted when a charged particle enters the crystal at a small angle with respect to the crystal planes or axes. Matsuda et al. [3] predicted a considerable enhancement of the phonon flux in the centre of the PXR pattern, if the photon energy of channeling radiation satisfies the Bragg condition, i. e. due to Bragg-reflected channeling radiation.

Since channeling radiation is emitted in a forward cone with an opening angle of $1/\gamma$ (Lorentz factor $\gamma = 1+\mathrm{E}_{el}/\mathrm{m}_o\mathrm{c}^2$), i. e. of several degrees only, it is generally accompanied by bremsstrahlung of a similar characteristic producing a continuous background in the channeling radiation spectrum. For several application purposes it would be desirable to have background-free channeling radiation and therefore, we started exploring the specifications to observe Bragg-reflected channeling radiation at the experimental set-up behind the injector of the superconducting electron accelerator (S-DALINAC) in Darmstadt [4].

For the given experimental geometry on can use the (110) plane to produce the channeling radiation and the (111) one for the Bragg reflection. The photon energy of the Bragg-reflected photons amounts to 3.95 keV for a silicon crystal. The observation angle is 45 degrees with respect to the incoming electron beam. The corresponding photon energy of the channeling line determines the electron energy to 6.84 MeV. To measure this new radiation type the crystal should be tilted stepwise from the planar channeling direction to a random direction out of the channeling condition. During the rotation of the crystal the Bragg condition must be fulfilled for any orientation. If this radiation type exists, it will fill up the minimum of the tilt angle behavior of normal PXR radiation observed in the plane of radiation. In 1998 a corresponding experiment is foreseen.

Continuing earlier investigations on coherent Bremsstrahlung [5] we looked for optimal conditions for the generation of forbidden X-ray reflections [6,7] at low electron energies of 4 MeV in a silicon crystal. Using its ⟨100⟩ axis is exspected to be observe the (100) forbidden reflection at a photon energy of 186 keV and in this case the so called row effect does not mask the forbidden reflection. (Row effect means allowed reflections arising from projections of the reciprocal lattice vectors in the direction of the electron momentum, which lead to the same photon energy). Thus this experimental requirements seems to provide the best opportunity to proof the existence of forbidden X-ray reflections experimentally.

References

[1] J. Freudenberger et al., Appl. Phys. Lett. 70 (1997) 267
[2] J. Freudenberger et al., Nucl. Instr. and Meth. in Phys. Res. B 119 (1996) 123
[3] Y. Matsuda et al., ucl. Instr. and Meth. in Phys. Res. B 115 (1996) 396
[4] J. Auerhammer et al., Nucl. Phys. A 553 (1993) 841c
[5] R. Zahn et al., Annual report 1996, FZR-179, p. 15
[6] J.U. Andersen and E. Laesgaard, Nucl. Instr. and Meth. in Phys. Res. 31 (1988) 11
[7] I. Endo et al., Annual Report 1995, Institute for Nucl. Study, Univ. of Tokyo, p. 58

Compton Scattering of Laser Light on an Electron Beam

H.W. Barz and E. Grosse

The interaction of laser light with relativistic electrons (i.e. Compton scattering) can be used to produce high energy photons. A photon with energy E_{ph} which is backscattered off an electron with a much larger relativistic energy of $E_e = \gamma m_e c^2$ gets a maximum energy of $E_f \simeq 4\gamma^2 E_{ph}$ in the direction of the electron. At ELBE light from a high intensity NdYAG laser can thus be transformed into ~ 30 keV X-rays for $E_e = 40 MeV$. The differential cross section is very strongly peaked in the direction of the electron momentum; it falls off at a characteristic angle of the order of $\Theta \simeq 1/(2\gamma)$. With increasing scattering angle also the energy of the rescattered photon decreases rapidly. Therefore, if laser light is scattered from an electron beam the angular spread $\Delta\Theta_e$ of the beam influences significantly the distribution of the rescattered photons in energy and angle.

In Figs. 1 and 2 the averaged double differential cross sections are shown for two different values of 0.5 mrad and 2 mrad for the angular spread $\Delta\Theta_e$ of the electron beam. The calculations were done for 40 MeV assuming zero energy spread. The averaged peak cross section is estimated to be $d\sigma/d\Omega dE_f \simeq 200\, mb/sr/(E_f\, \Delta\Theta_e^2)$. The smaller the angular spread of the electron beam the larger is the percentage of the total cross section of 660 mb which is available for the production of high energy photons. As the yield of backscattered photons is inversely proportional to the size of the zone of overlap between the laser and electron beams not only the angle divergence but rather the emittance of the electron beam has to be as small as possible to allow an effective use of the Compton backscattering effect.

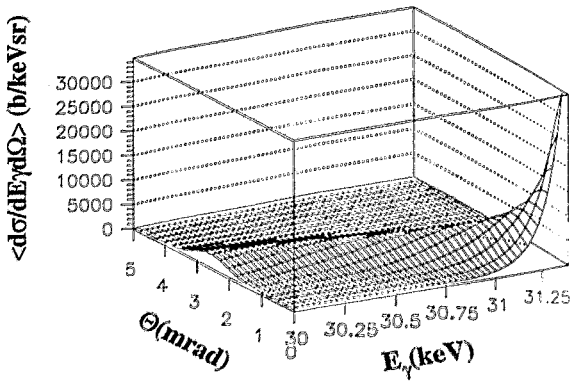

Fig. 1 *Averaged double differential cross section for the production of keV photons by scattering of laser light with a wavelength of 1 μm scattered off a 40 MeV electron beam. The cross section is averaged over the angular spread of 0.5 mrad of the electron beam.*

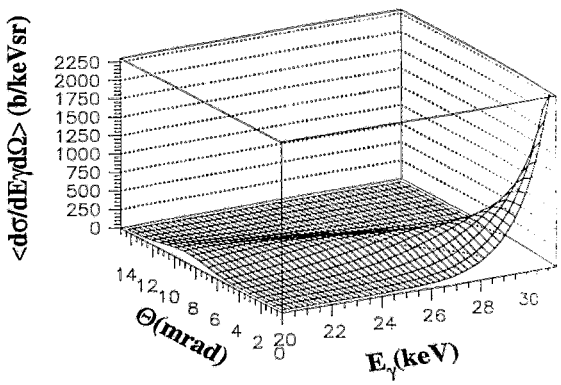

Fig. 2 *The same as Fig. 1, but now with an angular spread of 2 mrad. Notice the different scales compared to Fig. 1.*

Free Electron Laser Annealing of Ion Implanted SiC

M. Wenzel, P. Gippner, K.-D. Schilling, W. Seidel, E.Grosse
G. Irmer[1], F. Wirbeleit[2]
H. Wirth[3]

A direct excitation of lattice vibrations by an intense ultrashort laser pulse with an appropriate wavelength can induce a rearrangement of disordered atoms and a activation of dopants even at room temperature without a melt-recrystallization cycle. Infrared absorption spectroscopy confirmed [1] that the annealing at 12.6 μm (TO phonon frequency) was effective for removing the crystalline damage induced by the ion implantation. On the other hand, Hall effect measurements showed [1] an increase of carrier density for samples annealed with infrared light of 10.4 μm (LO phonon frequency), whereas the absorption was weak at this wavelength.

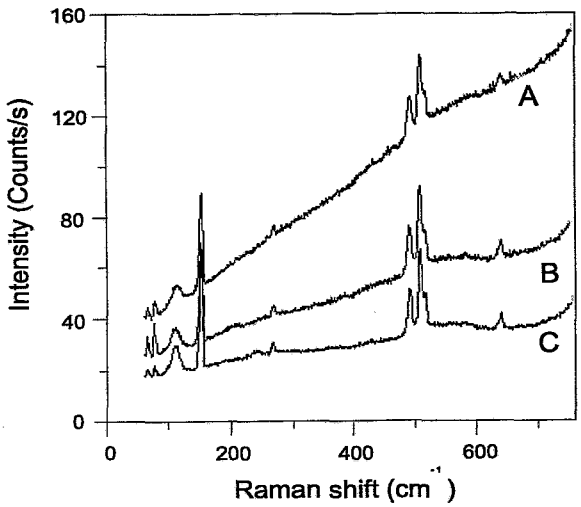

Fig. 1 *Raman spectra of a sample after ion implantation (B) and of two samples after implantation and laser annealing at λ=10.3 μm (C) and λ=12.6 μm (A), respectively.*

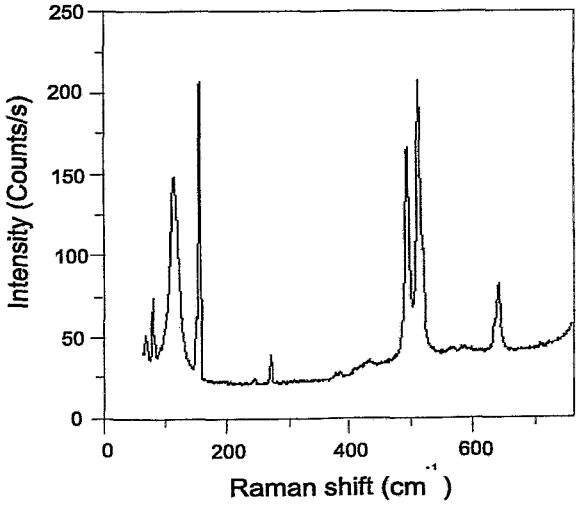

Fig. 2 *Raman spectra of a SiC sample before ion implantation. The low background and the small phonon linewidths (about 4.3 cm^{-1}) indicate a good crystal quality of the substrat material.*

In a first experiment at the free electron laser FELIX [2], we irradiated N- and Al-implanted 6H-SiC crystals (300 μm thick, area 4.5 x 4.5 mm^2) in the wavelength region from 9.5 μm to 15.7 μm. X-ray diffraction measurements before and after laser annealing suggest that the crystalline damages induced by Al-ion implantation are reduced [3]. The samples were also investigated by low-temperature Raman and Electron Paramagnetic Resonance (EPR) measurements. For different irradiation wavelengths, different recrystallization effects appear (Fig. 1). For comparison the spectrum of a virgin sample is shown in Fig. 2. We can see that ion implantation causes crystal damages, resulting in halfwidth broadening of about 1 cm^{-1} and an increased luminescence background. Annealing with 10.3 μm reduces the luminescence. The remaining discrepancies between the samples A and C are not completely understood and need further investigations.

[1] *Institut für Theoretische Physik, TU Bergakademie Freiberg*
[2] *Institut für Experimentelle Physik, TU Bergakademie Freiberg*
[3] *Institut für Ionenstrahlphysik und Materialforschung, FZR*

References

[1] H. Ohyama et al., Appl. Phys. Lett. 71 (1997), 823
[2] FOM Institute for Plasma Physics, Nieuwegein, The Netherlands
[3] F. Eichhorn, FZR, private communication

Neutrons at ELBE

H. Freiesleben[1], D. Richter[1], K. Seidel[1], S. Unholzer[1]

The neutron physics group at the TUD has been granted financial support (HBFG) for the installation of a neutron hall at ELBE. The scientific motivation to produce and use neutrons at the ELBE stems from fusion neutronics.

The energy yield by d-t fusion consists primarily of kinetic energy of 14 MeV neutrons which is converted in the blanket system (first wall, blanket and vacuum vessel) of a fusion reactor by nuclear and atomic processes of neutrons and photons into heat. The spectral distribution of the neutron and photon flux density in the back-plate of a shield-blanket mock-up for the International Thermonuclear Experimental Reactor (ITER) is shown in Fig. 1. The neutron spectrum consists of a 14 MeV-peak and a continuous distribution ranging up to thermal energy. The portion of these components in the total flux depends on the position in the blanket system. In the first wall e. g., the 14 MeV neutrons are dominating, whereas in the vacuum vessel more low-energy neutrons appear, resulting also in changed photon spectra. Hence, heat deposition, tritium breeding, gas production, activation and radiation damage in the blanket materials, which depend strongly on neutron and photon energy, need to be investigated as function of neutron and photon energy spectra.

At ELBE these neutron field spectra can be produced by mixing neutrons of two sources: The electron beam of ELBE generates via bremsstrahlung a continuous spectrum of photoneutrons which can additionally be modified by multiplier and/or moderator. A d-T neutron generator provides 14 MeV neutrons. Each of the sources has a strength of up to 10^{12} neutrons per second. They can be operated simultaneously or individually. That allows integral fusion neutronics experiments as well as investigations of the elementary nuclear and atomic processes.

Neutron fields of this kind are also suited for investigations concerning transmutation, neutron metrology, radiation safety physics and safe-guard problems.

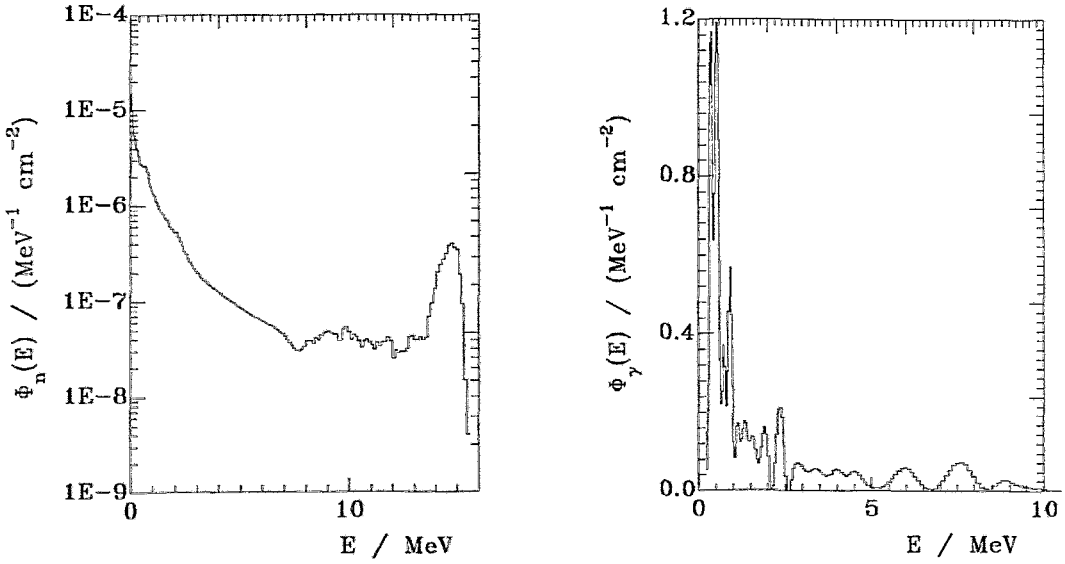

Fig. 1 *Measured neutron (left hand) and photon (right hand) fluence spectrum per one d-t neutron in an ITER shield-blanket mock-up [1]*

[1] *Institut für Kern- und Teilchenphysik, TU Dresden*

References

[1] H. Freiesleben et al., Fusion Technology 1996, page 1571, Elsevier Science B. V. 1997

Hadron Physics

Strangeness and electromagnetic radiation from strongly interacting systems (hadrons and nuclei) – these are the research topics of the hadron department.
To gain with these probes new insights in properties of hadrons and nuclear matter in collisions we participate in several experimental collaborations. At GSI/Darmstadt the detector systems KaoS and FOPI offer the possibility to study properties of hadrons produced in heavy-ion collisions. The kaon and anti-kaon production near or below the threshold are measured with the magnet spectrometer KaoS. An abnormal enhancement of anti-kaon production in heavy-ion collisions at equivalent beam energies has been detected. Preliminary interpretations of this effect point to an anti-kaon mass reduction due to partial restoration of chiral symmetry in dense nuclear matter. Very recent and forthcoming measurements at KaoS focus on kaon and anti-kaon detection in reactions with various beam and target combinations to get a systematic mass dependence.
With the 4π detector FOPI also hidden strangeness is measurable, e.g., in ϕ production which is identified via the kaon - anti-kaon decay channel. Presently the kaon spectra at midrapidity are analyzed, and evidence for kaon squeeze-out was found. The mentioned detector systems are multi-purpose installations. Therefore, a much wider set of various interesting aspects has been explored and reported in a series of publications.
Complementary to the mentioned measurements of hadron spectra in heavy-ion collisions one needs a detailed knowledge on hadron reactions in the same energy region. The cooler synchrotron COSY/Jülich provides a suitable device to study hadron-induced reactions at hadrons or nuclei. Essential components of the time of flight (TOF) detector installation have been built up in Rossendorf. The first series of measurements with COSY-TOF are devoted to the strangeness production in the reaction $pp \rightarrow pK\Lambda$ and to bremsstrahlung in the reaction $pp \rightarrow pp\gamma$. The results are going to be published soon. In addition, in close collaboration with the Technical University Dresden the reaction $pp \rightarrow pn\pi^+$ is measured by using the one-layered barrel.
ANKE is an internal spectrometer in the COSY ring. The decisive wire chambers are constructed in Rossendorf. Among the first experiments envisaged in 1998 is the exploration of anti-kaon production in light nuclei; the concept of this experiment has been mainly elaborated by scientists from our institute.
To ensure a participation in future developments, wire chambers for the HADES experiment at GSI are going to be built up in Rossendorf. It is the aim of this experiment to seek for a direct verification of the hypothesis that properties of hadrons are modified in a nuclear environment.
The theory group in the hadron physics department is accompanying these experimental activities. Predictions and interpretations of selected topics in the realm of strange and rare electromagnetic probes are provided. Some of these calculations refer to the energy range as covered by the experiments performed with FZR participation, others deal with the quark-gluon plasma accessible only at higher beam energies.

Off-plane Emission of K^+ Mesons in Au+Au Collisions at 1 AGeV [B,G]

Y. Shin[3], R. Barth[1], I. Böttcher[4], D. Brill[3], M. Dębowski[5], F. Dohrmann, F. Laue[1], A. Förster[2], E. Grosse, P. Koczoń[1], B. Kohlmeyer[4], M. Mang[1], M. Menzel[4], L. Naumann, H. Oeschler[2], F. Pühlhofer[4], E. Schwab[1], C. Schneider, P. Senger[1], J. Speer[2], H.Ströbele[3], C. Sturm[2], G. Surowka[1,5], F. Uhlig[2], A. Wagner[2,*], W. Waluś[5]

The azimuthal emission pattern of particles is an important observable for the study of the dynamics and the space-time evolution of a nucleus-nucleus collision. The in-plane directed flow and out-of-plane squeeze-out observed for protons and light fragments can be understood as hydrodynamical expansion phenomena. The preferential out-of-plane emission of pions at midrapidity was explained as an effect of shadowing due to the comoving spectator matter. The azimuthal angular distribution of K^+ mesons is of particular interest as it is sensitive to the strong kaon-nucleon potential in the nuclear medium.

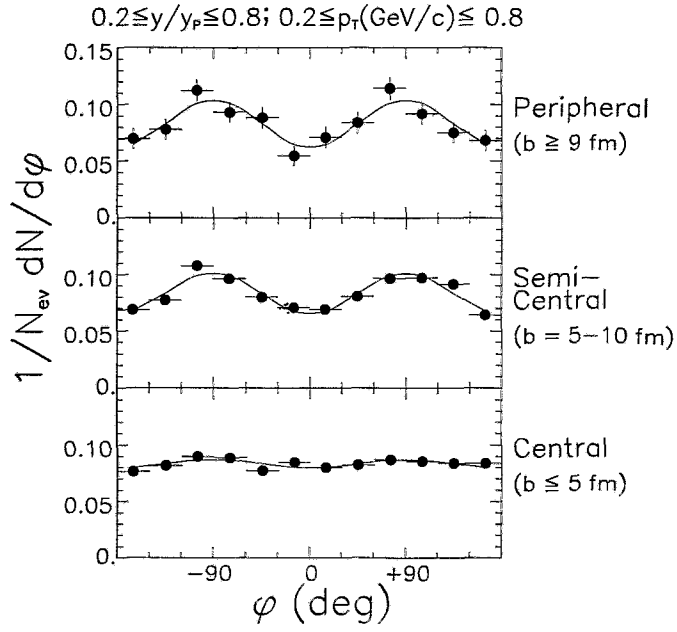

Fig. 1 *K^+ azimuthal angular distribution for peripheral, semi-central and central Au+Au collisions at 1 AGeV.*

We have performed a study of the K^+ emission pattern in Au+Au collisions at 1 AGeV. The kaons were measured with the spectrometer KaoS at Θ_{lab} = 34, 44 and 54°. The collision centrality was determined from the charged particle multiplicity measured around midrapidity and the orientation of the reaction plane was derived from the momentum vector of the projectile spectator fragments measured at forward angles. Fig. 1 shows the K^+ azimuthal angular distribution for peripheral, semi-central and central collisions for kaon momenta between 0.2 and 0.8 GeV/c and a range of normalized rapidities of $0.2 < y/y_{proj} < 0.8$. The data are corrected for the uncertainty of the reaction plane determination by a Monte Carlo method.
The K^+ yield is clearly enhanced at azimuthal angles of $\varphi = \pm 90°$ which is perpendicular to the reaction plane. The solid lines represent fits to the data according to $dN/d\varphi \propto a_1\cos(\varphi)+a_2\cos(2\varphi)$. We find values for a_1 consistent with zero which means that there is no in-plane flow (as expected at midrapidity). The strength of the off-plane anisotropy

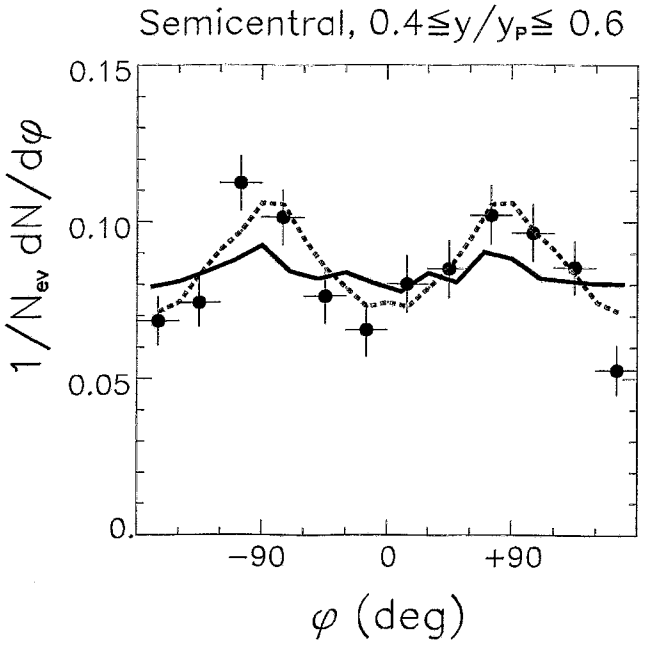

Fig. 2 K^+ *azimuthal distribution for semi-central collisions and* $0.4 < y/y_{proj} < 0.6$ *for Au+Au 1 AGeV. The lines represent results of RBUU calculations [1] (see text).*

can be parameterized by $R = \frac{N(90°)+N(-90°)}{N(0°)+N(180°)} = 1.56 \pm 0.04$ for semi-central collisions.
In fig. 2 we compare our data for semi-central collisions within a narrow rapidity window $0.4 < y/y_{proj} < 0.6$ to the prediction of a relativistic transport model for Au+Au at 1 AGeV and b = 7 fm [1]. Within the model calculation, the kaons propagate through participant and spectator matter and kaon-nucleon rescattering is taken into account. The dashed line corresponds to a calculation which includes a strong in-medium KN potential whereas the solid line is the result without an in-medium KN potential. According to the RBUU model, the strong KN potential is clearly needed to reproduce our data.
From our data we can also extract information on the K^+ in-plane flow near target and projectile rapidity. We divide the data set for semi-central collisions (center part of fig. 1) into three rapidity bins y/y_{proj} = (0.2-0.4, 0.4-0.6 and 0.6-0.8) and determine the a_1 and a_2 coefficients. The fit gives values of $a_1 = 0.087 \pm 0.046$, 0.048 ± 0.041 and 0.034 ± 0.052 which are very small or compatible with zero within the error bars. We find no signature for the existence of an in-plane directed flow of K^+ mesons. A similar result has been reported by the FOPI collaboration. The disappearance of kaon flow was predicted by RBUU calculations due to the repulsive KN potential. The K^+ mesons are repelled from the nucleons which exhibit a significant in-plane flow. Still missing is a full theoretical explanation of how this mechanism extinguishes the K^+ flow near target (and projectile) rapidity while it enhances the out-of-plane emission of K^+ mesons at midrapidity. In the latter case the kaon repulsion by the spectator matter seems to be the dominant effect.

[1] *GSI Darmstadt*
[2] *TU Darmstadt, Institut für Kernphysik*
[3] *Universität Frankfurt, Institut für Kernphysik*
[4] *Universität Marburg, Physikalisches Institut*
[5] *Jagiellonian University Cracow, Institute of Physics*
* *now at NSCL, Michigan State University, USA*

References

[1] G.Q. Li, C.M. Ko and G.E. Brown, Phys.Lett. B 381 (1996) 71 and G.Q.Li, private communication

Kaon Production in C+C Collisions [B,G]

C. Sturm[2], F. Laue[1], R. Barth[1], I. Böttcher[4], D. Brill[3], M. Dębowski[5], F. Dohrmann, A. Förster[2], E. Grosse, P. Koczoń[1], B. Kohlmeyer[4], M. Mang[1], M. Menzel[4], L. Naumann, H. Oeschler[2], F. Pühlhofer[4], E. Schwab[1], C. Schneider, Y. Shin[3], P. Senger[1], J. Speer[2], H. Ströbele[3], G. Surowka[1,5], F. Uhlig[2], A. Wagner[2,*] and W. Waluś[5]

First preliminary results for K^+ production from C+C measured at SIS-KaoS in dependence of the beam energy are reported and compared to recent K^+ data from Ni+Ni collisions [1].

Fig. 1 presents the K^+ invariant production cross sections as a function of the c.m. kinetic energy for C+C collisions at various beam energies. The data are measured at Θ_{lab}=44° (1 AGeV), 40° (1.2 AGeV) and 32° (1.5-2.0 AGeV). These angles correspond approximately to $\Theta_{cm}\approx$90°. We discuss here the midrapidity data only. The solid lines represent Boltzmann distributions fitted to the data (assuming isotropic emission in the c.m. system). The inverse slope parameters increase from T≈60 MeV at 1 AGeV beam energy to T≈80 MeV at 2 AGeV. We estimate the total K^+ production cross sections σ_{K+} by integrating the fit results over momentum and extrapolation to 4π assuming isotropic emission. The inclusive K^+ production multiplicities are determined by $M_{K+} = \sigma_{K+}/\sigma_R$ with $\sigma_R=4\pi(1.2 \times A^{1/3})^2 fm^2$. The K^+ multiplicities M_{K+} per average number of participating nucleons $<A_{part}>$ are shown in fig. 2 as a function of the beam energy together with results from Ni+Ni collisions ($<A_{part}> = 6$ in C+C and 29 in Ni+Ni according to a geometrical model). The solid lines represent fits to the data according to $M_{K+} \propto E_{beam}^{\alpha}$ with α=5.3±0.3 (Ni+Ni) and α=6.0±0.3 (C+C). We assume here an isotropic kaon emission although we found deviations from isotropy. However, the K^+ angular distribution in C+C collisions does not change significantly with beam energy. Therefore, the shape of the K^+ excitation function as shown in fig. 2 should not depend on the K^+ emission pattern. Fig. 2 indicates that the C+C data increase faster with beam energy than the Ni+Ni data. This effect is expected for a soft equation of state which leads to an enhanced K^+ production yield for heavy systems at low beam energies. The kaon data from C+C collisions complete the data set on subthreshold K^+ production as a function of the size of the collision system. Fig. 3 shows $M_{K+}/ <A_{part}>$ measured for different symmetric projectile-target combinations at a beam energy of 1 AGeV. The dominant role of multi-step-processes or other collective effects in subthreshold kaon production is visible from the rise with A.

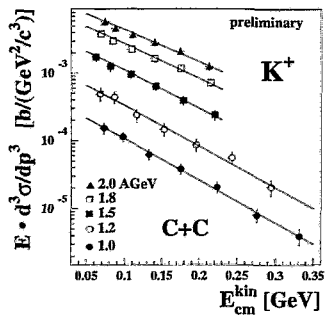

Fig. 1 *Invariant K^+ production cross sections as a function of c.m. kinetic energy (fits see text).*

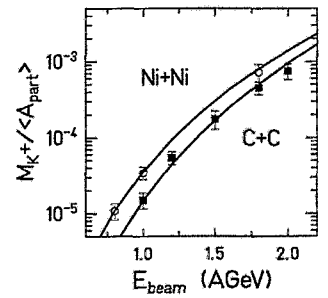

Fig. 2 *Inclusive $M_{K+}/<A_{part}>$ as a function of beam energy (fits see text).*

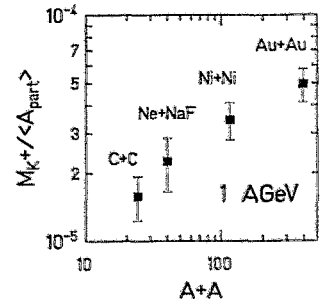

Fig. 3 *$M_{K+}/<A_{part}>$ as a function of system size (A+A).*

[1] *GSI Darmstadt*
[2] *TU Darmstadt, Institut für Kernphysik*
[3] *Universität Frankfurt, Institut für Kernphysik*
[4] *Universität Marburg, Physikalisches Institut*
[5] *Jagiellonian University Cracow, Institute of Physics*
[*] *now at NSCL, Michigan State University, USA*

References

[1] R. Barth and the KaoS Collaboration, Phys. Rev. Lett. 78 (1997) 4007

Antikaon Production in C+C Collisions [B,G]

C. Sturm[2], F. Laue[1], R. Barth[1], I. Böttcher[4], D. Brill[3], M. Dębowski[5], F. Dohrmann, A. Förster[2], E. Grosse, P. Koczoń[1], B. Kohlmeyer[4], M. Mang[1], M. Menzel[4], L. Naumann, H. Oeschler[2], F. Pühlhofer[4], E. Schwab[1], C. Schneider, Y. Shin[3], P. Senger[1], J. Speer[2], H. Ströbele[3], G. Surowka[1,5], F. Uhlig[2], A. Wagner[2,*] and W. Waluś[5]

We have studied the production of K^- mesons at SIS-KaoS. The yield of antikaons created in nucleus-nucleus collisions at subthreshold beam energies depends sensitively on the in-medium K^- rest mass. Calculations based on chiral Lagrangians predict a reduction of the antikaon mass in the dense nuclear medium. In Ni+Ni collisions at 1.8 AGeV we have found an unexpected large K^- yield [1] which was explained by an in-medium K^- mass reduction [2].

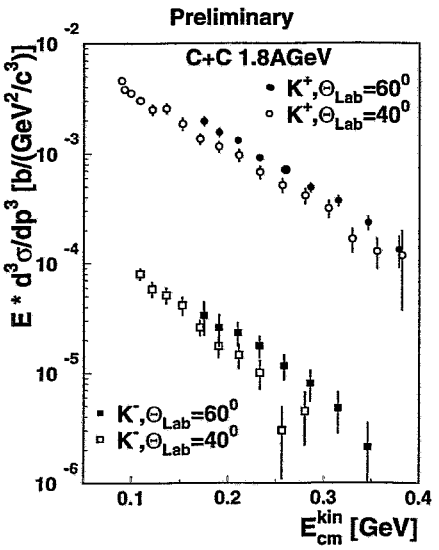

Fig. 1 *Invariant K^+ and K^- production multiplicities a as a function c.m. kinetic energy.*

Fig. 1 presents preliminary K^+ and K^- invariant production cross sections from C+C collisions at 1.8 AGeV for Θ_{lab}=40° and 60°. The kaon and antikaon yields measured at Θ_{lab}=60° are clearly above the 40° data. This corresponds to a forward-backward peaked angular distribution both for K^+ and K^- mesons. The fit of a Boltzmann distribution to the 40° data results in inverse slope parameters of T≈70 MeV for K^+ and T≈50 MeV for K^-. The K^+/K^- ratio is about 40. The corresponding value for Ni+Ni at 1.8 AGeV was 18±6 [1]. This difference is most probably due to the fact that K^+ production is above threshold (at 1.8 AGeV) whereas K^- production is still subthreshold. Hence the K^+ yield increases less with increasing mass than the K^- yield. In order to roughly correct for this phase space effect we compare K^- and K^+ production cross sections at equivalent beam energies, namely the K^- yield at 1.8 AGeV to the K^+ yield at 1 AGeV. In both cases the kinetic energy in the NN system is 230 MeV below the kinematical threshold energies which are E_{beam}=1.58 GeV for NN→$K^+\Lambda$N and E_{beam}=2.5 GeV for NN→K^+K^-NN. The K^- yield for 1.8 AGeV as shown in fig. 1 agrees roughly with the K^+ yield measured at 1 AGeV (see fig. 1 in the contribution on Kaon Production). Such an agreement was already found for Ni+Ni collisions [1] which suggests that the K^-/K^+ ratio for equivalent beam energies does not depend on the size of the system in the mass range from C to Ni. This result is surprising as one would expect for the K^- mesons strong absorption effects in contrast to the K^+. The cross section for the absorption of a K^- meson with a momentum of about 400 MeV/c via the strangeness exchange process $K^-N\rightarrow\pi\Lambda$(or Σ) is about 40 mb. This value corresponds to a mean free path of $\lambda \approx 1.6$ fm in normal nuclear matter (ρ_0=0.16 fm^{-3}). Assuming a survival probability according to exp(-r/λ) with r=1.2×A$^{1/3}$ fm we estimate that the K^- absorption in the Ni+Ni system is about 3 times stronger than for C+C. This factor has to be compensated by an enhanced K^- production in the Ni+Ni system in order to get as large K^-/K^+ ratios, as observed experimentally.

[1] *GSI Darmstadt* [2] *TU Darmstadt, Institut für Kernphysik* [3] *Universität Frankfurt, Institut für Kernphysik*
[4] *Universität Marburg, Physikalisches Institut* [5] *Jagiellonian University Cracow, Institute of Physics*
* *now at NSCL, Michigan State University, USA*

References

[1] R. Barth and the KaoS Collaboration, Phys. Rev. Lett. 78 (1997) 4007
[2] W. Cassing et al., Nucl.Phys. A 614 (1997) 415

Fast Tracking Trigger for the Kaon Spectrometer [G]

M. MENZEL[1], I.M. BÖTTCHER[1], M. BORN[1], J. HOFFMANN[2], P. KOCZOŃ[2], B. KOHLMEYER[1], L. NAUMANN, F. PÜHLHOFER[1], B. RIMARZIG, J. SPEER[1] AND THE KAOS COLLABORATION

A new scintillator wall (G-detector) was installed at the Kaon Spectrometer [1] at SIS in a position behind the focal plane. The G-detector contains 30 vertically mounted paddles built of $47 \times 7.5 \times 2$ cm^3 BICRON BC408 scintillators, 11 cm long lucite light guides and HAMAMATSU H1949 photomultiplier tubes. Together with the two existing scintillator arrays (D- and F-detector) this setup allows for a fast online particle tracking [2] within 150 ns. In addition to the 1^{st}-level TOF trigger this online tracking serves as a 2^{nd}-level trigger.

The tight timing requires fast processing of the track information from the 76 detector paddles (fig. 1). The strategy is to compare precompiled track patterns with the actual hit patterns. $2^{76} = 7.5 \cdot 10^{22}$ combinations are possible and accepted in the input stage of the electronics. This number is reduced to a few thousands realistic hit patterns, because multiplicities higher than two can be ignored in practice. A block diagram of the electronic logic is shown in fig. 1. The hit pattern of the F- and G-detector is split in two 15-bit wide data words, which are used as addresses for fast SRAM-IC's. The data output consists of a binary number that is unique for each one- or two-hit pattern. The next row of SRAM's uses the output of the first one as addresses to perform the same task by connecting the information of the two parts of each detector array. This coding delivers an 18-bit wide binary number that encodes every one- or two-hit pattern to a memory lookup unit (MLU). The MLU is filled with the hit patterns of allowed trajectories, so that the output gives the possible D-hits depending on the F- and G-hits. In the last step the predicted hit pattern of the D-detector is compared with the real pattern by logic AND's. If one of the comparisons is successful a 2^{nd}-level trigger signal is generated. This trigger logic, together with the necessary auxiliary logic, is realized as CAMAC module. Before each experiment the SRAM's are filled via the CAMAC dataway. During the data acquisition the modul is working without any external support. The generation of the 2^{nd}-level trigger signal takes 110 ns starting at the arrival of a 1^{st}-level signal.

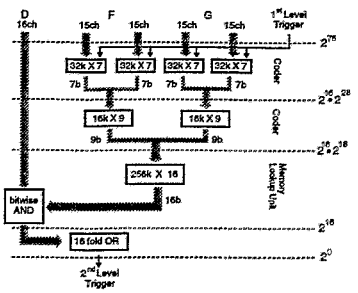

Fig. 1 *Block diagram of the tracking trigger logic.*

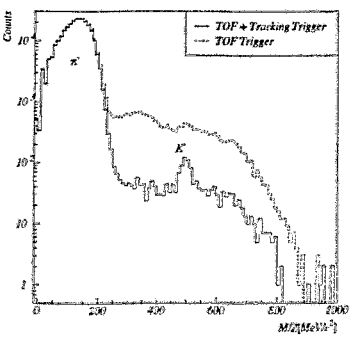

Fig. 2 *Negatively charged particle spectra taken online with and without the 2^{nd}-level trigger. (Ni+Ni, 1.93 AGeV, Θ=50°, B=-0.9 T)*

In a Ni-experiment in November 1997 the new tracking trigger operated successfully. Using a high trigger efficiency of 95% we found background suppression factors up to one order of magnitude in the region of the kaon mass. These factors depend on the used 1^{st}-level TOF trigger and on the momentum range. In fig.2 particle mass spectra are shown, which demonstrate clearly the background reduction, in particular around the kaon mass. The efficiency for the allowed particles is about 95%. (The pion peak is cut by the 1^{st}-level trigger.) The new scintillators are connected to the existing laser calibration system. For minimum ionizing particles the paddles show a time resolution of 170 ps (FWHM). The additional TOF information will improve the spectrometer mass resolution.

[1] *Universität Marburg* [2] *GSI Darmstadt*

References

[1] P. Senger et al., Nucl. Inst. and Meth. A 327 (1993) 393
[2] I.K. Yoo et al., GSI Scientific Report 1994 (1995) 274

Identification of Midrapidity Kaons with FOPI [B,G]

C. Plettner, R. Kotte, W. Neubert and D. Wohlfarth
FOPI collaboration

With the goal of providing additional information on kaon properties around midrapidity we continued the strangeness research started in 1996 with the CDC/Plastic Barrel combination [1,2] of the FOPI detector system [3], but now with the Helitron/Plastic Wall combination.

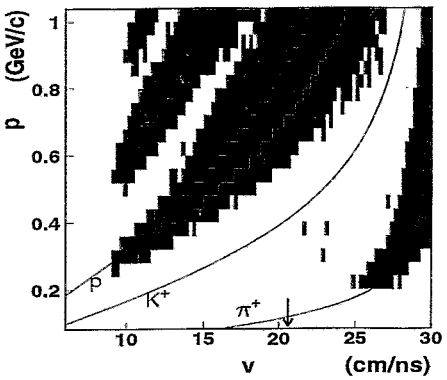

Fig. 1 *The experimental momentum* **p** *from the Helitron drift chamber vs. the velocity* **v** *taken from the Plastic Wall for charge +1 particles of the reaction 1.69 AGeV Ru+Ru. The lines give the nominal particles masses. The arrow indicates the c.m. velocity.*

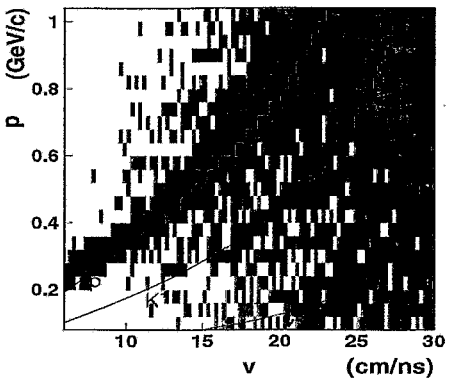

Fig. 2 *The same as Fig. 1, but now results of GEANT simulations using as event generator the IQMD transport model (b=2 fm, stiff EoS, momentum dependent forces, no cluster formation). Additionally, one thermal K^+ meson (fireball temperature T=100 MeV) is added per event.*

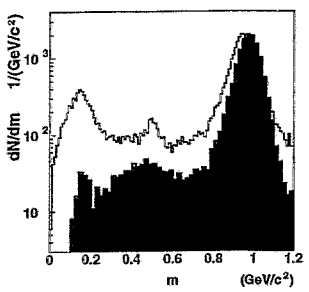

Fig. 3 *Experimental mass distribution (hatched histogram) of charge +1 particles produced in the reaction 1.69 AGeV Ru+Ru and reconstructed from the Helitron momentum and the Plastic Wall velocity. The free histogram gives the reconstructed masses of the GEANT simulations.*

Figs. 1 and 2 show the distribution of charge +1 particles in the plane of momentum **p** from Helitron vs. velocity **v** from the Plastic Wall. For Fig. 1 cuts are applied on the polar angle ($15^o < \theta_{lab} < 26^o$), on the tracking and matching qualities. No cuts are applied on the GEANT data of Fig. 2.

Fig. 3 gives the mass distributions after linearization via $m = p/v\sqrt{1-(v/c)^2}$. For the experimental data additional cuts are applied on the energy loss in the plastic scintillators (less than 2 times the loss of minimum ionizing particles) and on the momentum ($p < 0.5$ GeV/c). The latter one strongly suppresses the π^+ signal. In a very rough estimate for the K^+ yield we get about 0.0015 per central event which is amost a factor of 2 below the value one expects from systematics [1]. The combined efficiencies of track finding in the Helitron and the matching of Helitron tracks with Plastic Wall hits will be determined with the help of GEANT simulations and from the experimental data itself taking advantage of the nearly 100% detection efficiency of the plastic scintillator wall. In the near future we will study the background below the kaon mass peak (arising both from protons and π^+ mesons), the kaon detection efficiency and the influence of the various cuts on the final results.

References

[1] D. Best et al., (FOPI collaboration), Nucl. Phys. A 625, 307 (1997)
[2] C. Plettner, R. Kotte, W. Neubert, D. Wohlfarth, FZR-179, 100 (1997)
[3] A. Gobbi et al., (FOPI collaboration), Nucl. Instr. Meth. A 324, 156 (1993);
J. L. Ritman, Nucl. Phys. B - Proc. Suppl. 44, 708 (1995)

Squeeze-Out Signal for low-p_t K^+-Mesons [B,G]

C. Plettner, R. Kotte, W. Neubert, D. Wohlfarth and the FOPI collaboration

Subthreshold strangeness production in heavy-ion collisions is an interesting field of present research. With the data of the reaction ^{96}Ru +^{96}Ru at a projectile energy of $E_{\mathrm{proj}} = 1.69$ A·GeV measured by the FOPI collaboration with the 4π-detector system [1] at GSI Darmstadt the kaon production around midrapidity can be investigated. This is feasible with the Helitron and outer Plastic Wall detector combination [2] which covers the polar angle range of $8° < \Theta_{\mathrm{lab}} < 26°$.

The present analysis is restricted to the region around the center of mass rapidity Y_{cm} and to polar angles between $15° < \Theta_{\mathrm{lab}} < 26°$. From the azimuthal distribution $\mathrm{dN/d\Phi}$ (Φ being the angle with respect to the reaction plane) we can learn about the anisotropic emission of particles. The out-of-plane ratio R'_N quantifies the strength of the emission [3,4]:

$$R'_N = \frac{N(90°) + N(-90°)}{N(0°) + N(180°)}$$

$R'_N > 1$ means preferential out-of-plane emission, $R'_N < 1$ preferential in-plane flow. In Fig. 1 the azimuthal distributions for π^+ mesons, K^+ mesons and protons are plotted. The precision of the reaction plane determination is 32°. From the data we find for K^+ mesons and protons an out-of-plane emission but for the π^+ mesons an in-plane-flow. So far no precise estimate of the background contained in the azimuthal K^+ distribution has been made. But we want remark

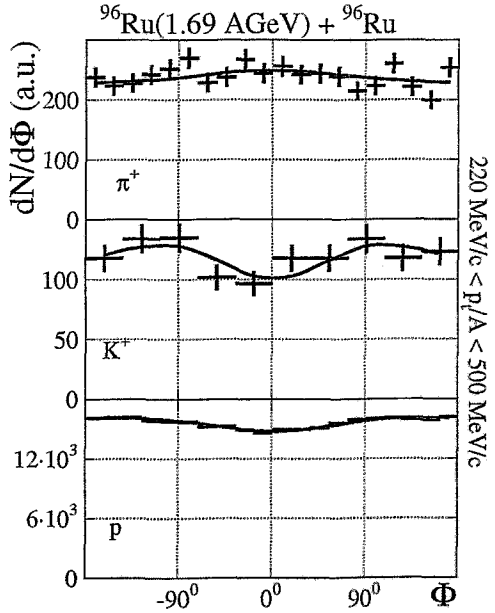

Fig. 1: *Azimuthal distributions $dN/d\Phi$ of semicentral events ($b \simeq 2-6$fm) for π^+, K^+, and protons for $-0.1 \leq Y^0 \leq 0.1$ where $Y^\circ \equiv (Y_{\mathrm{lab}} - Y_{\mathrm{cm}})/Y_{\mathrm{cm}}$. The curves correspond to Fourier series fits (cf. [3,4]). The extracted values for R'_N are displayed in Table 1.*

- that the pion background is almost negligible because for kaon identifikation the pions are strongly suppressed by certain cuts ([3]). Furthermore, low-p_t pions exhibit an in-plane-flow (see also [5]).
- that the proton background cannot conceal the kaon signal; otherwise the value of R'_N for K^+ would be closer to the one of the protons.
- and that for Au+Au at 1 A·GeV a very similar R_N for K^+ is found (cf. [6]).

We expect that with better statistics – so far only 10% of the available data have been analysed – we can extract a more reliable kaon squeeze-out signal.

Table 1. *Out-of-plane emission ratios R'_N (uncorrected) and R_N (corrected for the precision of the reaction plane determination)*

	π^+	K^+	p
R'_N	0.99 ± 0.19	1.16 ± 0.24	1.03 ± 0.02
R_N	0.98 ± 0.19	1.37 ± 0.28	1.06 ± 0.02

References

[1] A. Gobbi and the FOPI collaboration, Nucl. Instr. Meth. A 324, 156 (1993)
[2] C. Plettner et al., this report
[3] N. Bastid and the FOPI collaboration , Nucl. Phys. A 622, 573 (1997)
[4] P. Crochet and the FOPI collaboration, Nucl. Phys. A 624, 755 (1997)
[5] D. Brill and the KaoS collaboration, Z. Phys. A 357, 207 (1997)
[6] Y. Shin and the KaoS Collaboration, GSI Scientific Report 1997, GSI 98-1 (1998)

Dilepton and Vector Meson Production in Heavy-Ion Reactions [G,W]

GY. WOLF

I have studied heavy-ion reaction dynamics on the basis of a microscopical model of the BUU type. In this model the nucleons, baryonic resonances up to 2 GeV/c^2 as well as pions, η's, ρ's and σ's are explicitly propagated. The model appears to describe the hadronic processes quite reliably.

I have applied this model to the process of dilepton production by calculating the contributions from proton-neutron bremsstrahlung, the Dalitz-decay of the Δ, η and ω, $\pi^+\pi^-$ annihilation as well as the direct decay of the ρ and the ω mesons, pion-nucleon bremsstrahlung, the Dalitz-decay of the $N(1440)$ and π^0. The π^0 decay dominates the invariant mass spectra below the pion mass not shown here. It is found that for all systems considered, the η Dalitz-decay dominates the spectra up to an invariant mass $M \approx 450$ MeV, and the ω decay around the ω meson mass. At 1 AGeV for 500 MeV $< M <$ 750 MeV practically all the cross section stems from $\pi^+\pi^-$ annihilation. At 2 AGeV, however, I find sizeable bremsstrahlung contributions, too. For studying especially $\pi^+\pi^-$ annihilation in the ρ mass regime a bombarding energy of 1 AGeV therefore seems to be optimal either for ^{197}Au+^{197}Au or ^{40}Ca+^{40}Ca collisions.

By dilepton measurements medium effects on the ρ and ω meson may be also explored. According to the vector meson-dominance model $\pi^+\pi^-$ annihilation proceeds via the production and decay of the ρ meson which might differ substantially in the medium [1]. Since the $\pi^+\pi^-$ annihilation dominates the dilepton invariant mass spectra below the ρ mass region, a change of the mass or width of the ρ as also suggested by QCD inspired models [2] should be seen experimentally. In order to estimate the magnitude of this effect I have performed calculations with the free ρ meson properties and compared to dilepton spectra that involve a density dependent form factor suggested in ref. [1] and ref. [2]. The spectra differ substantially (Fig. 1). Any future experiments looking for this effect would thus have to be sensitive to changes of this order.

We studied, futhermore, the σ–ω mixing in nuclear matter. Due to the mixing the ω meson broadens substantially [3]. I investigated its effect on the dilepton spectra in π^-+^{208}Pb collision at 1.3 GeV bombarding energy. I found that by selective measurements with respect to the ω momentum the mixing can be experimentally observed by HADES at SIS.

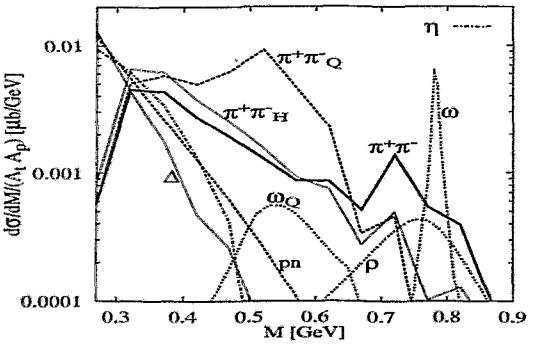

Fig. 1 *Dilepton spectra in Au+Au at 1 AGeV. I index Q denotes the modified contributions using the QCD sum rule estimates for ρ and ω [2], while index H indicates the annihilation contribution with the modified ρ in the hadronic model [1].*

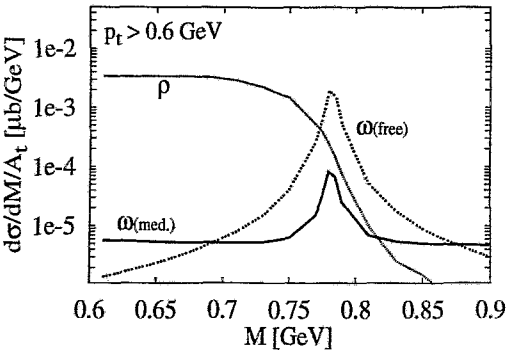

Fig. 2 *Dilepton production in π^-+^{208}Pb collision at 1.3 GeV bombarding energy. The figure shows the spectra with $p_t > 0.6$ GeV momentum cut. The broadening of the ω damps the contribution at the peak position.*

References

[1] M. Herrmann, B. Friman and W. Nörenberg, Nucl. Phys., A 560 (1993) 415.
[2] T. Hatsuda and S.Y. Lee, Phys. Rev. C 46(1992) R34.
[3] Gy. Wolf, B. Friman, M. Soyeur, Submitted to Nucl. Phys. A., eprint: nucl-th/9707055

Combined Effect of Nuclear Coulomb Field and Radial Flow on Two-Meson Correlations in Relativistic Heavy Ion Collisions

H.W. Barz

Measurements of correlations of pions as a function of their relative momenta are used to determine the source size in heavy ion reactions at intermediate and relativistic energies. The Hanbury-Brown and Twiss effect predicts a width of the correlation function $\Delta q = \hbar c/R_0$ for a randomly emitting spherical source with radius R_0 in the absence of any interaction. However this relation is distorted if flow and Coulomb interaction between particles and source become important. Flow shrinks the volume from which particles with a certain momentum can be emitted while Coulomb forces falsify the pion momenta characterizing the source size.
A source with flow is described by a source function $S(t, \mathbf{r}, \mathbf{p})$ which contains a correlation between emission point $\mathbf{r}$ and momentum $\mathbf{p}$. To determine the correlation function for two pions with momenta $\mathbf{p}$ and $\mathbf{p}'$ the calculation of the density matrix ρ is required

$$\rho(p,p') = \int d^4x \int d^4x' \, \rho(x,x') \psi_p^*(x) \psi_{p'}(x'), \tag{1}$$

$$\rho(x,x') = \delta(t-t') \int d\mathbf{p} \; e^{i\mathbf{p}(\mathbf{r}-\mathbf{r}')} S(t, \frac{\mathbf{r}+\mathbf{r}'}{2}, \mathbf{p}). \tag{2}$$

Here x comprises $(t, \mathbf{r})$, and the wave function ψ_p describes the motion of the meson in the field of the source. We aim to investigate the effect of the charge of the source and use solutions ψ_p of the Klein-Gordon equation with the Coulomb potential included [1]. Using a Gaussian source distribution characterized by R_0 the obtained correlation function C_2 [which is essentially the normalized square of (1)] has still the typical Gaussian shape $\sim exp(-q^2R^2)$, $q = |\mathbf{p} - \mathbf{p}'|$, as in the case of the unperturbed motion of the mesons. However, the observed radius R depends now on the momentum $\mathbf{K} = \frac{1}{2}(\mathbf{p} + \mathbf{p}')$. In Fig. 1 we show the ratio R/R_0 for the sideward and outward correlation for a system typical for a collision of heavy ions at 1 GeV per nucleon. The existence of flow decreases the extracted radius R with increasing pair momentum. The Coulomb field reduces (increases) the observed radii for positively (negatively) charged pions obtained from the side correlation. The Coulomb effect is opposite and weaker for the outward correlation.

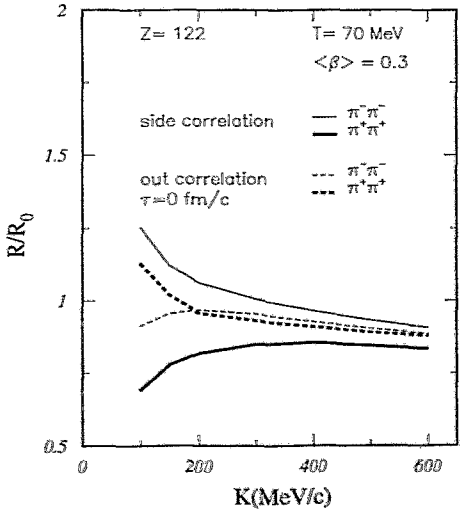

Fig. 1 *Ratios of HBT radii to the geometrical radius extracted from sideward and outward correlations of a source with charge number of 122, temperature of 70 MeV and a mean radial flow velocity of 0.3 c as a function of the average momentum K of the pion pair.*

References

[1] H.W. Barz, Phys. Rev. **C53** (1996) 2536

Coulomb Effects in Relativistic Heavy-Ion Reactions [B]

H.W. Barz, J.P. Bondorf[1], J.J. Gaardhøje[1], and H. Heiselberg[2]

An asymmetry in the number of opposite charge pions has recently observed in heavy ion collisions at SIS, AGS and SPS energies around 1 A·GeV [1], 11.4 A·GeV [2] and 158 A·GeV [3]. This effect can be explained by the Coulomb interaction between the produced pions and the positive charge of the reaction partners.

The long ranged Coulomb force changes the initial momentum p_0 and the energy E_0 a pion has at freeze-out. At low bombarding energies approximately a slowly expanding spherical source is formed which leads to a change of the energy for $\pi^{\pm}$ by $V_c = \pm\frac{6}{5}Ze^2/R_f$, where Z is the stopped charge and R_f the freeze-out radius. At ultrarelativistic collision energies it is important to include the rapid longitudinal expansion of the system as well as retardation effects. For rapid longitudinal Bjorken expansion we find [4] that the pions get a constant change of their transverse momentum $p_c \simeq \pm 2\frac{e^2}{R_f} dN^{ch}/dy$ which is proportional to the net charge (proton) rapidity distribution dN^{ch}/dy.

Assuming that the original distribution at freeze-out is thermalized either as $\exp(-E_0/T)$ or $\exp(-p_{\perp 0}/T)$ for SIS or ultrarelativistic energies, respectively, one can easily derive the final distribution for positive and negative pions. Using the measured slope parameters T and adjusting the respective values for the energy and momentum shifts the experimental π^-/π^+ ratios are well reproduced (see Fig. 1).

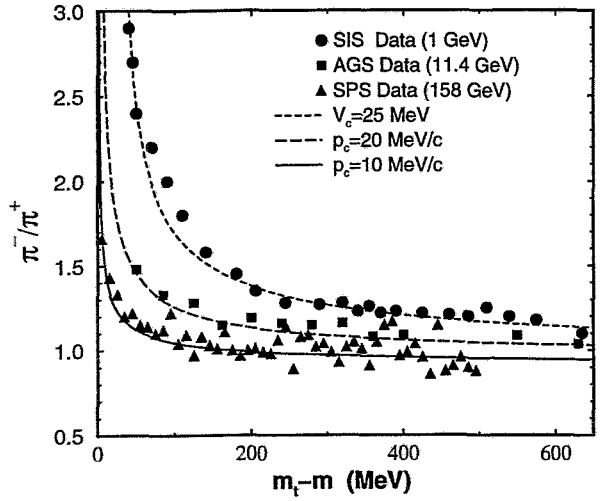

Fig. 1 *π^-/π^+ ratios measured in collisions of two heavy nuclei with mass numbers of 200 as a function of $m_\perp$ at SIS, AGS and SPS energies compared to calculations (curves).*

For collisions of $Au+Au$ at SIS energies we find $V_c \simeq 27$MeV which implies a radius of $R \simeq 8$fm using a common charge of $Z = 110$ (14% centrality). At ultrarelativistic energies we obtain $p_c^{AGS} \simeq 20$ MeV/c and $p_c^{SPS} \simeq 10$ MeV/c. From the measured proton rapidity distribution, $dN^p_{AGS}/dy \simeq 70$ and $dN^p_{SPS}/dy \simeq 37$ we can extract the size of the systems at freeze-out: $R_f^{AGS} \simeq R_f^{SPS} \simeq 10$ fm. These conclusions agree well with the refined analysis [4] based on calculations of pion trajectories.

[1] *Niels Bohr Institute, Copenhagen, Denmark*
[2] *NORDITA, Copenhagen, Denmark*

References

[1] A. Wagner et al., submitted Phys. Lett.; D. Pelte et al., Z. Phys. A 357 (1997) 215
[2] L. Ahle et al., Nucl. Phys. A 610 (1996) 139c
[3] H. Bøggild et al. (NA44), Phys. Lett. B 372, 343 (1996)
[4] H.W. Barz et al., Phys. Rev. C 56 (1997) 1553 and nucl-th/9711064

Bremsstrahlung within the One-Boson Exchange Model [B]

V.V. Shklyar[1], B. Kämpfer, A.I. Titov[1]

Previous estimates [1] of bremsstrahlung spectra in intermediate-energy nucleon reactions have been completed [2]. Within the effective one-boson exchange model we have calculated the complete set of Feynman diagrams on the tree level with π, σ, ω and ρ exchange for the reactions $pp \to pp\gamma$ and $pn \to pn\gamma$ including the anomalous magnetic moments of nucleons and internal radiative conversions of mesons. Delta decays $\Delta \to N\gamma$ are fully taken into account as well as all interference terms. Older data at 730 MeV proton beam energy are reproduced and give confidence in our model.

Examples of energy spectra and angular distributions are displayed in Fig. 1 for a non-coplanar detector geometry. It should be stressed that high-energy photons come from Δ decays, while soft photons stem from pure bremsstrahlung at beam energies 0.7 - 1.7 GeV.

While the model parameters are adjusted in the 1 GeV region, we apply our model also for beam energies near the pion threshold. As seen in Fig. 2 the shape of the angular distributions is fairly well reproduced.

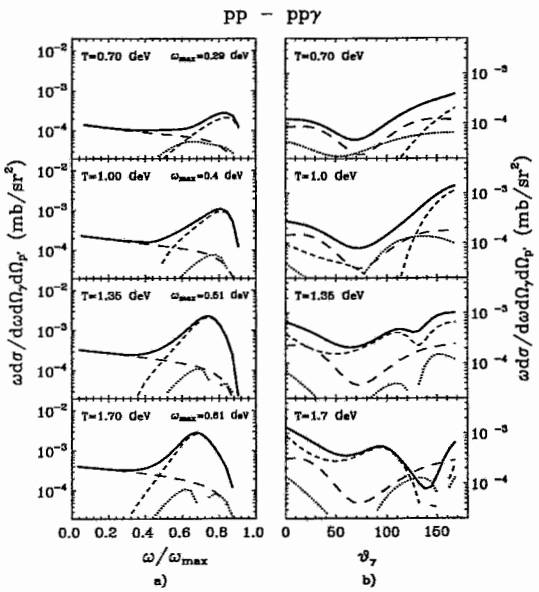

Fig. 1 *The cross section $\omega\, d\sigma/d\omega\, d\Omega_\gamma d\Omega_{p'}$ as a function of ω/ω_{max} for $\vartheta_\gamma = 30°$, (left panel) and as a function of ϑ_γ at $\omega/\omega_{max} = 0.5$, (right panel) for the reaction $pp \to pp\gamma$ at various beam energies ($\vartheta_{p'} = 40°$, $\phi = 60°$). Long-dashed lines: pure bremsstrahlung, dashed lines: Δ contribution, dotted lines: interference.*

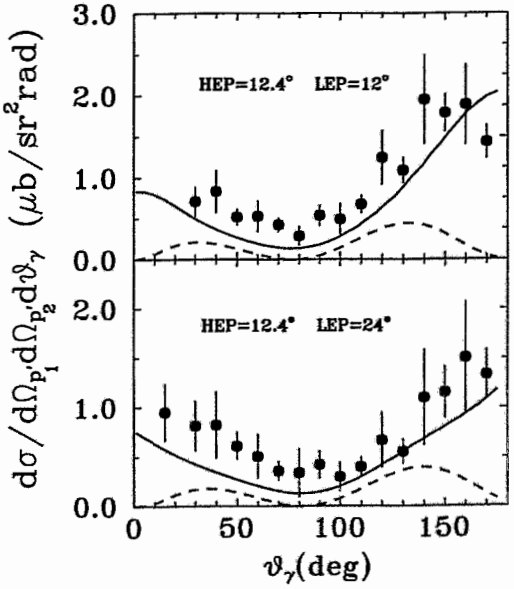

Fig. 2 *Comparison of our calculated cross section for the reaction $pp \to pp\gamma$ with data [3] (scaled by the often debated normalization factor 2/3) at 280 MeV beam energy. The dashed line is the result of the soft photon approximation.*

[1] *Bogoliubov Institute of Theoretical Physics, JINR Dubna, Russia*

References

[1] A.I. Titov, B. Kämpfer, B.L. Reznik, V.V. Shklyar, Phys. Lett. B 372 (1996)

[2] V.V. Shklyar, B. Kämpfer, B.L. Reznik, A.I. Titov, FZR-191 (1997), Nucl. Phys. A in print

[3] K. Michaelian et al., Phys. Rev. C 45 (1992) 2001

The Hard Photon Component in ppγ [B,K]

E. KUHLMANN[1] FOR THE COSY-TOF COLLABORATION

The study of pp bremsstrahlung is one of the original experiments to be performed with the COSY TOF spectrometer. First data at p = 797 MeV/c have been taken in October 1996 [1]; here only one of the main results will briefly be presented.

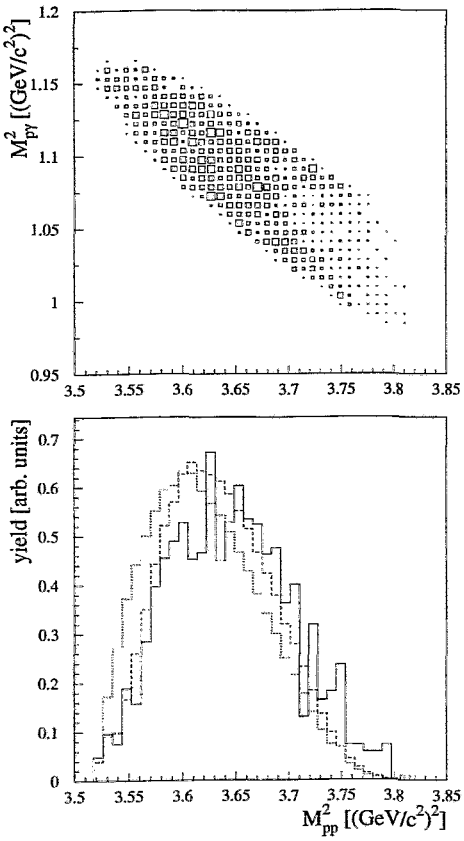

Fig. 1 *top: Dalitz plot of (kinematically fitted) bremsstrahlung events; bottom: projection onto the x-axis; the dotted and dashed curves represent Monte Carlo simulated distributions (see text).*

With the "Quirl" alone already a large fraction of the available phase space could be covered. When focussing onto the high energy end of the bremsstrahlung spectrum this percentage accounts for roughly 80% of the upper third in E_γ allowing a detailed view into the nature of the hard photon component. A Dalitz plot of all (kinematically fitted) bremsstrahlung events is shown in fig. 1 (top); in the bottom part the projection onto the x-axis is shown, where the dashed and dotted curves represent Monte Carlo (MC) simulated data (see below). Suitably normalized empty target runs have been subtracted. The most surprising result is the absence of sizeable FSI-effects at lowest M^2_{pp} which govern the corresponding Dalitz plots of the ppπ° [2] and pnπ^+ reactions [3] at comparable bombarding energies.

From kinematics only a low yield for two-proton emission at near-zero relative momentum was to be expected; an important additional reason, however, seems to stem from the structure of the ppγ transition matrix element for the magnetisation current operator which is believed to govern the processes relevant in the high energy part of the photon spectrum. This matrix element can be written [4] as the sum of two terms which for identical particles cancel each other to a large degree in all those cases where a spin-singlet state is involved thus favoring triplet $\rightarrow$ triplet transitions. The impact of the otherwise dominant $^1S_0$ state, which in NN scattering has by far the largest T-matrix elements, is except for the uppermost end of the photon spectrum widely reduced. Yet sizeable FSI effects are only to be expected if the two protons are in such a $^1S_0$ state as in the π° producing reaction mentioned above which close to threshold proceeds via the transition $^3P_0 \rightarrow {}^1S_0 s_0$. The order of the multipole radiation can also be deduced from fig. 1, namely, that in the projection (fig. 1, bottom), agreement with the MC data is only found, when the "simple" simulation (dotted curve) which only includes phase space and detector efficiency is additionally folded with a $(1/3 + cos^2\Theta_{CM})$- factor which is characteristic for dipole radiation [5]; this result is given by the dashed curve.

[1] *Institut für Kern- und Teilchenphysik, TU Dresden*

References

[1] P. Herrmann et al., Annual Report 1996 Jül-3365 p. 8 and earlier volumes
[2] A. Bondar et al., Phys. Lett. B 356 (1995) 8
[3] J.G. Hardie et al., Phys. Rev. C 56 (1997) 20
[4] V. Herrmann et al., Phys. Lett. B 251 (1990) 6
[5] B. v. Przewoski et al., Phys. Rev. C 45 (1992) 2001

Test of the One-Layer Barrel Detector for the COSY-TOF with Cosmic Rays [B,K]

B. Hübner[1], A. Böhm[1], K.-Th. Brinkmann[1], S. Dshemuchadse, J.S. Lange[1], H. Freiesleben[1], P. Michel, K. Möller, A. Schamlott, P. Schönmeier[1], M. Steinke[2] and M. Würschig-Pörsel[1] for the COSY-TOF collaboration

In the beginning of 1997 the first barrel for the COSY Time-of-Flight spectrometer TOF based on the one-layer barrel concept [1] [2] was assembled in Rossendorf and tested with cosmic rays. These experiments were carried out using the same electronics and data acquisition as in the COSY-TOF experiments in Jülich. The tests proved the functionality of all scintillator bars. The properties of the full detector set-up were as follows: The average light velocity in the scintillators was found to be 15 cm/ns with a variation of ± 0.5 cm/ns. The attenuation lengths of the bars were measured to be 2 to 5 m, where the variation is correlated with the transparency of the bar judged by optical inspection, i.e. the light attenuation in darker bars was higher than in bright ones. This effect is illustrated in Fig. 1. The ongoing analysis of the July 97 beamtime [3] will show if this affects the quality of the experimental data.

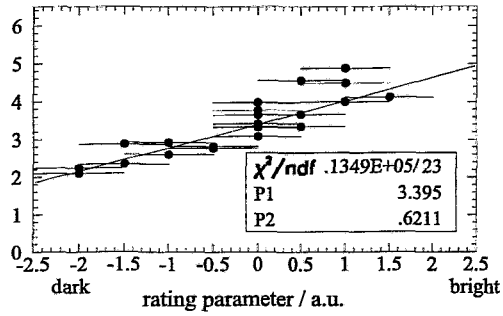

Fig. 1 *Correlation of the attenuation length and the optical appearance of the bar.*

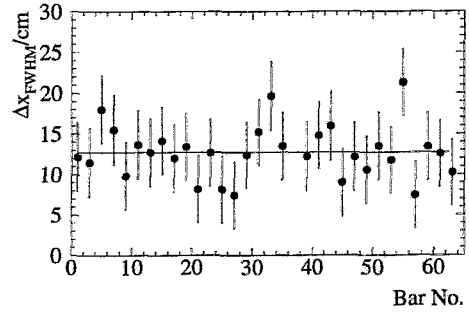

Fig. 2 *Position resolution for a set of 32 bars obtained from the edge steepness of the time difference spectrum.*

The average position resolution determined from the edge steepness of the time difference spectra is $\Delta x(FWHM) = 13$ cm. The individual resolutions for a set of 32 bars are shown in Fig. 2. In these experiments, walk effects due to the leading edge discriminators used could not be corrected. Since these effects are strongest at the edges of the time difference spectra, the resulting position resolution should be taken as an upper limit only. The time resolution obtained from the difference of the calculated and measured time of flight between two bars for cosmic particles, applying restrictive cuts on the QDC values in order to minimize walk effects, is $\Delta t(FWHM) = 1$ ns. Hence, the position resolution is $\Delta x(FWHM) = 7.5$ cm. These results are in good agreement with prototype tests using constant fraction discriminators [2]. In the experiments at COSY, the barrel will be equipped with a laser calibration system in order to correct for walk effects. Furthermore, we found that there is no cross talk between the bars. Double hits can be recognized by compairing the position information obtained from the time difference ($x_{TDC} \propto TDC_{rear} - TDC_{front}$) to the position calculated independently from the ratio of the QDC values ($x_{QDC} \propto \ln(QDC_{rear}/QDC_{front})$).

[1] *Institut für Kern- und Teilchenphysik, TU Dresden* [2] *Institut für Experimentalphysik, RU Bochum*

References

[1] K.-Th. Brinkmann et al., Review: "The barrel scintillator hodoscope for the COSY-TOF spectrometer" RU Bochum, TU Dresden, FZ Rossendorf.
[2] S. Dshemuchadse et al., Annual Report 1996, IKP, Jül-3365, p. 17
[3] G.Y. Sun et al., this report

First Results of the One-Layer COSY-TOF Barrel Hodoscope [B,K]

G.Y. Sun[1], K.-Th. Brinkmann[1], H. Freiesleben[1], B. Hübner[1], S. Dshemuchadse, P. Michel, K. Möller and A. Schamlott for the COSY-TOF collaboration

The one-layer COSY-TOF barrel was built in Rossendorf in 1996 [1]. After the first tests with cosmic rays, it was dismantled and moved to COSY, where it was mounted and utilized for the first time in the July-97 beamtime. The calibration of the barrel hodoscope was performed using elastic pp scattering data from this experiment at beam energies around 300 MeV. The pp elastic scattering events were identified by requiring two coplanar hits in the barrel and two coplanar hits in the outer ring of the start detector [2] with the same azimutal angle as the hits in the barrel and putting additional cuts on the hit positions of the two correlated elastic events in opposite scintillator bars. The yield obtained in this way for the first 48 bars is shown in Fig. 1. Apart from some cases where problems with individual electronic channels exist a rather constant value is observed as is expected from the cylindrically symmetric setup.

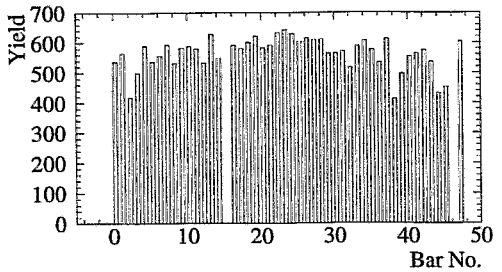

Fig. 1 *Yield of the pp elastic scattering events in the first 48 scintillator bars.*

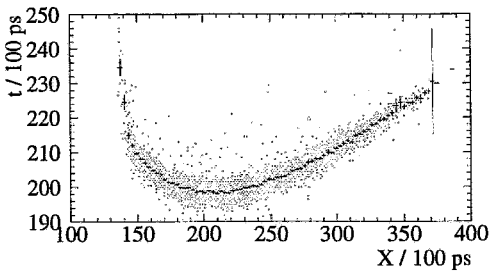

Fig. 2 *Position dependence of tof for one of the scintillator bars.*

Fig. 2 shows an example of the position dependence of time of flight (tof) of elastic scattering events to one of the bars. The displayed time, t, is related to tof through an offset. The time difference $X = TDC_{front} - TDC_{rear}$ is a direct measure of the hit position.

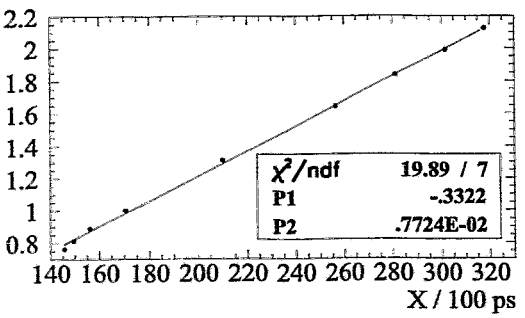

Fig. 3 *Position calibration for one of the scintillator bars.*

By comparing the tof determined by kinematics with experimental data we obtain the offset of tof. Setting certain cuts on tof we get the X values from experimental data and the position values from kinematics. Hence the hit position in scintillator bars can be calibrated with pp elastic scattering events as shown in Fig. 3. The slope of the fitted line is a measure of the effective speed of light (c_{sz}) in the scintillator. We get $c_{sz} = 15.5$ cm/ns which is consistent with the result obtained in the cosmic-ray tests [3].

[1] *Institut für Kern- und Teilchenphysik, TU Dresden*

References

[1] S. Dshemuchadse et al., "Set-up of the one-layer COSY-TOF Barrel Hodoscope", Annual report 1996, Forschungszentrum Jülich

[2] P. Michel et al., "MARS: A start detector system for the COSY-TOF spectrometer", accepted for publication in Nuclear Instruments and Methods

[3] B. Hübner et al., "Test of the One-Layer Detector for the COSY-TOF with Cosmics", this Annual report

Comparision of Measured (p,2p) COSY-TOF Data with Simulated INC- and MICRES-Code Events at the Pion Threshold [B,K]

B. NAUMANN, L. NAUMANN, P. HERRMANN[1], U. ZIELINSKI[1] AND THE COSY-TOF-COLLABORATION

Data of proton induced two prong events from reactions on nuclei of the target foil material (mainly carbon and oxygen) were taken in 1996 at the COSY run on pp-bremsstrahlung with the COSY-TOF spectrometer [1]. The proton momentum was chosen as 797 MeV/c, thus, the pion production channels $pp \rightarrow d\pi^+$ and $pp \rightarrow pp\pi^0$ were accessible. The COSY-TOF spectrometer has been described previously [2]. The spectrometer detects the trajectory, time of flight and energy loss of each charged particle. The angular acceptance covering the scattering angle in the range of $3° \leq \theta_{lab} \leq 33°$ and the azimuthal range of 2π. About 10^4 two prong events from the "empty target" were accumulated in a missing mass spectrum under the proton pair hypothesis. About 10^7 events were simulated with the INC-code [3] and the MICRES-code [4]. The figure illustrates the comparison of the experimental data with the INC-code simulation (a) and the MICRES-code simulation (b) as a function of squared missing mass.

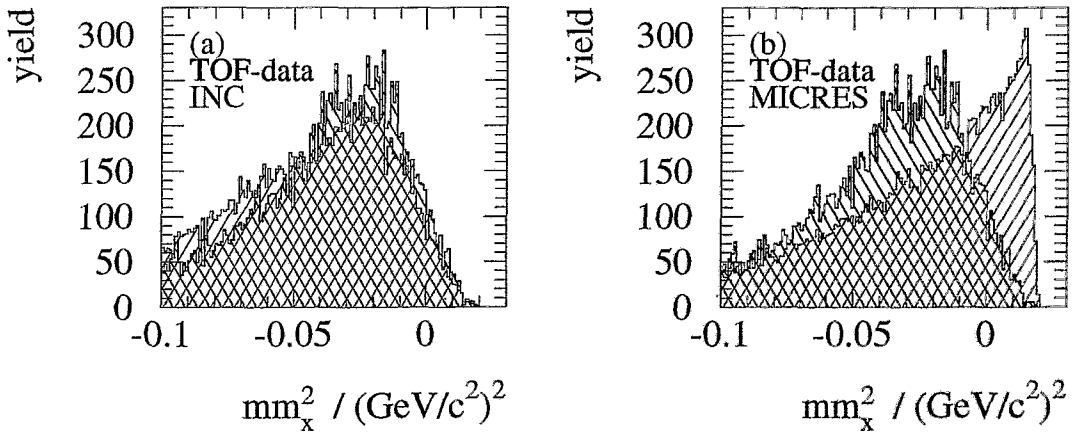

Fig. 1 *Comparision of simulated and measured proton nucleus reaction as a function of the missing mass squared.*

The geometrical acceptance of the spectrometer and the β-determination with an error of 5 % are taken into account. The spectra are normalized to the integrals of the shapes. The comparison shows, that our data are in better agreement with the INC-model than with MICRES. The reason may be, that in the MICRES-code the emitted nucleons are kinematically uncorrelated after passing through the scattering cascade. New data for proton scattering on carbon were measured with the COSY-TOF spectrometer in 1997 at the same beam momentum. The target [5] was filled with liquid methan to obtain a significantly higher luminosity. The data are under preparation.

[1] *Institut für Experimentalphysik I, Ruhr-Universität Bochum*

References

[1] P. Hermanowski et al., Annual Report 1996, FZR-179 (1997) 33
[2] U. Bechstedt et al., Annual Report 1995, Jül-3200 (1996) 5
[3] W. Bertini, Phys. Rev. V.188, N.4 (1969) 1711
[4] D. Theis, Ph. D. thesis, ISKP Bonn (1992)
[5] V. Jaeckle et al., Nucl. Instr. and Meth. A 349 (1994) 15

The Large Multiwire Chamber MWC2 for the ANKE Spectrometer [B]

Ch. Schneider, M. Freitag, J. Hutsch, T. Kirchner[1], M. Sobiella

In the side detector of the ANKE spectrometer a particle track will be measured by two multiwire chambers. The smaller MWC1 is placed near the dipole magnet D2 and is well tested [1]. The larger chamber MWC2 is located between MWC1 and the stop telescopes. The production of MWC2 has been finished and the operation behavior can now be compared to that of MWC1. The large size (2160x900 mm) of MWC2 leads to differences in the parameters and production in respect to MWC1. The tension of the longer sensitive anode wires of MWC2 must be higher to withstand the electrostatic forces in the chamber and keep them inside a spatial deviation of $\sim 2\%$. In MWC1 tungsten wires with ø 20 μm had been used with a force of 0.5 N. This results in a tension near the limit of the linear elastic response behavior of tungsten. Therefore it was necessary to use for MWC2 a wire diameter of 25 μm to achieve a force of 0.8 N.

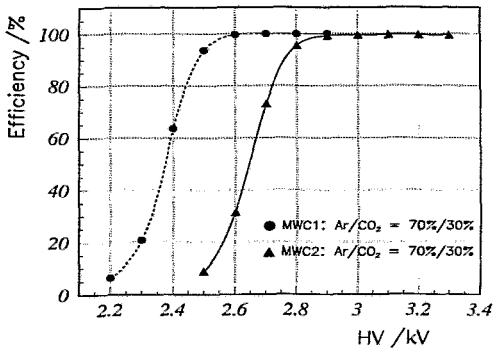

Fig. 1 *Efficiency curves of MWC1 and MWC2.*

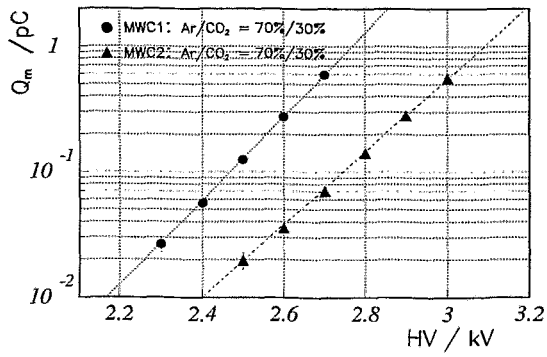

Fig. 2 *Mean charge of signals Q_m from MWC1 and MWC2 as a function of high voltage HV.*

In a multiwire chamber the multiplication factor M between the primary charge and the final charge collected at a wire depends on the capacity C and the high voltage HV besides the parameters of the gas. In a multiwire arrangement C can be approximated by $2\pi\epsilon_0/(\pi L/s - ln(2\pi r_w/s))$; here L is the gap between anode and cathode, s the distance between the wires and r_w the radius of a wire. Since $r_w \ll L, s$ the capacity C decreases with increasing r_w. As a consequence the multiplication factor M in MWC2 is smaller than in MWC1 at the same HV. Using the same amplifier threshold the efficiency in MWC2 will be smaller too.

This behavior can be seen in the two measured efficiency curves of MWC1 and MWC2 in fig. 1. The efficiency curve of MWC2 is shifted by about 250 V to higher voltage. The length of the plateau of MWC2 is about 400 V and seems to be slightly longer than the plateau of MWC1. This can be seen from the curves for the mean charge Q_m of the signals as a function of HV, see fig. 2. Both curves show the expected exponential law of the proportional operation mode very well what indicates a normal chamber behavior. Due to the thicker wire of MWC2 a smoother rise of the curve for MWC2 exists. The endpoint of operation will therefore be reached at a somewhat higher voltage. For both chambers the results are inside the expected range so one can assume also for MWC2 a normal operation at the ANKE spectrometer.

[1] *now: Subatech, University of Nantes, France*

References

[1] Ch. Schneider. "Untersuchung der Subschwellenerzeugung von Kaonen am COSY-ANKE-Spektrometer", Ph.D. thesis, Technischen Universität Dresden (1997)

Search for Virtual Δ^{++} Knock-out from ^9Be at 1 GeV [W]

L.N. Andronenko[1], M.N. Andronenko[1], Yu.I. Gusev[1], A.A. Kotov[1], W. Neubert, D.M. Seliverstov[1], I.I. Strakovski[1], L.A. Vaishnene[1], Yu.I. Zalite[1]

The existence of nucleon resonances in the ground state of nuclei is a long-standing problem. A method for the observation of one signature in the $pA \to p\Delta^{++}X$ reaction was described in ref. [1]. In the special case of ^9Be the detection of the recoil nucleus ^8He ($\Delta A = -1, \Delta Z = -2$ with respect to the target) allowed to eliminate all background from interactions of incident protons with single nucleons. Indeed, the expected enhancement of the cross section in the spectator (i.e. low- momentum) range was observed at $\Theta_{lab} = 60^o$ [1] but further measurements at lower momenta are desired. Our spectrometer based on Bragg Ionization Chambers [2] with low registration thresholds offers a feasible method. The detection of the low abundant ^8He requires in addition to the first level trigger (which selects fragments) a more restrictive condition. The Bragg peak height $BP \propto Z$ must match the limits of Z=2 and the condition $4 < A < 12$ must be fullfilled simultaneously. In this case the data transfer from the front-end electronics is started and the full pulse-shape information from the FADCs is written on disk. The data rates accepted by the first level trigger are scaled down what allows the simultaneous storage of the full information necessary to compare with the previous data in the overlap region. The comparison of the invariant cross sections (shown in fig. 1 for selected fragments) confirms the results of ref. [1]. The increasing enhancement of the cross section in the low momentum range due to the virtual Δ^{++} knock-out seems to be present (as shown in fig. 2) despite the large statistical uncertainties.

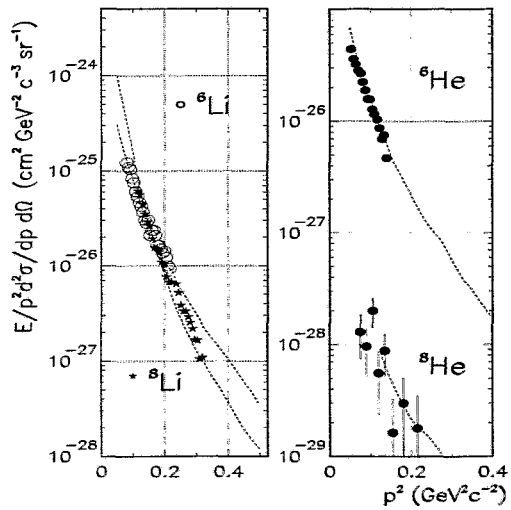

Fig. 1 *Differential cross sections vs. momentum square. Dashed lines: shapes obtained by a spline fit of data from ref. [1].*

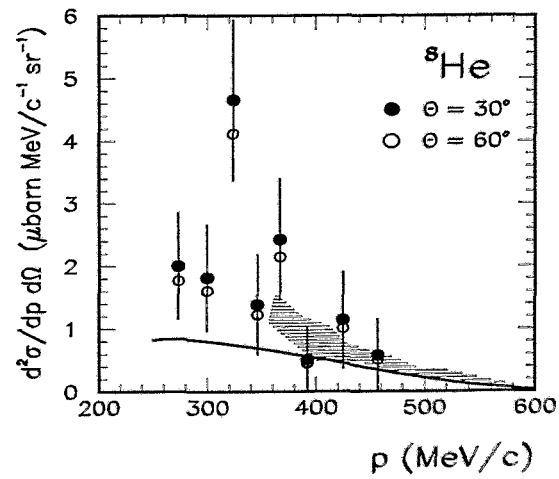

Fig. 2 *Differential cross section vs. momentum. Shadowed area: range of data from [1], open circles: present data extrapolated to 60° using the angular dependence of ^6He emission, ref. [3], solid line: expected shape without Δ^{++} contribution.*

[1] *St. Petersburg Nuclear Physics Institute, 188350 Gatchina,Russia*

References

[1] A.I. Amelin et al., Phys. Lett. B 337 (1994) 261
[2] L.N. Andronenko et al., Nucl. Instr. Meth. A 312 (1992) 467
[3] R.E.L. Green et al., Physics Auxiliary Publication Service PRVCA-35-1341-42

Calculation of ω Production in $p + d$ Interactions [B]

H. MÜLLER

There are plans [1] to study the reaction $p + n \rightarrow \omega + d$ at ANKE using a deuterium target and detecting the spectator proton in a similar way as in a recent experiment [2] at CELSIUS for the reaction $p + n \rightarrow \eta + d$. Since experimental data for ω production in $p + d$ interactions are not available, in Fig. 1 an order of magnitude estimate is given calculated with the ROC model [3]. These results may serve as a basis for estimating the counting rates which can be expected.

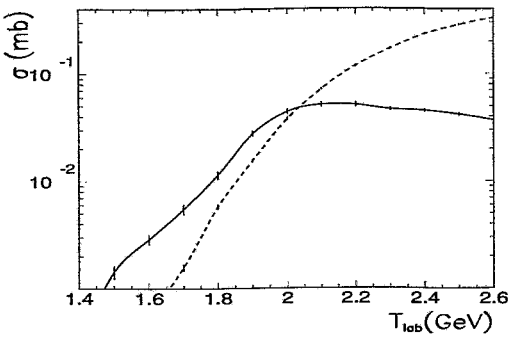

Fig. 1 *Calculated cross sections for the reactions $pd \rightarrow \omega pd$ (full line) and $pd \rightarrow \omega 2pn$ (dashed line). The vertical bars indicate the statistical uncertainties of the Monte-Carlo calculations.*

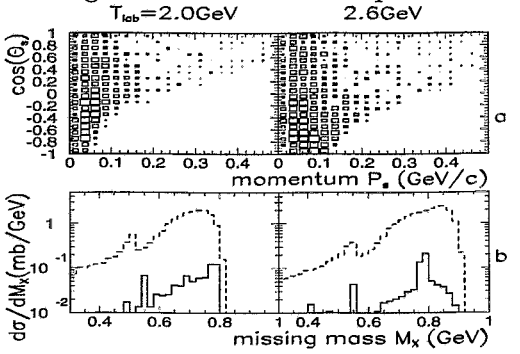

Fig. 2 *(a) Angle ($\cos(\Theta_s)$) versus momentum (P_s) of protons from the reaction $p+d \rightarrow p_s+\omega+d$ in coincidence with d at angles $\Theta_d \leq 5°$.*
(b) Missing mass spectrum for protons ($\Theta_s \geq 90°$, $0.05 \leq P_s \leq 0.2$ GeV/c) in coincidence with d at $\Theta_d \leq 5°$ and $P_d \geq 1$ GeV/c (full line).

At ANKE a detection system for high-momentum particles emitted under small angles will be installed [4]. It will be used for detecting the deuterons, while the design of the detector for the spectator protons is still under discussion. In Fig. 2a the distribution of these spectator protons from $p + d \rightarrow p_s + \omega + d$ is shown. As can be expected from the assumption of a quasi-free production process there is no pronounced correlation between the directions of the deuteron and the spectator proton except the kinematical constraints from the three-body phase-space. Due to the decrease of the $p+n$ center-of mass energy for backward going spectators ω production becomes impossible for high enough spectator momenta as can be seen in Fig. 2a. The momentum distribution within the allowed kinematical region decreases strongly at large momenta due to the deuteron wave function. In order to give an impression of the expected background from other reactions the missing-mass spectra are plotted in Fig. 2b under the idealized assumption that the spectator detector covers the whole backward hemisphere. At both energies the ω peak at 0.78 GeV is clearly distinguished from the background. The necessity of a good particle identification in the forward detector is demonstrated by the dashed curves in Fig. 2b, which represent the missing-mass spectra resulting from a misidentification of forward going p's as d's. This background is structure-less in the region of the ω peak and the amount of misidentified p's still tolerable will depend to a large extent from the achievable missing-mass resolution.

References

[1] L.A. Kondratyuk, C. Wilkin, private communication
[2] S. Häggström, Acta Universitatis Upsalensis,
Uppsala Dissertations from the Faculty of Science and Technology 13 (1997)
[3] H. Müller, Z. Phys. A 355, 223 (1996)
[4] V.I. Komarov et al., COSY Proposal 18, FZ Jülich (1992)

Elastic Proton-Deuteron Backward Scattering [B]

L.P. KAPTARI[1], B. KÄMPFER, S.M. DORKIN[2], S.S. SEMIKH[1]

In recent studies [1, 2] the static properties of the deuteron and the exclusive deuteron break-up reaction have been calculated within the Bethe-Salpeter (BS) approach. We have extended our BS approach to the elastic proton-deuteron backward scattering [3]. Precision measurements of this reaction are envisaged in near future at COSY with the ANKE and TOF installations. Some results of our approach are compared with older data in Figs. 1 and 2. A set of polarization observables is provided in [3].

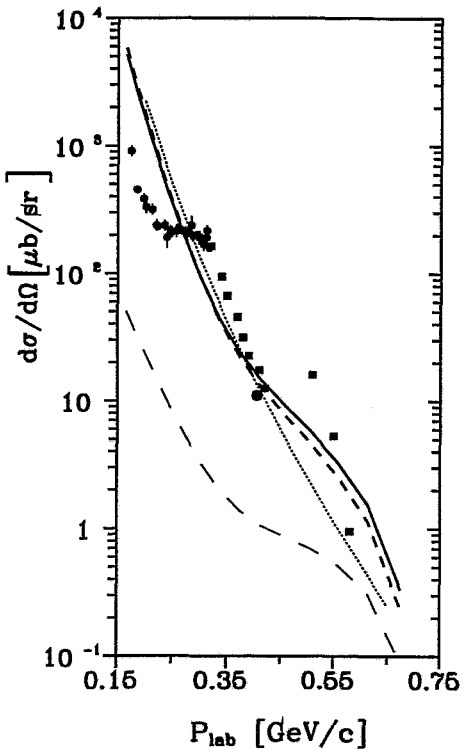

Fig. 1 *The spin averaged differential cross section as a function of the proton momentum. Dashed curve: positive energy contributions, long-dashed curve: contributions from Lorentz boost, full curve: BS calculation, dotted curve: non-relativistic calculations with Bonn potential. For details and quotation of data cf. [3].*

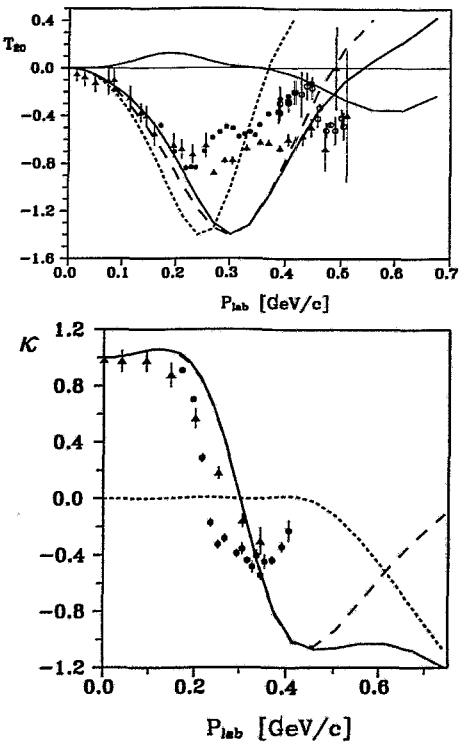

Fig. 2 *Tensor analyzing power T_{20} (upper panel), and polarization transfer κ (lower panel). Dotted curve: purely relativistic corrections, short-dashed curves: calculations with minimal relativization scheme and Paris potential, full curves: the net result within the BS approach. For more details and quotation of data cf. [3].*

[1] *Bogoliubov Institute of Theoretical Physics, JINR Dubna, Russia*
[2] *Far-Eastern State University, Vladivostok, Russia*

References

[1] L.P. Kaptari, A.Yu. Umnikov, S.G. Bondarenko, K.Yu. Kazakov, F.C. Khanna, B. Kämpfer, Phys. Rev. C 54 (1996) 986
[2] L.P. Kaptari, B. Kämpfer, S.M. Dorkin, S.S. Semikh, Phys. Lett. B 404 (1997) 8
[3] L.P. Kaptari, B. Kämpfer, S.M. Dorkin, S.S. Semikh, FZR-194 (1997), Phys. Rev. C in print

Polarization Observables in the Reaction $NN \to NN\phi$ [B]

A.I. TITOV[1], B. KÄMPFER, V.V. SHKLYAR[1]

The reaction $NN \to NN\phi$ is calculated [1] within the one-boson exchange model. In the tree level Feynman diagrams the ϕ arises from the internal conversion vertex $\rho\pi\phi$. The parameters (effective coupling constants, cut-offs in monopole formfactors) can be partially adjusted by the reaction $\pi^- p \to n\phi$. The corresponding total exclusive cross section as a function of the beam energy (cf. Fig. 1) describes the few experimental data [2,3] near threshold fairly well.
Presently there is a wide discussion on the apparent violation of the OZI rule in the reaction $\bar{p}p \to \phi X$. One possible resolution of this puzzle is the assumption of a substantial hidden strangeness (i.e. $s\bar{s}$) content in the proton. As test of this hypothesis we have calculated the sensitivity of polarization observables on the $s\bar{s}$ admixture in the proton in $pp \to pp\phi$ reactions [1]. In doing so the one-boson exchange model is supplemented by a *uud* knock-out mechanism. Results for the beam-target asymmetry $C_{zz}^{BT} = [d\sigma(S_i = 1) - d\sigma(S_i = 0)]/[d\sigma(S_i = 1) + d\sigma(S_i = 0)]$ (here S_i denotes the total spin in the entrance channel) are displayed in Fig. 2. It should be stressed that already slightly above the threshold the interaction dynamics becomes important. While the total cross section is hardly sensitive to a small admixture of hidden strangeness, the polarization observables do so.

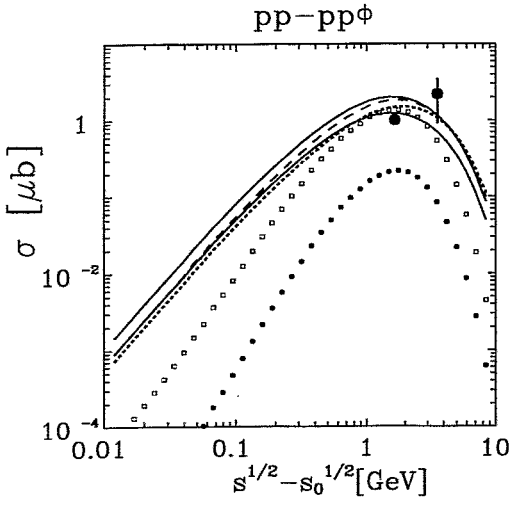

Fig. 1 *The total cross section for the reaction $pp \to pp\phi$ as a function of center-of-mass energy above threshold. The solid lines and the short-dashed line are for various parameter sets described in [1]; dashed line: result of a calculation with constant near-threshold matrix element. Open squares and full dots: the contributions of the uud knock-out channel for two different parameter sets with a strangeness weight of 1%. Data from [3].*

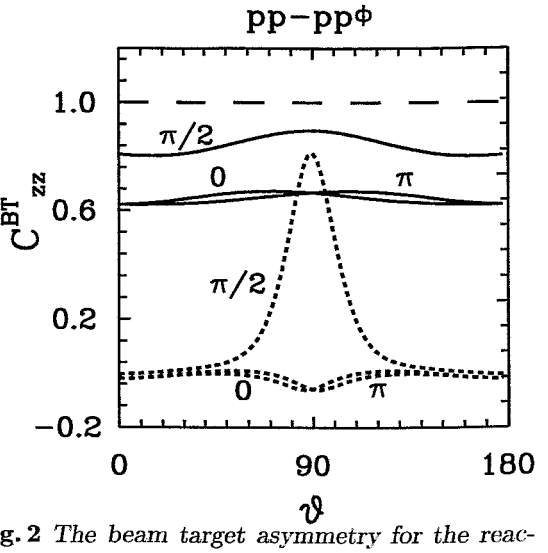

Fig. 2 *The beam target asymmetry for the reaction $pp \to pp\phi$ as a function of the center-of-mass polar angle ϑ of the ϕ for a beam energy of 100 MeV above threshold. Long-dashed line: threshold result, solid lines: contributions of the conventional one-boson exchange model, dotted lines: contribution of the uud knock-out channel; the curves are labelled by the polar angles of the recoil proton. The assumed strangeness weight is 2%.*

[1] *Bogoliubov Institute of Theoretical Physics, JINR Dubna, Russia*

References

[1] A.I. Titov, B. Kämpfer, V.V. Shklyar, FZR-202 (1997)
[2] A. Brenschede, Ph.D. thesis, Uni Giessen (1997), DISTO collaboration, to be published
[3] R. Baldi et al., Phys. Lett. B 68 (1977) 381

Large Trapezoidal Drift Chambers for the HADES Experiment [B]

F. Dohrmann, W. Enghardt, E. Grosse, M. Sobiella and the HADES-Collaboration

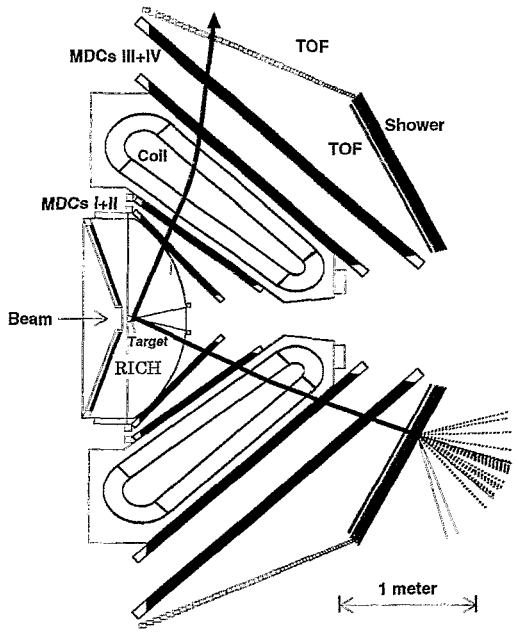

Fig. 1 *Cross section through the HADES spectrometer.*

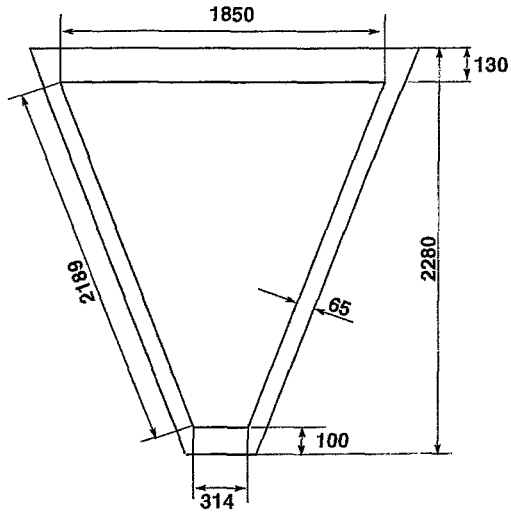

Fig. 2 *Schematic view of a MDC-III frame.*

HADES is a high acceptance di–electron spectrometer to be set up at GSI, Darmstadt, for measuring lepton pairs produced in heavy ion and hadron induced reactions. HADES investigates in-medium properties of vector mesons like ρ, ω, and ϕ. Model calculations [1,2] and QCD sum rules [3] predict mass shifts of particles inside nuclear matter.

The short lived ρ meson (lifetime $\sim$ 1fm/c), if produced in Au–Au collisions at $1-2$ AGeV, mainly decays inside the dense reaction medium (2–3 times the normal nuclear density ρ_0). Furthermore, in reactions such as π^- Pb, a significant fraction of ω mesons, being a narrower resonance (lifetime 23.5 fm/c), are produced at low momentum and thus would also decay inside the nucleus.

The spectrometer is depicted in fig. 1. It consists of a fast, hadron blind Ring Imaging Cherenkov counter (RICH), a set of four tracking planes of Multi Wire Drift Chambers (MDC), a six coil superconducting magnet, a set of shower detectors and a Time of Flight (TOF). The spectrometer covers about 40% of the azimuthal angle ($18^\circ \leq \theta \leq 85^\circ$).

The FZ Rossendorf currently participates in constructing and testing of the low-mass drift chambers. The second largest tracking plane (MDC III) is constructed at the detector laboratory of the institute. 6 modules (active area: $2.3\times2\,\mathrm{m}^2$, drift cell size $8\times12\,\mathrm{mm}^2$) form the entire plane. Each module contains 6 drift cell layers, i.e. 6 anode and 7 cathode frames. New technologies for winding and fixing thin aluminum wire (80 μm diam.) and handling thin large frames made of fiber reinforced epoxy resins are developed. For handling the shear size of the frames, fig. 2, a new larger clean room and specially shaped tables and containers have been installed.

References

[1] S. Klimt et al. Phys. Lett. B 249 (1990) 386
[2] G.E. Brown and M. Rho, Phys. Rev. Lett. 66 (1991), 2720
[3] T. Hatsuda and H.S. Lee, Phys. Rev. C 46 (1992) R34

Estimates of Dilepton Yields from Correlated Semi-Leptonic Decays of Open Charm and Bottom Mesons in Relativistic Heavy-Ion Collisions [B]

K. GALLMEISTER, B. KÄMPFER, O.P. PAVLENKO[1]

The dileptons, stemming from correlated semi-leptonic decays of open charm and bottom mesons in central ultra-relativistic heavy-ion collisions, represent a huge background to the dilepton signal from thermalized deconfined matter. In Fig. 1 we show the invariant mass spectra of these contributions at RHIC energies; the designed acceptance of the PHENIX detector system is taken into account. As pointed out by Shuryak in 1997 the energy loss of heavy quarks, due to gluon radiation propagating through deconfined matter. can diminish substantially their relative kinetic energy, and as a consequence the invariant mass of the resulting dileptons is reduced too. We have modelled such energy loss effect in various scenarios described in detail in [1]. Even using a comparatively strong energy loss it becomes evident from Fig. 1 that the thermal signal can hardly be extracted from the full spectrum.

We have therefore revived a previous study [2] of the transverse momentum dependence of thermal dileptons and compared with results of Monte Carlo calculations of the background from charm and bottom decays. In Fig. 2 the corresponding spectra for LHC energies are displayed. The acceptance of the ALICE detector system is taken into account, and only leptons with transverse momenta $p_\perp > 2$ GeV are considered. One can infer that suitable kinematical cuts in the double differential spectrum suppress sufficiently the background, and in a certain window the thermal signal dominates. Other contributions to the background, like dileptons from Dalitz decays of π^0 and η, contribute only at the kinematic limit of large values of the transverse pair momentum. Whether the proposed strategy of extracting the thermal signal is experimentally feasible depends on the possibility to subtract the combinatorical background.

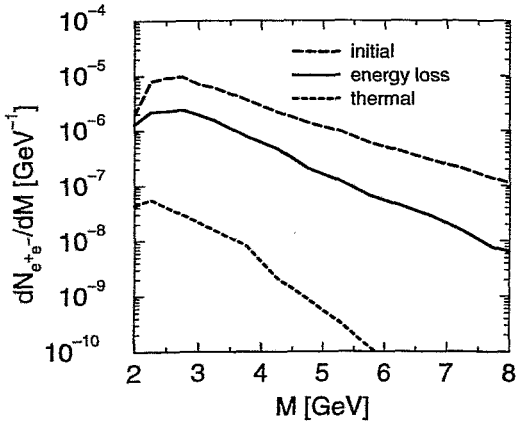

Fig. 1 *Various contributions to the invariant mass spectrum of dielectrons at RHIC energies observable in the PHENIX acceptance. The dashed (solid) line is the sum of charm and bottom contributions without (with) energy loss.*

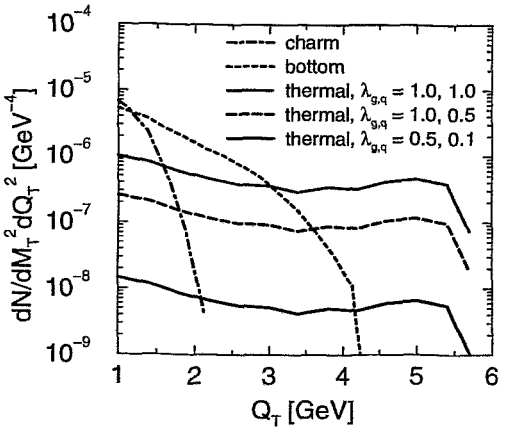

Fig. 2 *Contributions to the transverse momentum spectrum of dileptons which occupy the transverse mass region $M_\perp$ = 5.25 - 5.75 GeV at LHC energies observable in the ALICE acceptance. The thermal yield is depicted for various quark/gluon fugacities $\lambda_{g,q}$ [2].*

[1] *Institute for Theoretical Physics, Kiev, Ukraine*

References

[1] B. Kämpfer, O.P. Pavlenko, K. Gallmeister, FZR-188 (1997), Phys. Lett. B in print
[2] B. Kämpfer, O.P. Pavlenko, A. Peshier, G. Soff, Phys. Rev. C 52 (1995) 2704

Iso-Rotational Moment of Inertia and Δ-Nucleon Mass Splitting at Finite Temperature and Density [B]

M. SCHLEIF AND R. WÜNSCH

To study nucleonic properties in nuclear matter we consider the chiral one-loop hedgehog soliton of the bosonized $SU(2)_f$ Nambu & Jona-Lasinio model which is embedded in a hot gas of constituent quarks with a dynamically generated mass [1,2]. Such a model incorporates the restoration of chiral symmetry and the possible dissolution of the soliton, which simulates the deconfinement transition of hadronic matter.

Due to the hedgehog ansatz the soliton violates rotational and iso-rotational invariance. Instead of a particle with definite spin and isospin the soliton represents a mixture of nucleon and Δ isobar. The quasi-classical cranking approach [3] constitutes a feasible way to restore the symmetry and to equip the soliton with the correct values of spin and isospin. The resulting Δ-nucleon mass splitting $\Delta E_{\Delta N} = \frac{3}{2\mathcal{J}}$ is controlled by the iso-rotational moment of inertia $\mathcal{J}$. Fig. 1 illustrates the moment of inertia as a function of medium temperature and density [2]. At vanishing density, the moment is nearly independent of temperature and remarkably increases only in the neighborhood of the critical temperature at 185 MeV. At finite medium density, the increase starts earlier. The larger moment at higher temperature leads to a smaller mass difference between nucleon and Δ isobar (lower part of Fig. 1). Notice that the lines end at the critical temperature with a finite mass splitting.

The behavior at finite density and low temperature is affected by our naive representation of the medium as a gas of constituent quarks. The Pauli-blocking of quark levels in the neighborhood of the valence level reduces the moment of inertia remarkably and leads to a large mass splitting. In a more realistic picture, the medium quarks should be bound in solitons and the corresponding transition matrix elements are not blocked to that degree.

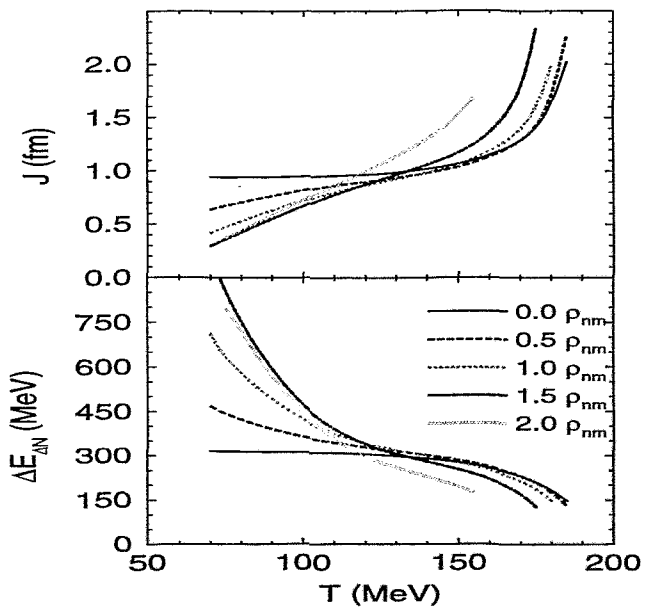

Fig. 1 *Moment of inertia $\mathcal{J}$ (upper part) and Δ-nucleon mass splitting $\Delta E_{\Delta N}$ (lower part) as a function of the medium temperature T for various values of the density (in units of the normal nuclear density $\rho_{\rm nm} = 0.16\,{\rm fm}^{-3}$) using a constituent quark mass $M = 420\,{\rm MeV}$ in vacuum.*

References

[1] J. Berger and C.V. Christov, Nucl. Phys. A 609 (1996) 537
[2] M. Schleif and R. Wünsch, Eur. Phys. J. A 2 (1998) in press; FZR-182 (1997)
[3] P. Ring and P. Schuck, The Nuclear Many-Body Problem, Springer Verlag, New York, 1980

Quasiparticle Model for the Equation of State of Deconfined Matter with Strange Quarks [B]

A. Peshier, B. Kämpfer, O.P. Pavlenko[1], G. Soff[2]

Recently a quasiparticle model has been proposed [1] to describe the lattice results [2] for pure SU(3) gauge field thermodynamics. The model is based on a parametrization of the strong interaction by massive gluon excitations with temperature dependent effective mass $m_g^2 \propto G^2(T)\,T^2$. The appropriately parametrized coupling constant G is adjusted to the data [2]. In the high-temperature limit $T \to \infty$ the coupling strength G approaches the one-loop QCD running coupling constant. In this spirit our model incorporates the asymptotic limit of QCD, and the pressure described below coincides with the leading-order QCD result.

We have extended [3] the model to describe the lattice data [4] of a quark-gluon plasma with four quark flavors in the chiral limit, cf. Fig. 1. We proceeded to include also strange quarks with finite rest mass. This modifies the equation of state as seen in Fig. 2.

A foundation of our model can be derived [5], in case of the ϕ^4 model theory, from the Luttinger-Ward selfconsistency relation between thermodynamical potential, propagators and selfenergies. It turns out that in the tadpole approximation the pressure reads like an ideal gas of particles which acquire a thermal mass due to interactions plus a small correction term.

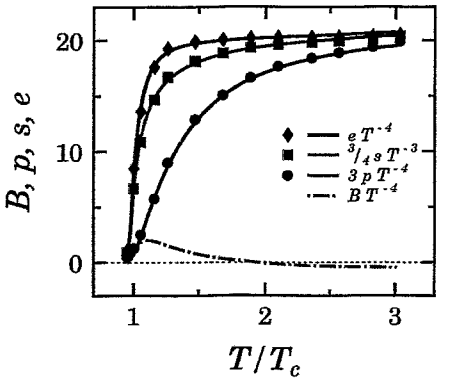

Fig. 1 *Description of the 4-flavor lattice QCD data [2] (symbols) by our model [1], which rests on the entropy density $s = s_{\rm id}(T, m(T))$, energy density $e = e_{\rm id}(T, m(T)) + B(T)$, pressure $p = p_{\rm id}(T, m(T)) - B(T)$, with a temperature dependent quasi-particle masses $m(T)$. The subscript "id" means the corresponding ideal gas expressions; the function $B(T)$ follows from thermodynamical selfconsistency.*

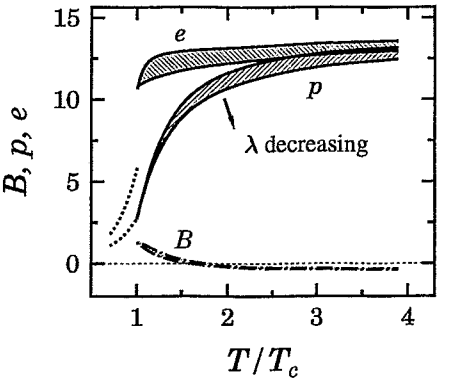

Fig. 2 *Our prediction of the equation of state (scaled by T^4) of interacting gluons, light u, d quarks and massive strange quarks. The quasiparticle model is adjusted to a constructed 1st-order phase transition to a resonance gas at T_c (dotted lines). The temperature dependent strange quark mass becomes here $m_s(T) \to m_s/2 + (m_s^2/2 + m(T)^2)^{1/2}$ according to the hard thermal loop results. λ is an internal model parameter.*

[1] *Institute for Theoretical Physics, Kiev, Ukraine*
[2] *Institut für Theoretische Physik, TU Dresden*

References

[1] A. Peshier, B. Kämpfer, O.P. Pavlenko, G. Soff, Phys. Rev. D 54 (1996) 2399
[2] G. Boyd et al., Phys. Rev. Lett. 75 (1995) 4169
[3] B. Kämpfer, O.P. Pavlenko, A. Peshier, M. Hentschel, G. Soff, J. Phys. G 23 (1997) 2001
[4] J. Engels et al., Phys. Lett. B 396 (1997) 210
[5] A. Peshier, Ph.D. thesis, TU Dresden (1998)

Nuclear Physics

In the nuclear structure theory group the disappearance of the pair correlations in rotating nuclei and mesoscopic aluminium particles in a magnetic field has been studied. Instead of the well defined phase transition from the superconducting (suprafluid) to the normal state seen in a macroscopic system there is in the considered mesoscopic systems a transition region where the gap parameter approaches zero in steps caused by subsequently breaking pairs. Surprisingly and contrary to the commonly accepted view, rapidly rotating nuclei when approaching the unpaired state do not rotate with the moment of inertia of a macroscopic rigid body. These deviations are the nuclear pendant to the normal persistent currents found in magnetic response of mesoscopic metal particles. They dramatically modify the transition super to normal.
Further, the T=1 proton - neutron pair correlations in N=Z nuclei have been investigated, which lead to a spontaneous breaking of the isospin symmetry with observable consequences for the rotational spectra of odd-odd nuclei.

The phenomenon of the magnetic rotation has been discovered by a Bonn-Rossendorf collaboration in a series of lead isotopes. According to the theoretical predictions this new excitation mode should exist in other mass regions too. The experimental work of the nuclear spectroscopy group has focussed to the search for magnetic rotation in nuclei in the mass region around A=80. For this purpose, the nuclides $^{82,83,84}Rb$ have been investigated in an experiment at LNL Legnaro using the 4π spectrometer GASP. Magnetic dipole bands have been found in all these nuclei. Indeed the bands in $^{82,84}Rb$ show the characteristics of magnetic rotation and are the first evidence of this rotational mode in odd-odd nuclei in this mass region. The study of the nuclide ^{79}Br has been refined by the analysis of level lifetimes which support the interpretation of the observed magnetic dipole band as an intermediate case including a strong magnetic component and electric rotation as well.
Another effort concerned the vibrational modes in magic nuclei with N=50 where the investigation has been extended to the nuclide ^{88}Sr. In a nuclear resonance fluorescence experiment at the electron accelerator S-DALINAC of the TU Darmstadt photons scattered on ^{88}Sr were measured with two CLUSTER detectors. Excited states identified in this experiment have been compared with predictions of the quasiparticle-phonon model which suggest an interpretation as two- or three-phonon excitations.

The FOBOS group completed a series of measurements at the U-400 M synchrotron in Dubna which was devoted to binary and ternary fission of hot nuclei. Thus, the reactions $^{40}Ar(36\ MeV)$ + nat. Ag, ^{232}Th and ^{248}Cm have been investigated. In these experiments the FOBOS gasball, scintillator shell and forward array were operated together for the first time. Furthermore, a spontaneous fission measurement for ^{248}Cm was performed. The extensive work concerning the data analysis has been continued providing the following new results:
Together with older results the new $^{248}Cm(sf)$ data allowed a comparative analysis of the influence of the two-Sn mode in the cold fission of Cm and Cf isotopes.
The unexpectedly small fragment mass dispersion measured at FOBOS in the fission of excited nuclei near Th found a quantitative interpretation both in the frame of a phenological model and also within a new three-dimensional version of the combined dynamical-statistical model of fission developed by a collaborating group in Omsk, Russia.
At excitation energies above 250 MeV evidence was found for a new mechanism of fast fission which cannot be explained in the frame of existing fast fission scenarios. The Omsk model is being refined to understand these findings.

The analysis of ternary events was continued by comparing the results of trajectory calculation with FOBOS data.

Striking differences were found in light charged particle data recorded in coincidence either with single heavy residues or with fragments from binary or ternary fission. The final state of a decaying hot heavy nucleus is strongly influenced by fluctuations in the early evaporation cascade.

Properties of heated nuclear matter can best be studied via fragment production at not too high excitation energies. For this aim experiments carried out within the FOPI collaboration and at the Gatschina synchrotron were analysed. The degree of thermal and chemical equilibrium was tested by comparing isotope yields to the results of thermal models. Deviations from the complete equilibrium established for fast fragments signal the presence of preequilibrium emission. Further, model calculations have shown that the enhanced ^{3}He yield can be understood by a late fragment formation due to coalescence.

Rotation of Nuclei in the Unpaired State [W]

S.Frauendorf, J. Sheikh[1], P.M. Walker[1], V. V. Pashkevich[2], A. Unzhakova[2], and F. Chu[3], M. A. Deleplanque[3]

Experiments with modern γ - ray detector arrays permit to study the rotation of nuclei after the transition from the suprafluid to the normal state. Fig. 1 shows as an example high K bands in the mass 180 region. A clear signal of the disappearance of pairing is the absence of rapid alignment processes [1]. Fig. 1 containing unpaired bands does not show such alignments which are seen in Fig. 2 as upbends of the K=7 and 15 bands. For the latter two quasi neutron bands the neutron pairing is still present. Tilted Axis Cranking (TAC) calculations reproduce very well the experimental angular momenta. The moments of inertia of the unpaired bands are substantially smaller than the values for rigid rotation indicating the presence of mass currents of quantal origin in the body fixed frame of reference. A systematic comparison of the calculated moments of inertia with the experimental ones known at high spin reveals that they are larger than the rigid body value in the lower part of a shell but smaller than it for most of the remaining part. The interpretation in terms of mesoscopic persistent currents is being worked out. The relation to quantum size effects in the magnetic susceptibility of quantum dots and metallic clusters is being studied

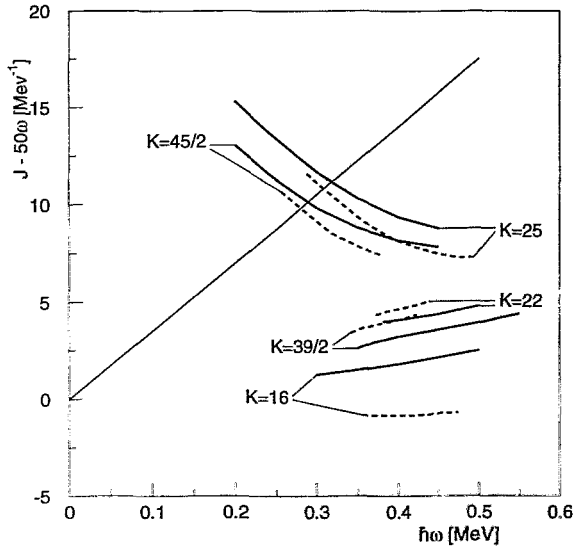

Fig. 1 *Angular momenta for high K bands in $^{178,179}W$ and ^{178}Hf (K=16). Full lines: TAC calculations assuming zero pairing. Dashed lines: Experiment. Straight line: The limit of strong coupling and rigid rotation. A constant rotor term of $50MeV^{-1}\hbar\omega$ is subtracted from all angular momentum.*

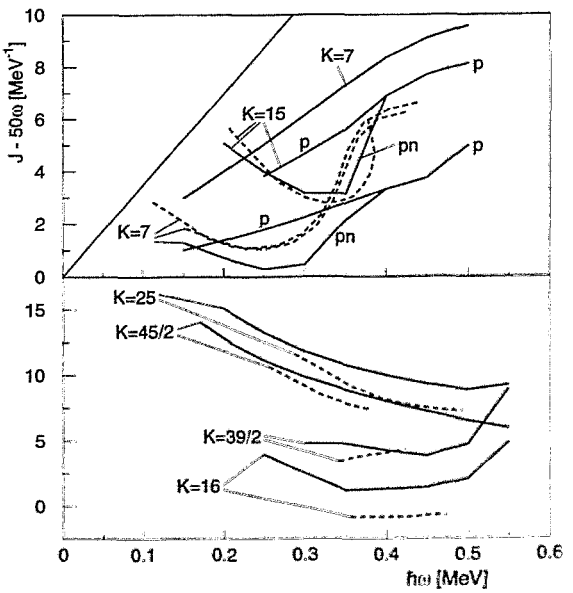

Fig. 2 *Same as fig. 1. In addition results with finite pairing are shown. The different cases are distinguished by letters, pp : proton pairing, nn: neutron pairing, no label: zero pairing. Lower panel: Results from the Lipkin - Nogami treatment of pairing. Full drawn lines: TAC calculations. Dashed: experiment.*

[1] *Department of Physics, University of Surrey, UK* [2] *LTP JINR, Dubna, Russian Federation*
[3] *Nuclear Science Division, Lawrence Berkeley National Laboratory, USA*

References

[1] S. Frauendorf. Nucl. Phys. 409 (1983) 243c

N-dependence Effective Pairing Strength in Al-grains and Phase Transition in Superconducting Grains [W]

S.FRAUENDORF, N.K. KUZMENKO [1] AND V.M. MIKHAJLOV[1]

The size dependence of the effective electron attraction strength (G) in Al nanometer-scale clusters is established on the basis of empirical critical temperatures (T_c) and pairing gaps (Δ). A substantial increase of NG, which is constant for bulk superconductors, is found. The model of electrons in a spherical cavity is studied. It permits to solve the pairing problem exactly and to calculate the canonical partition function. Calculations of T_c, Δ and specific heats are performed with in both grand canonical and canonical approaches. As compared to the bulk (BCS limit) the transition becomes smeared out. Still a transition temperature may be defined which coincides with the bulk value. This definition turns out to be reasonable, because it designs the region of the most dramatic changes of many physical quantities. The electronic magnetic susceptibility is strongly reduced by the pair correlations. Still it is positive (paramagnetic) for most of the cases. The paramagnetic enhancement is a finite size effect that is in sharp contrast to the bulk superconductor which has a negative susceptibility (diamagnetic). The value of the susceptibility is strongly affected at $N \simeq 10^3$ by N-dependence of G.

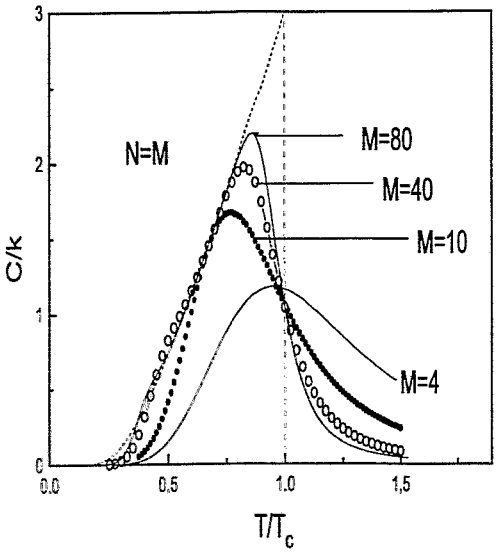

Fig. 1 *Specific heat C of the single-shell v.s. T/T_C at different values of the degeneracy of the Fermi level$M \sim N^{1/3}$. Solid and dashed lines correspond to canonical and BCS results, respectively.*

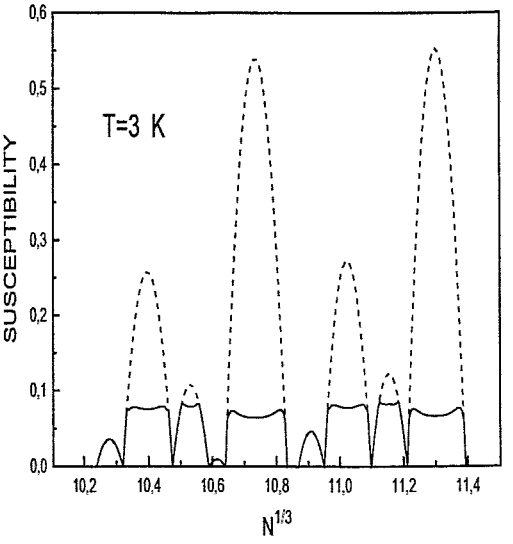

Fig. 2 *Susceptibility (in units $\mid \chi_L \mid \cdot 10^5$ where χ_L is the Landau expression for diamagnetism of the degenerate free electron gas) v.s. $N^{1/3}$. Dashed lines: $G = 0$, solid lines: $G > 0$.*

[1] *V.G. Khlopin Radium Institute, 194021, St.-Petersburg, Russia*

Rotating Quasi Particles near $N = Z$

S. FRAUENDORF AND J.A. SHEIKH[1]

The classification of rotational bands as quasiparticle configurations in a rotating mean field (CSM) has led to the understanding of the near yrast spectra of rapidly rotating nuclei. Such high spin studies have revealed new insight into the nature of the pair correlations between like particles. Modern γ - ray detector arrays permit to study high spin states for nuclei near the $N = Z$ line in the mass 80 region, where proton - neutron (pn) pair correlations are expected to play an important role. To study their nature it is necessary to reformulate the CSM in such a way that the pn - pairing is included. We have solved exactly the model problem of protons and neutrons in an $f_{7/2}$ shell interacting with a δ - force, by numerical diagonalizations. Then the approximate mean field solution is constructed for the same model case. Only $T = 1$ (pn - pairs coupled to zero spin) pairing is found. The mean field solution breaks spontaneously the isospin symmetry, where different orientations of the pair field in isospin space are equivalent. A particular convenient choice is the orientation with the pn - field equal to zero. This permits to construct excitation spectrum by combining quasi proton and quasi neutron excitations in the same way as for nuclei with $Z \neq N$ (CSM). The strength of the pn - pair correlations follows from the isospin symmetry, i. e. it is given by an isotropic distribution of the pair field. The influence of the Coulomb field that breaks isospin symmetry on the orientation of the $T = 1$ pair field is being studied.

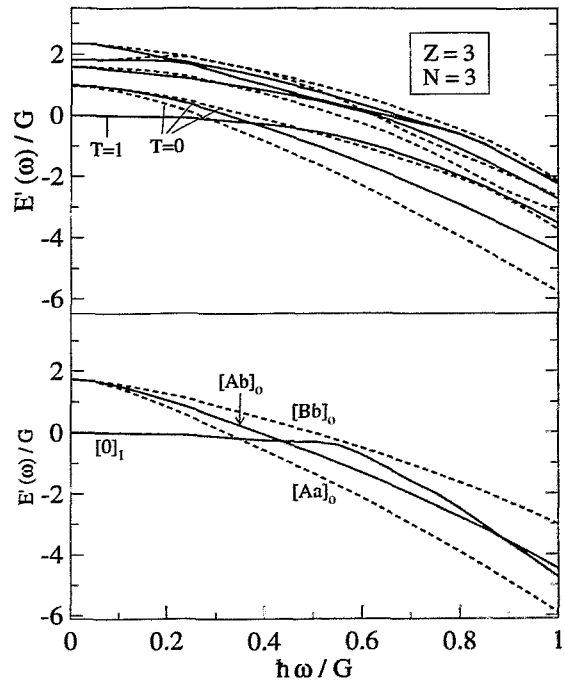

Fig. 1 *Total routhians for the $Z = N = 3$ system. The upper panel shows the Shell Model results and the lower the CSM approximation. Full lines correspond to even spins and dashed ones to odd spins. The CSM approximation reproduces the exact Shell Model result rather well indicating that the assignment of quasi particle configurations is correct. The conventional letter notation is used, where A, B denotes the lowest quasi neutron and a, b the lowest quasi proton states.*

[1] *Tata Institute of Fundamental Research, Colaba, Bombay, 400 005, India*

Magnetic Rotation in the Odd-Odd Nuclei ^{82,84}Rb [B]

H. Schnare, R. Schwengner, F. Dönau, S. Frauendorf, E. Grosse, L. Käubler, H. Prade, J. Eberth[1], S. Skoda[1], K.P. Lieb[2], A. Jungclaus[2], C. Lingk[2], G. Lo Bianco[3], G. de Angelis[4], A. Gadea[4], E. Farnea[4] and C.A. Ur[4]

Nuclei in a certain (N,Z) range around $A = 80$ are predicted to exhibit the features of magnetic rotation [1]. Experimental evidence is deduced from regular sequences of strong magnetic dipole transitions at high-spin in contrast to the irregular low-spin spectra being the common characteristic of nearly spherical nuclei.

To investigate the appearance of magnetic rotation in the nuclei ^{82}Rb,^{83}Rb [2] and ^{84}Rb, excited states have been populated using the fusion-evaporation reaction ^{76}Ge(^{11}B,xn) at a beam energy of 50 MeV, delivered by the Legnaro XTU Tandem accelerator. A target stack consisting of two thin Ge foils with a thickness of 0.2 mg/cm^2 was used. The emitted γ-rays were observed by the GASP array in its standard configuration with 40 Compton-suppressed HPGe detectors and the BGO inner ball with 80 elements. Approximately 1.5×10^8 high-fold events were collected and sorted into a $E_\gamma - E_\gamma$ matrix as well as a $E_\gamma - E_\gamma - E_\gamma$ cube.

Analysis of the data resulted in a considerable extension of the previously known level schemes [3], see Fig. 3a,3b. The strong $\Delta I = 1$ structures were observed in both nuclei and represent the first evidence for magnetic rotation in odd-odd nuclei of the $A = 80$ region. Both bands show the characteristic features of no signature splitting (Fig. 1) and a decreasing $B(M1)/B(E2)$ ratio with increasing spin (Fig. 2). Above spin $I = 15$ an upbend is observed in the $B(M1)/B(E2)$ plot for the ^{84}Rb data. Possibly this upbend indicates an alignment process which interferes the shears mechanism of magnetic rotation in this nucleus. A detailed interpretation on the basis of the tilted-axis cranking model is in progress.

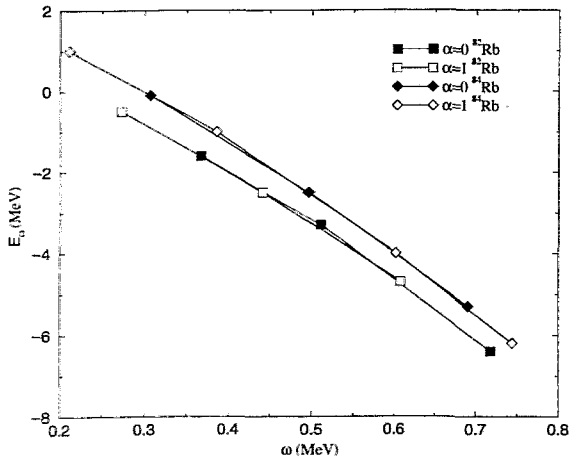

Fig. 1 *Experimental Routhian as function of rotational frequency for both signatures of the $\Delta I = 1$ bands marked in Figs. 3a,3b*

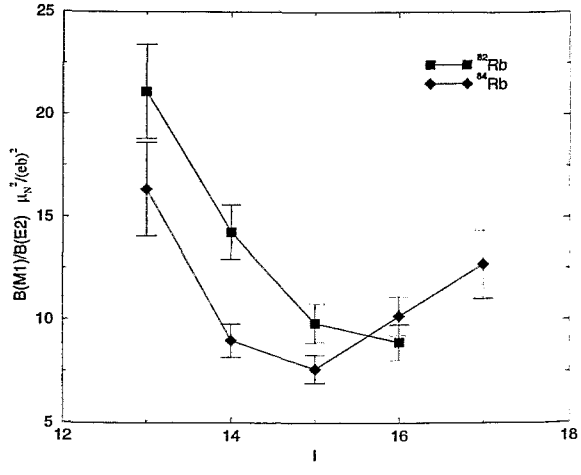

Fig. 2 *Experimental B(M1)/B(E2) ratios for γ-transitions of the bands marked in Figs. 3a,3b*

[1] *Institut für Kernphysik, Universität zu Köln*
[2] *2. Physikalisches Institut, Universität Göttingen*
[3] *INFN - Sezione di Milano*
[4] *Laboratori Nazionali INFN Legnaro*

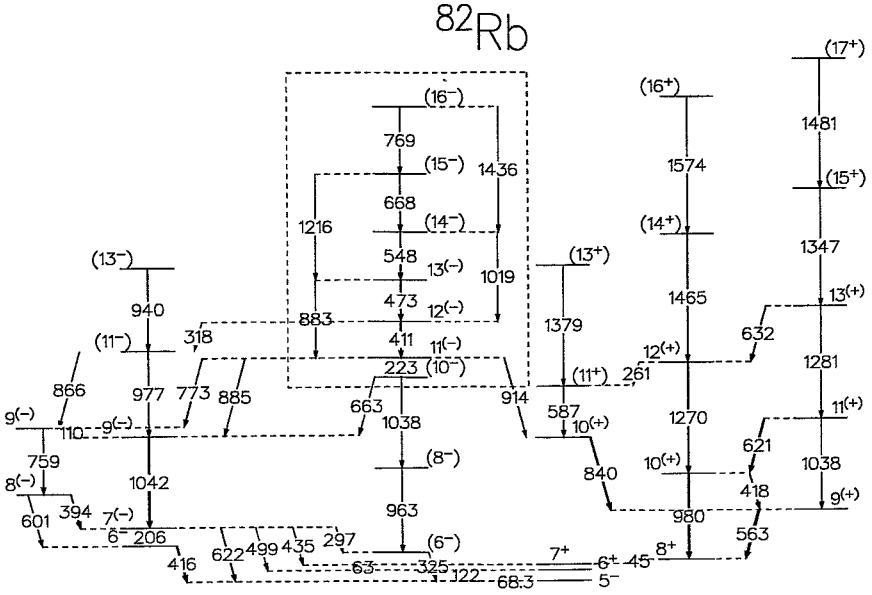

Fig. 3a *Partial level scheme of* ^{82}Rb. *Encircled region displays the magnetic shears band.*

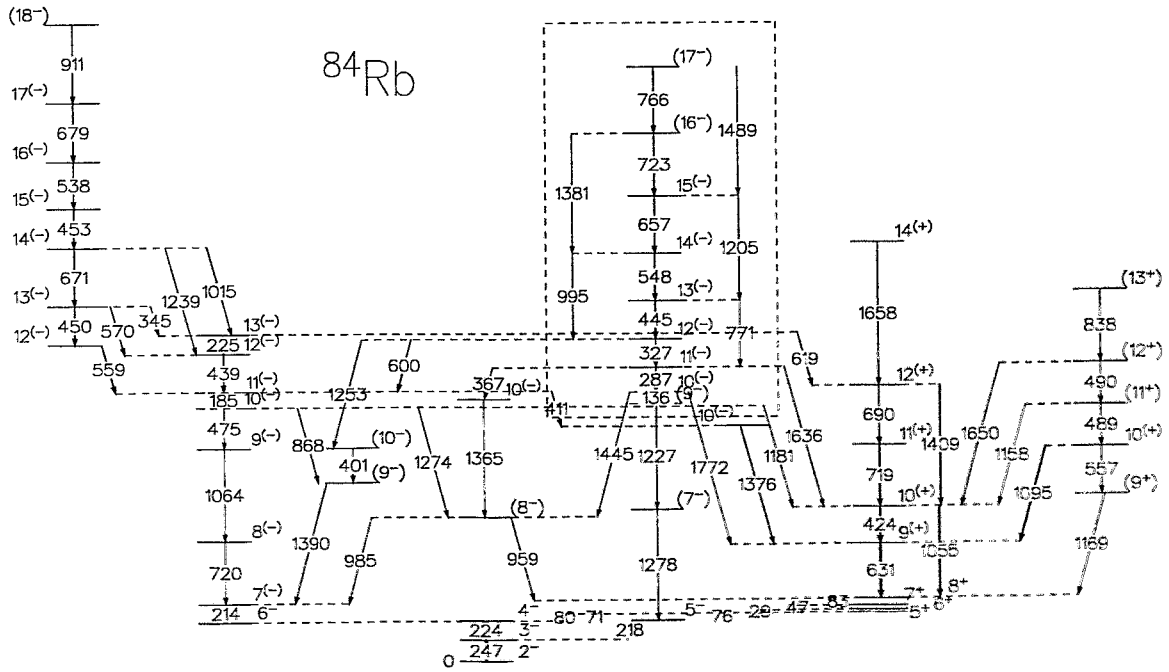

Fig. 3b *Partial level scheme of* ^{84}Rb. *Encircled region displays the magnetic shears band.*

References

[1] S. Frauendorf, Z. Phys. A 358 (1997) 163

[2] R. Schwengner et al., this report

[3] J. Döring et al., Z. Phys. A 338 (1991) 457 and Z. Phys. A 339 (1991) 425

Magnetic Dipole Bands in ^{83}Rb [B]

R. SCHWENGNER, H. SCHNARE, S. FRAUENDORF, F. DÖNAU, L. KÄUBLER, H. PRADE, E. GROSSE, A. JUNGCLAUS[1], K. P. LIEB[1], C. LINGK[1], S. SKODA[2], J. EBERTH[2], G. DE ANGELIS[3], A. GADEA[3], E. FARNEA[3], C. A. UR[3] AND G. LO BIANCO[4]

Magnetic rotation is predicted in several mass regions including a certain region near $A = 80$ [1] where the deformation is small and the particle-like protons fill the $g_{9/2}$ orbital and the (fp) shell while there are only few $g_{9/2}$ neutron holes in the $N = 50$ shell. This rotational mode leads to regular bands with strong $M1$ but weak $E2$ transitions. A characteristic feature of these so-called shears bands is the decrease of the $M1$ transition strengths with increasing spin caused by the alignment of the spins of the involved orbitals.

To search for magnetic rotation in the mass region around $A = 80$ we have studied the isotopes $^{82}Rb_{45}$, $^{83}Rb_{46}$ and $^{84}Rb_{47}$. Excited states in these nuclei were populated via the reaction ^{11}B + ^{76}Ge at $E = 50$ MeV using the ^{11}B beam of the XTU tandem accelerator of the LNL Legnaro. Gamma rays were detected with the spectrometer GASP. A total of 1.5×10^8 three-fold coincidence events was recorded. The preliminary level scheme of ^{83}Rb deduced from the present coincidence experiment is shown in Fig. 1. It has been largely extended with respect to previous work [2]. In particular, four level sequences labelled A, B, C and D in Fig. 1 have been observed for the first time.

Sequence A includes strong $M1$ transitions connecting $13/2^-$, ..., $21/2^-$ states. At $J = 23/2$ the character of this sequence changes and is dominated by $E2$ transitions at high spin. Sequence B includes $E2$ transitions only and might be the signature partner of sequence A. Sequences C and D are dipole bands including $M1$ as well as $E2$ transitions. An inspection of the level spacings of sequence C shows that these are not regular as expected for shears bands. Moreover, the plot of ratios of $B(M1)$ and $B(E2)$ values of transitions deexciting a certain state given in Fig. 2 reveals a pronounced staggering. This behaviour contrasts with that of the magnetic dipole bands in the odd-odd neighbours ^{82}Rb and ^{84}Rb, where the $B(M1)/B(E2)$ ratios show the behaviour expected for magnetic rotation [3]. This remarkable difference may be related to the different configurations of the dipole bands including 3- and possibly 5-quasiparticle configurations in ^{83}Rb but 2- and 4-quasiparticle configurations in ^{82}Rb and ^{84}Rb. A detailed interpretation of the dipole bands in comparison with predictions of the tilted-axis cranking model [1] is in progress.

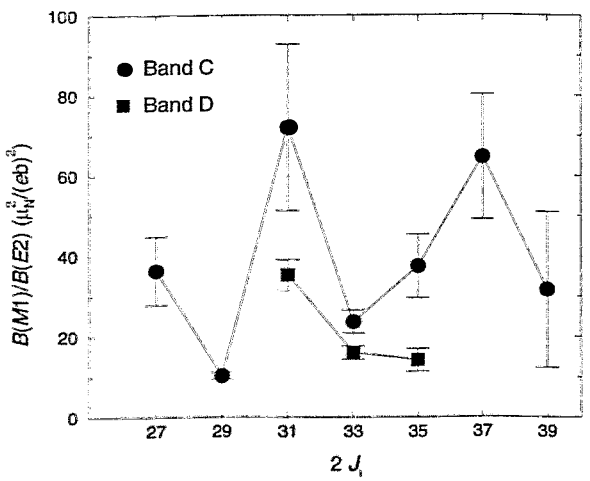

Fig. 2 *Experimental $B(M1)/B(E2)$ ratios for γ transitions of the bands labelled C and D in Fig. 1.*

[1] *II. Physikalisches Institut, Universität Göttingen*
[2] *Institut für Kernphysik, Universität zu Köln*
[3] *INFN, Laboratori Nazionali di Legnaro*
[4] *INFN, Sezione di Milano*

References

[1] S. Frauendorf, Z. Phys. A 358 (1997) 163
[2] W. Gast et al., Phys. Rev. C 22 (1980) 469
[3] H. Schnare et al., this report

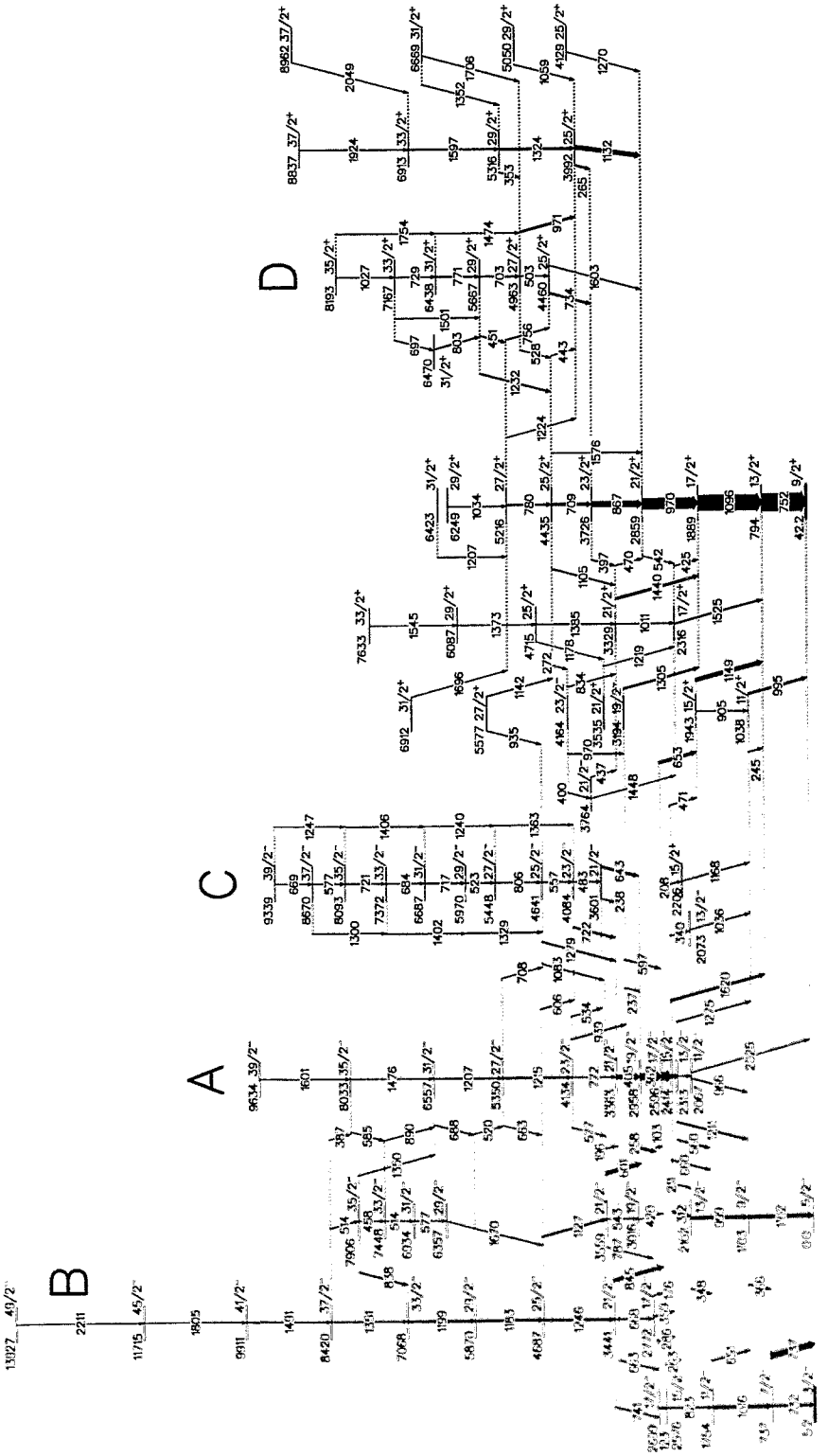

Fig. 1 *Preliminary level scheme of* ^{83}Rb *deduced from the present experiment.*

Lifetimes in the Magnetic Dipole Band in ^{79}Br [B]

T. Servene, J. Reif, H. Schnare, R. Schwengner, H. Prade, G. Winter[†], L. Käubler, J. Eberth[1], H.G. Thomas[1], F. Becker[1], B. Fiedler[1], S. Freund[1], S. Kasemann[1], S. Skoda[1], T. Steinhardt[1], O. Thelen[1], T. Härtlein[2], Ch. Ender[2], F. Köck[2], P. Reiter[2], D. Schwalm[2],

Level lifetimes in the nucleus ^{79}Br were determined in the reaction ^{76}Ge(^{7}Li,4n) at $E(^{7}\mathrm{Li})$=35 MeV using the Doppler shift attenuation method (DSAM). The recoiling nuclei were stopped in the backed target (0.6 mg/cm^2 ^{76}Ge on 2.5 mg/cm^2 ^{179}Au). Doppler-shifted γ-rays were detected with an array of six EUROBALL-Cluster detectors. Details of the experimental setup are described in [1,2]. The coincidence data were sorted into two $E_\gamma - E_\gamma$ matrices, one for each of the observation angles 40° and 140°.

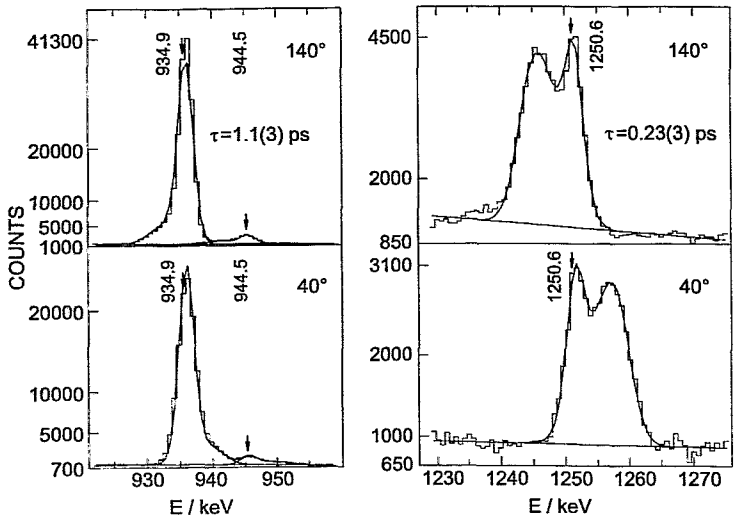

Fig. 1 *Examples for the lineshape analysis of transitions in the yrast band in ^{79}Br. The given lifetimes are results of the presented fits.*

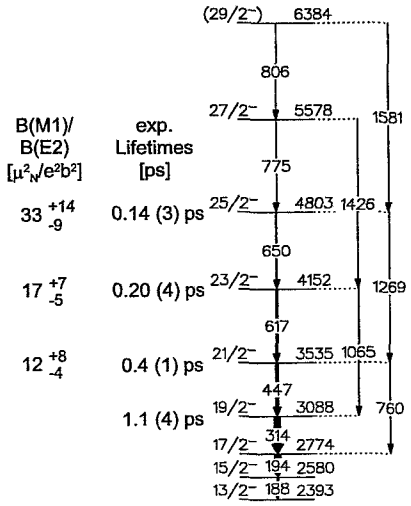

Fig. 2 *Experimental lifetimes and the ratios B(M1)/B(E2) in the magnetic dipole band in ^{79}Br.*

The lifetime of a specific level is deduced from a detailed analysis of the lineshape taking into account the feeding from other levels. For the lineshape analysis the program DOPPIDIF [4] was used. Examples for the lineshape analysis are given in Fig. 1. In Fig. 2 the magnetic dipole band in ^{79}Br is shown together with the determined lifetimes and the ratios B(M1)/B(E2, ΔI=2). Spin and parity assignments are taken from the analysis of DCO-ratios [5] and linear polarization data respectively.

[1] *Institut für Kernphysik der Universität zu Köln*
[2] *Max-Planck-Institut für Kernphysik, Heidelberg*

References

[1] J. Eberth, Prog. Part. Nucl. Phys. 28 (1992) 495
[2] T. Servene et al., Annual Report 1995, FZR-130 (1996) 73
[3] R. Schwengner et al., Annual Report 1995, FZR-130 (1996) 71
[4] G. Winter, program DOPPIDIF, FZR, unpublished
[5] T. Servene et. al., Annual Report 1996, FZR-149 (1997) 69

States of Seniority 3 and 5 in the $N = 48$ Nucleus ^{87}Y

R. SCHWENGNER, J. REIF, H. SCHNARE, G. WINTER†, T. SERVENE, L. KÄUBLER, H. PRADE, M. WILHELM[1], A. FITZLER[1], S. KASEMANN[1], E. RADERMACHER[1] AND P. VON BRENTANO[1]

Our investigation of the $N = 48$ nucleus ^{87}Y revealed excited states up to $J^\pi = 33/2^-$ [1]. Mean lifetimes of eight high-spin states have been determined using the Doppler-shift attenuation method. Reduced transition strengths deduced from these lifetimes are given in Table 1. These values may serve as a stringest test for theoretical model predictions.

The structure of ^{87}Y has been interpreted in terms of the shell model. The calculations performed in the model space $\pi(0f_{5/2}, 1p_{3/2}, 1p_{1/2}, 0g_{9/2})$ $\nu(1p_{1/2}, 0g_{9/2})$ describe the observed high-spin states on the basis of seniority $v = 3$ and $v = 5$ configurations. The majority of calculated level energies and transition strengths agree well with experimental values as demonstrated in Fig. 1 and Table 1, respectively. Especially the large experimental $B(M1)$ values of up to 1.8 W.u. for transitions between yrast states with $J > 21/2$ are well reproduced. In the calculations they result from a recoupling of the spins of the involved proton and neutron orbitals. For example, the $v = 5$ configuration $\pi[0f_{5/2}^{-1}(0g_{9/2}^2)_{J_g}]_{J_\pi}$ $\nu(0g_{9/2}^{-2})_8$ predominates in the $27/2_1^-$ to $33/2_1^-$ states with spin values of $J_g = 4$, 6, 8 and $J_\pi = 13/2$, $17/2$.

Table 1 *Experimental and calculated transition strengths in* ^{87}Y

J_i^π	J_f^π	$\sigma\lambda$	$B(\sigma\lambda)$ (W.u.) EXP	$B(\sigma\lambda)$ (W.u.) SM
$\frac{21}{2}^+_1$	$\frac{17}{2}^+_1$	$E2$	4.5(3)	6.2
$\frac{23}{2}^+_1$	$\frac{21}{2}^+_1$	$M1$	$0.69^{+0.23}_{-0.14}$	1.23
$\frac{25}{2}^+_1$	$\frac{23}{2}^+_1$	$M1$	$1.10^{+0.35}_{-0.21}$	0.87
$\frac{25}{2}^+_2$	$\frac{21}{2}^+_1$	$E2$	$4.7^{+3.5}_{-1.9}$	4.6
$\frac{25}{2}^+_2$	$\frac{23}{2}^+_1$	$M1$	$0.08^{+0.04}_{-0.03}$	0.04
$\frac{25}{2}^+_2$	$\frac{25}{2}^+_1$	$M1$	$0.05^{+0.03}_{-0.02}$	0.02
$\frac{27}{2}^+_1$	$\frac{23}{2}^+_1$	$E2$	$2.5^{+2.0}_{-1.0}$	0.23
$\frac{27}{2}^+_1$	$\frac{25}{2}^+_1$	$M1$	$0.010^{+0.009}_{-0.004}$	0.0004
$\frac{27}{2}^+_1$	$\frac{25}{2}^+_2$	$M1$	$0.55^{+0.27}_{-0.16}$	0.14
$\frac{27}{2}^-_1$	$\frac{23}{2}^-_2$	$E2$	< 2.4	0.3
$\frac{27}{2}^-_1$	$\frac{25}{2}^-_1$	$M1$	< 0.004	0.07
$\frac{27}{2}^-_1$	$\frac{25}{2}^-_2$	$M1$	< 0.01	0.03
$\frac{29}{2}^-_1$	$\frac{25}{2}^-_1$	$E2$	$12.0^{+5.2}_{-3.6}$	5.0
$\frac{29}{2}^-_1$	$\frac{25}{2}^-_2$	$E2$	$11.4^{+6.1}_{-4.1}$	4.0
$\frac{29}{2}^-_1$	$\frac{27}{2}^-_1$	$M1$	$0.79^{+0.29}_{-0.20}$	1.12
$\frac{31}{2}^-_1$	$\frac{29}{2}^-_1$	$M1$	$0.56^{+0.14}_{-0.09}$	1.40
$\frac{33}{2}^-_1$	$\frac{31}{2}^-_1$	$M1$	$1.78^{+0.60}_{-0.35}$	1.41

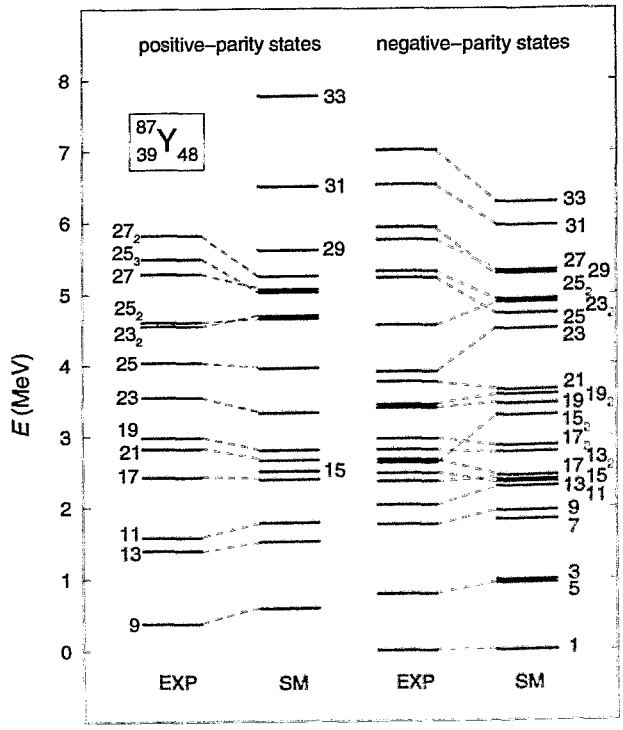

Fig. 1 *Comparison of experimental with calculated level energies of states in* ^{87}Y. *Spins are given as* $2J$.

[1] *Institut für Kernphysik, Universität zu Köln*

References

[1] R. Schwengner et al., Annual report 1996, FZR-179 (1997) 72

High-Spin States in the N=49 Nuclei ^{88}Y and ^{87}Sr

C. Borcan, R. Schwengner, H. Schnare, T. Servene, M. Wilhelm[1], A. Fitzler[1], S. Kasemann[1] and P. von Brentano[1]

The nuclei near the shell closure at N=50 are of particular interest because they offer useful information about multi-particle excitation modes (see e.g. [1]). Moreover, their investigation could improve our knowledge about the effective proton-neutron interaction.
A recent investigation [2] of the N=49 nucleus ^{86}Rb revealed an improved shell model description of states with $J \geq 15$ by including the excitation of one $g_{9/2}$ neutron over the shell gap at N=50 into the $d_{5/2}$ orbital.
In order to extend the knowledge about N=49 nuclei we have undertaken the study of the nuclei ^{88}Y and ^{87}Sr. High-spin states of these nuclei have been studied via the reactions ^{80}Se(^{11}B,3n) and ^{80}Se(^{11}B,p3n), respectively. The coincidence experiment was carried out with a 45 MeV beam delivered by the FN Tandem accelerator of the University of Cologne. γ-γ coincidences were measured using the six detector array OSIRIS CUBE. The level schemes have been extended up to excitation energies of $E \approx 7$ MeV as shown in Fig. 1. In both nuclei $\Delta J = 1$ sequences have been observed for the first time. Spin assignments are based on the directional correlations of coincident γ rays. The analysis of level lifetimes is in progress.

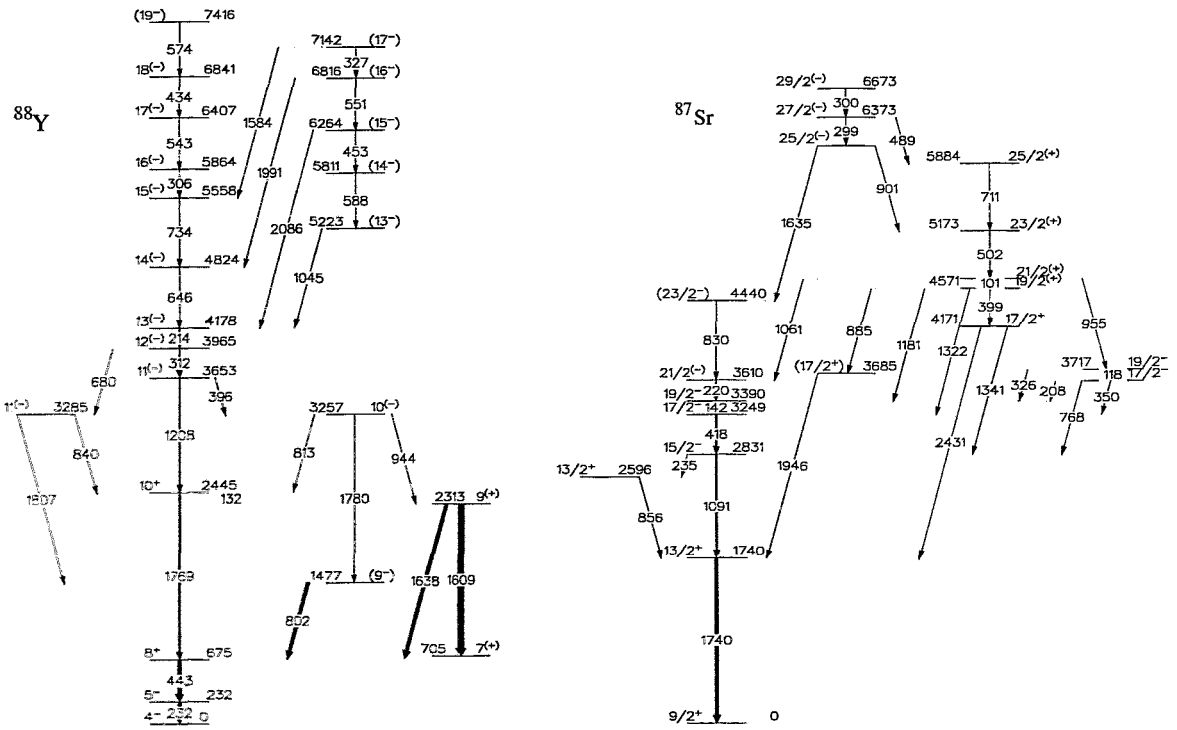

Fig. 1 *Preliminary level schemes of* ^{88}*Y and* ^{87}*Sr deduced from the present work.*

[1] *Institut für Kernphysik, Universität zu Köln, 50937 Köln*

References

[1] R. Schwengner et al., Nucl. Phys. A 584 1995 (159) and Phys. Scr. T 56 (1995) 126
[2] G.Winter et al., Phys. Rev. C 49 (1994) 2447

Nuclear Resonance Fluorescence Experiment on ^{88}Sr with two EUROBALL CLUSTER Detectors [B,D,H]

L. KÄUBLER, H. PRADE, H. SCHNARE, R. SCHWENGNER, M. GRINBERG[3], F. DÖNAU, E. GROSSE, P. v. BRENTANO[1], J. EBERTH[1], J. ENDERS[2], A. FITZLER[1], C. FRANSEN[1], R.-D. HERZBERG[1], H. KAISER[2], P. v. NEUMANN-COSEL[2], N. PIETRALLA[1], A. RICHTER[2], CH. STOYANOV[3], H.-G. THOMAS[1], H. TIESLER[1], D. WEISSHAAR[1], I. WIEDENHÖVER[1] AND A. ZILGES[2]

For the understanding of complex states in the odd-mass N=50 nuclei ^{87}Rb and ^{89}Y [1], which arise from the coupling of an unpaired proton to two- or three-phonon states in the N=50 core nucleus ^{88}Sr, the detailed knowledge of the core states is important. Therefore a (γ,γ') experiment on ^{88}Sr has been performed with an endpoint energy of the bremsstrahlung of 6.8 MeV at the S-DALINAC accelerator using two EUROBALL CLUSTER detectors at 90° and 127°. To illustrate the experimental progress, in Fig. 1 the high energy part of the total (single and add-back events of both CLUSTER detectors added) gamma-ray spectrum is shown. For the 6335 keV peak we obtained during 8 days beam time about 70.000 counts, whereas in a previous experiment [2] only about 1.000 counts could be recorded in about 60 days . Many new transitions have been found, e.g. the 6202 and 6348 keV γ-rays. For the corresponding 6348 keV level a spin of J=1 could be determined from angular correlation data. A gamma-ray branch from the 4743 keV state to the 2_1^+ level has been observed. In accordance with QPM calculations, an interpretation as a $2^+ \otimes 3^-$ two phonon state for the 4743 keV level and as three-phonon $2^+ \otimes 2^+ \otimes 3^-$ structures for the 6215 and 6335 states is proposed.

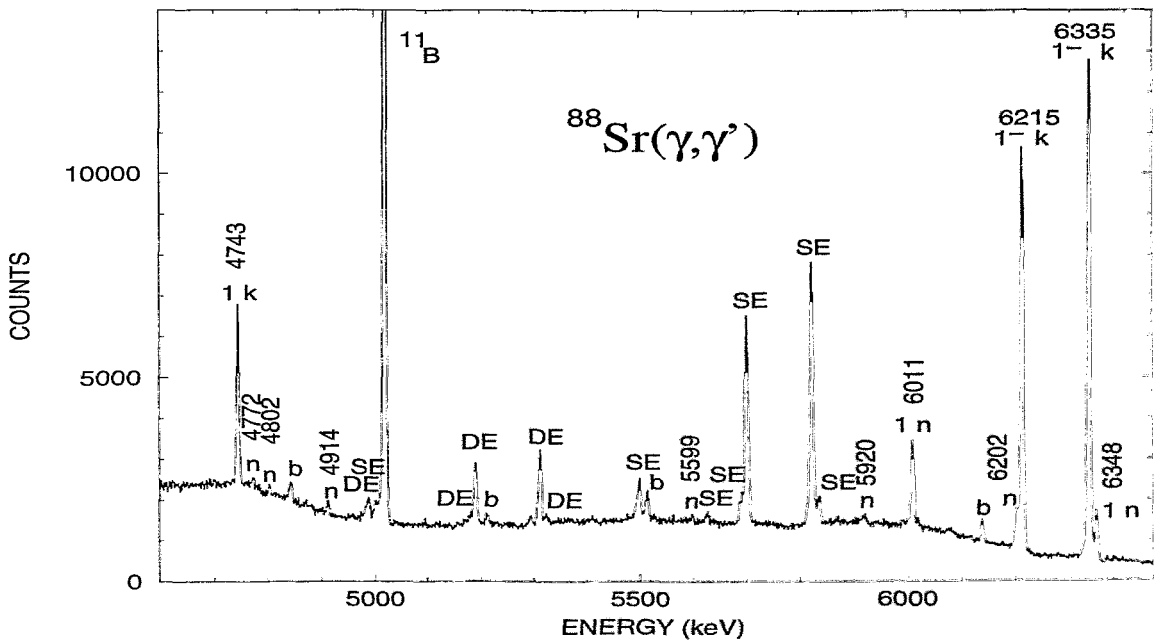

Fig. 1 *Section of the total gamma-ray spectrum; if known J or J^π is given; k means - seen in previous (γ,γ') experiments; n - new in (γ,γ'); b,SE,DE - background or single or double escape.*

[1] *Institut für Kernphysik, TU Darmstadt, D-64289 Darmstadt*
[1] *Institut für Kernphysik, Universität zu Köln, D-50937 Köln*
[1] *Institute of Nuclear Research and Nuclear Energy, Sofia, BG-1784 Sofia*

References

[1] J. Reif. et al., Nucl. Phys. A 620 (1997) 1
[2] G. Isoyama et al., Nucl. Phys. A 342 (1980) 124

Lifetimes and Collectivity of Low-lying States in ^{115}Sn [H]

YU. N. LOBACH[1], L. KÄUBLER, R. SCHWENGNER AND A. A. PASTERNAK[2]

The structure of low-lying states of the spherical and semimagic tin nuclei is characterized by the competition of spherical many-quasi particle neutron excitations, of phonon contributions from the vibrational mode as well as of admixtures from low-lying proton 2p2h intruder rotational states. To study this behaviour in more detail, mean lifetimes of 19 and lifetime limits for 5 excited states in ^{115}Sn have been measured at the cyclotron U-120 in Kiev, using the Doppler-shift attenuation method in connection with the reaction ^{113}Cd(α,2nγ)^{115}Sn at a beam energy of 27 MeV [1]. The results for negative-parity states are given in Fig. 1. The analysis of the transition probabilities leads to the following conclusions: (i) the experimental $B(\sigma L)$ values are generally enhanced, thus giving an indication for collective admixtures even to low-lying states in ^{115}Sn; (ii) the picture of core-particle coupling describes the properties of the $\nu h_{11/2} \otimes 2_1^+$ multiplet (2_1^+ is the first 2^+ state in ^{114}Sn), whereas this picture gives only a rough estimate for the $\nu h_{11/2} \otimes 4_1^+$ multiplet; (iii) The agreement of the B(E2) value for the transition from the 3319 keV state of the $\nu h_{11/2} \otimes \pi 2p2h$ band to the 2024 keV state of the $\nu h_{11/2} \otimes 2_1^+$ multiplet [1], with the B(E2) value of the corresponding transition from the 2614 keV state in ^{114}Sn is a strong evidence for the proposed configuration $\nu h_{11/2} \pi (g_{9/2}^{-2} g_{7/2}^2)$ for this band in ^{115}Sn [2].

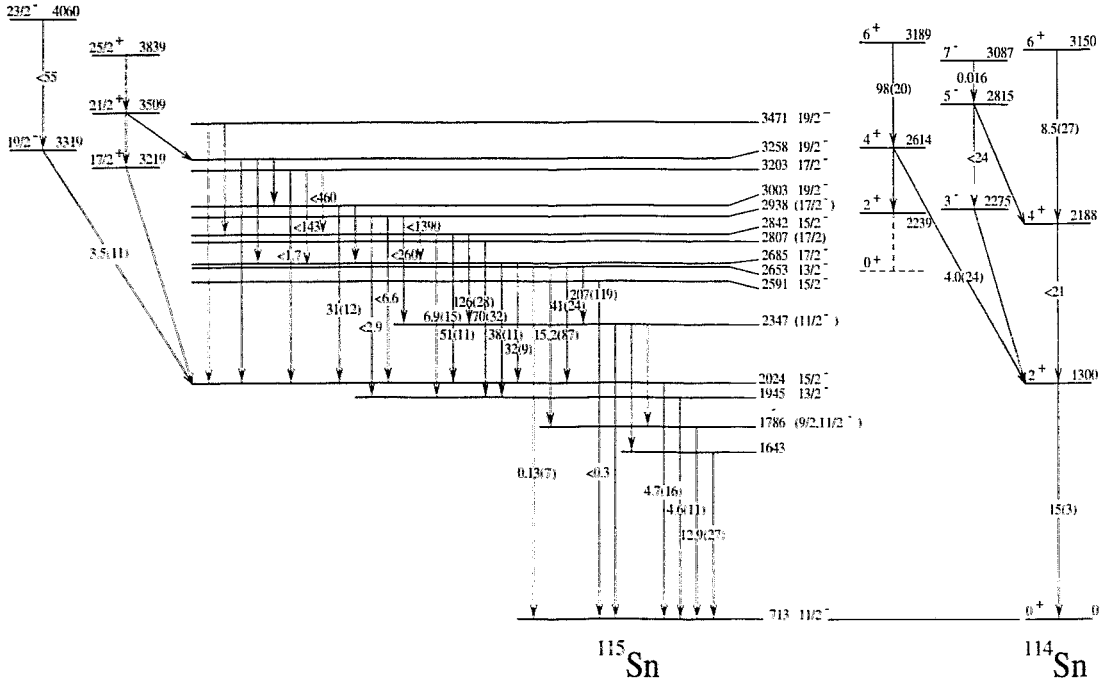

Fig. 1 *Partial level scheme of ^{115}Sn showing states built on the $\nu h_{11/2}$ single-particle state at E_x = 713.3 keV in comparison with yrast states and some members of the π2p2h intruder band in ^{114}Sn, shifted to 713.3 keV. For ^{115}Sn, labels on the arrows indicate our measured B(E2) values given in W.u..*

[1] *Institute for Nuclear Research of the Ukrainian Academy of Science, 252028 Kiev, Ukraine*
[2] *Physico-Technical Institute "A.F.Ioffe", ul. Politechnitscheskaja 26, 194021 St.Petersbourg, Russia*

References

[1] Yu. N. Lobach et al., to be published
[2] J.M. Sears et al., Phys. Rev. C 55 (1997) 1096

The Local Trigger and Data Acquisition System of the EUROSiB Array [W]

H.-G. Ortlepp, G. Pausch, K. Heidel, M. Moszynski[1], H. Prade and D. Wolski[1]

The completely mounted compact 4π Si-array EUROSiB [1] together with all bias supply channels, preamplifiers and pulse-shape analysis [2] electronics became operational in 1997. All analogue functions for each two detection channels (pulse recognition, trapezoidal spectroscopic shaping, conversion of zero crossing and flight times into amplitudes) are performed in one especially developed NIM module. An own local trigger and data acquisition system has been designed which allows to combine EUROSiB with other detection systems, in particular with EOROBALL III. The trigger is housed in two NIM modules and provides a linear multiplicity signal, a logical signal indicating exceeding of an adjustable multiplicity threshold, the ADC gate and clear pulses, and a local busy signal.
A coincidence with the outer system is recognized within a fast trigger sampling interval and generates a local trigger signal which can be used by the master trigger [3] for event selection and for the decision to read out the EUROSiB sub-event.

The three signals from each detector delivered by the analogue electronics - energy, rise time and time of flight - are digitized in altogether 15 8-channel peak sensing VME ADC modules CAEN V556S. The VME crate (see figure) further contains a modified Struck STR8080 readout engine which includes the conversion results of fired ADC channels in the EUROBALL DT32 data stream [3], and a Wiener AT-VME interface for initializing the ADC's and loading the readout program into the STR8080. The AT-VME is coupled to a PC and it can be replaced by a VME processor card containing an Ethernet connnection. A further module must be designed for interfacing the VXI-typical EUROBALL system control signals with the EUROSiB local trigger and the local readout part. In its first implementation only the EUROBALL common dead-time mode is foreseen.

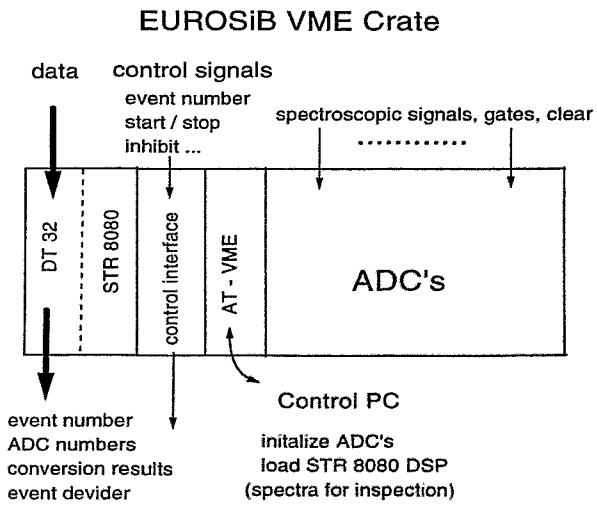

[1] *Soltan Institute for Nuclear Studies, Dept. of Nuclear Electronics, PL-05-400 Otwock-Swierk, Poland*

References

[1] G. Pausch et al., Annual Report 1995, FZR-130 (1996), pp. 135-142,
G. Pausch et al., Annual Report 1996, FZR-179 (1997) 101
[2] G. Pausch et al., IEEE Transact. Nucl. Sci. 43, No.3 (1996) 1097
[3] I. Lazarus and P.J. Coleman-Smith, IEEE Transact. Nucl. Sci. 42, No.4 (1995) 891

Time Scale of Fission-Like Ternary Decay into Fragments of Similar Masses [B]

C.-M. Herbach and H.-G. Ortlepp for the FOBOS collaboration

Coulomb trajectory calculations have been used to deduce the time scale of the mass-symmetric ternary decay that was investigated in the reactions ^{14}N(53AMeV) + ^{232}Th and ^{197}Au [1]. The formation of the fragments with masses corresponding to the experimental events (A_1,A_2,A_3) is simulated as a sequence of two fissions. Within the time interval Δt the fragment A_1 generated by the first scission and the remaining complex (A_2+A_3) are accelerated by Coulomb forces. After this time the second scission occurs and the velocities of the three fragments are calculated up to their asymptotic values. For $\Delta t < 1000$ fm/c the motion of the fragments is remarkably affected by the final state Coulomb interaction. The mutual angle Θ_{axis} between the direction of A_1 and the axis A_2-A_3 has been choosen as a selective observable which was calculated in the rest frame of the residual complex with the orientation pointing to the heavier of both fragments A_2 and A_3. Considering the acceptance of the detector set-up, the correlation function

$$Y(\Theta_{axis}) = \frac{N(\Theta_{axis})^{cor} - N(\Theta_{axis})^{mix}}{N(\Theta_{axis})^{cor} + N(\Theta_{axis})^{mix}} \qquad (1)$$

was used to display the distributions that are deduced from simulated (Fig.1) and measured data (Fig.2). It refers to physical events ('cor') of correlated fragments and to artificial data ('mix') composed by fragments which are taken from different events. The complex (A_2+A_3) has been identified from the asymptotic velocity vectors both for the experimental and the simulated data. The used method - adapted from [2] - selects the fragment combination which is distinguished by the best agreement of the relative fragment velocities at the two scissions with the corresponding values from binary fission systematics.

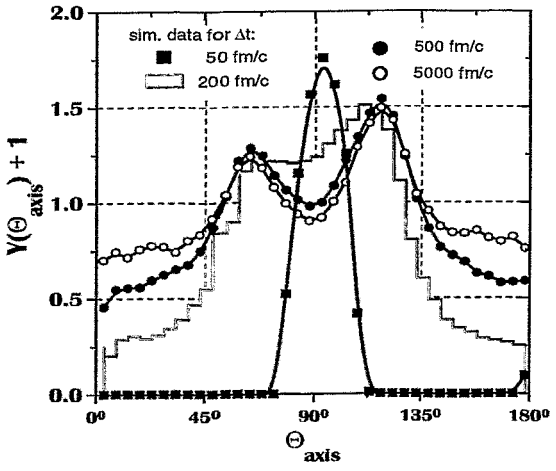

Fig. 1 *Results of trajectory calculations*

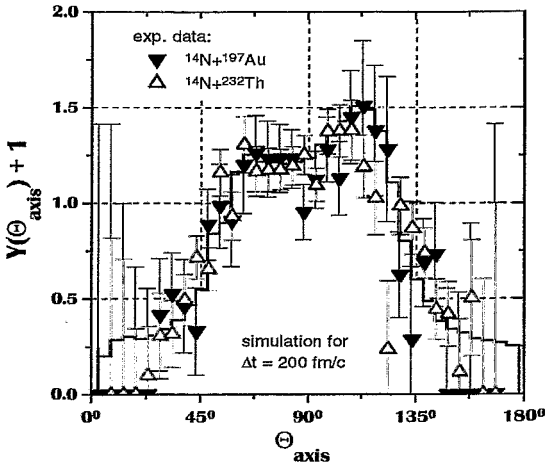

Fig. 2 *Comparison with experimental data*

The measured data for both reactions (Fig.2) are in agreement with the simulations at $\Delta t = 200$ fm/c. This time scale corresponds to about 1% of typical values for the collective motion in binary fission. When the second scission occurs, the fragments from the first scission have increased their distance only by < 20 fm. Consequently, the assumption of a common fission-like decay is supported and a mechanism of two independent reaction steps can be excluded.

References

[1] C.-M. Herbach, H.-G. Ortlepp, Annual Report 1996, FZR-179 (1997) 52
[2] G. Bizard et al., Phys. Lett. B 276 (1992) 413

Decay of Heavy Excited Nuclei with Large Fissility [B]

A.A. Aleksandrov[1], I.A. Aleksandrova[1], L. Dietterle[1], V.N. Doronin[1], P. Gippner, C.-M. Herbach, S.A. Ivanovsky[1], D.V. Kamanin[1], F. Koscielniak[2], A. Matthies[1], T. Möhlenkamp, W. von Oertzen[3], H.-G. Ortlepp, Yu.E. Penionzhkevich[1], Yu.V. Pyatkov[4], K.D. Schilling, D.I. Shishkin[1], O.V. Strekalovsky[1], V.G. Tichtchenko[1], I.P. Tsurin[1], C. Umlauf[1], W. Wagner, M. Wilpert[3], R. Wolski[2], R. Yanez, V.E. Zhuchko[1] and L. Zrodlowski[2]

Using the 4π-fragment-spectrometer FOBOS [1] at the heavy ion cyclotron U-400M of the JINR Dubna, the study of the multi-fragment decay of heavy nuclei at intermediate excitation energies [2] has been continued. Composite systems with mass A_c = 200-250, excitation energy ϵ_c^* = 1-4 MeV/u and large values of the fissility Z^2/A were generated by the reactions ^{40}Ar(36AMeV) + ^{248}Cm and ^{232}Th. So far, the analysis of the data has been restricted to events from fission and decay into three massive fragments. In both cases, the reconstruction of the linear momentum transfer (LMT) as a measure of the induced excitation energy was deduced from the momentum balance of the fragments. While the binary fission yield is dominated by contributions from peripheral collisions, the ternary events are correlated with larger values of the LMT (Fig.1). As displayed by Dalitz-plot of the fragment masses (Fig.2), most of the detected ternary events are characterized by the formation of a lighter fragment $A_{min} \approx A_{Ar}/2$ with about half the projectile mass followed by symmetric fission of the residual. This may indicate some memory from the entrance channel. The latter is assumed to be negligible for ternary events under the restriction of $A_{min} > 50$. For these events, the ternary yields relative to binary fission N_3/N_2 amount to $4{\cdot}10^{-3}$ and $2{\cdot}10^{-3}$ for the measurements at ^{248}Cm and ^{232}Th, respectively. Considering our results at ^{14}N(53AMeV)+^{197}Au and ^{232}Th with $N_3/N_2 \approx 1.5{\cdot}10^{-3}$ for both reactions, the increase of N_3/N_2 with Z^2/A is smaller than expected from the data of [3].

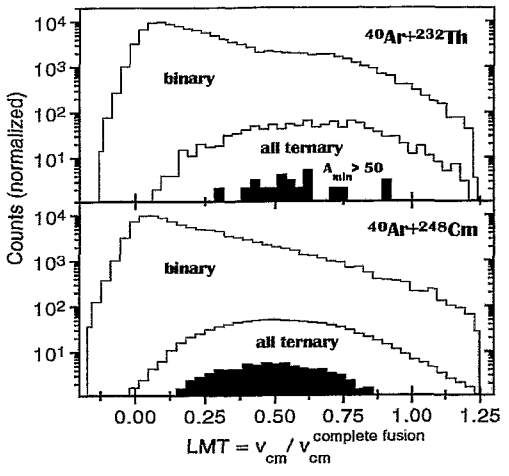

Fig. 1 *LMT distribution for binary fission and ternary decays into massive fragments*

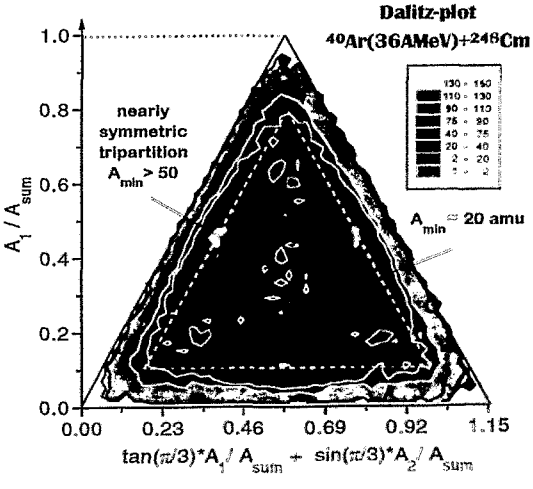

Fig. 2 *Fragment masses of ternary events (A_{sum}=A_1+A_2+A_3, 100% efficiency at Z>8)*

[1] *Joint Institute for Nuclear Research, 141980 Dubna, Russia*
[2] *Henryk Niewodniczansky Institute of Nuclear Physics, 31-324 Cracow, Poland*
[3] *Hahn-Meitner-Institut GmbH, 14109 Berlin, and Freie Universität Berlin, 14195 Berlin, Germany*
[4] *Moscow Engineering Physics Institute, 115409 Moscow, Russia*

References

[1] H.-G. Ortlepp et al., Nucl. Instrum. Methods A 403 (1998) 65
[2] C.-M. Herbach et al., Annual Report 1996, FZR-179 (1997) 51
[3] V.E. Perelygin et al., Nucl. Phys. A 127 (1969) 577

Fragment Mass Distributions Generated by a New Three-Dimensional Combined Dynamical Statistical Model for Fission of Hot Nuclei [B]

A.E. Gettinger[1], I. Gontchar[1], R.S. Kurmanov[1], L.A. Litnevsky[1], H.-G. Ortlepp and V.V. Pashkevich[2]

The well known Combined Dynamical Statistical Model (CDSM) [1] of the fission of hot nuclei does not consider explicitely the mass asymmetry degree of freedom. The dynamics is one-dimensional. We developed a new model which includes also asymmetric nuclear shapes of the fissioning system. It is realized in the code SAND running on a PC. The shape parametrization is based on a restricted set of Cassini ovals. Shell effects are not included. The dynamics is described by a Langevin equation for the corresponding coordinates. Particle evaporation is treated in the same way as in the former CDSM version. An example of a fragment mass distribution generated by the SAND code is shown in fig.1. Within the full width at half maximum the distribution can be well fitted by a Gaussian. For excitation energies between 50 and 200 MeV the dispersion of these Gaussians well agrees with FOBOS results (fig. 2) for the reaction ^{7}Li (43 AMeV) + ^{232}Th [2]. The considerable deviation of the experimental mass dispersion from an extrapolated semiempirical systematics is qualitatively interpreted in ref. [2] as cooling effect. The present extended CDSM allows a quantitative theoretical description of this effect.

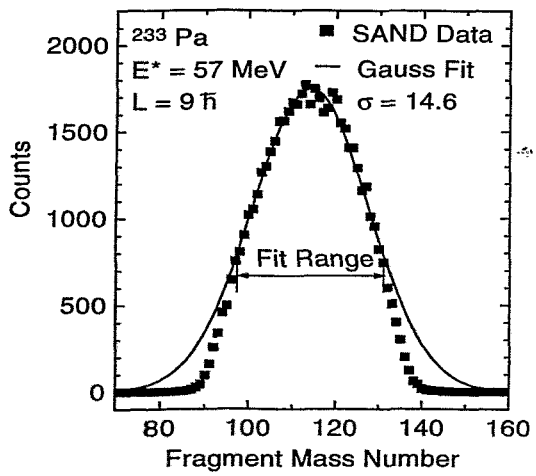

Fig. 1 *Fission fragment mass distribution generated by the SAND code and fitted by a Gaussian over the indicated range.*

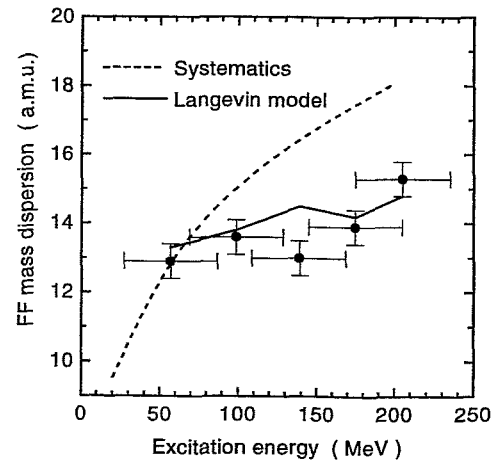

Fig. 2 *Mass dispersion measured at five excitation energies (points) compared with an extrapolated systematics and SAND results*

For fragment mass ratios larger than $A_1/A_2 = 1.35$ the simulated distribution decreases stronger than a Gaussian (fig. 1). This effect is caused by too steep rise of the potential energy at larger asymmetries. A minimization using higher Cassini ovals was not performed because of high numerical effort. Presently, the code is being rewritten using a more appropriate coordinate system.

[1] *Omsk State Railway Academy, Omsk, Russian Federation*
[2] *Joint Institute for Nuclear Research, Dubna, Russian Federation*

References

[1] P. Fröbrich, I.I. Gontchar and N.D Mavlitov, Nucl. Phys. A 556 (1993) 281
[2] H.-G. Ortlepp et al., Annual Report 1996, FZR-179 (1997) 54

Analysis of Pre-Fission Charged Particle Spectra from the Reactions ^{14}N (53 AMeV) + ^{197}Au and ^{232}Th [B]

D.V. KAMANIN, H.-G. ORTLEPP, C.-M. HERBACH, W. WAGNER

Light charged particle (LCP) data measured by the FOBOS [1] scintillator shell have been transformed into spectra in the rest frame of the fissioning system determined event-wise from the fragment data. The calibration of the CsI(Tl) counters is described in [2]. Acceptance corrections have been simulated for different velocities of the fissioning system. Up to now only the pre-scission component has been analyzed because it is not affected by registration thresholds. The measured LCP spectra are affected by a 50 μm Ni supporting grid of 75% transparency. A special iterative procedure has been applied to accumulated spectra for the correction of this effect. Results of this correction are shown in Fig. 1 for a simulated alpha-spectrum. Experimental LCP spectra have been accumulated only for the most backward angles in order to exclude pre-equilibrium particles and also only perpendicular to the fission axis in order to suppress the post-scission component. LCP yields and nuclear temperatures have been derived by means of fitting using the parametrization of ref. [2] (Fig. 2). Initial excitation energies after incomplete fusion have been estimated from the linear momentum transfer determined from the fragment parameters. For the Th Target at $E^*_{init} \approx 400\ MeV$ the mean multiplicities amounted to 1.63 ± 0.07 for protons and 0.74 ± 0.06 for alphas. The temperatures turned out to be nearly independent of the initial excitation energy and amounted to (4.0 ± 0.2)MeV for protons and (4.3 ± 0.3)MeV for alphas.

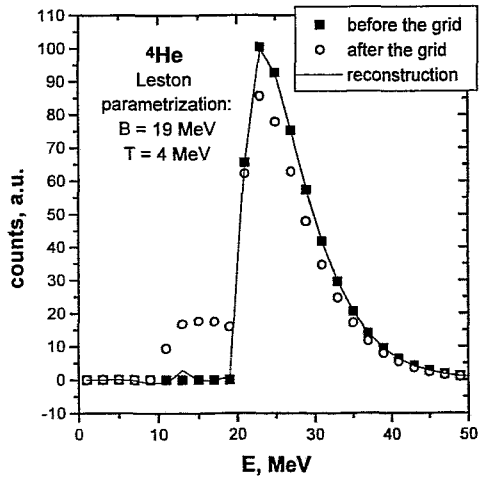

Fig. 1 *Simulated initial alpha spectrum, distorted one after a grid and result of the reconstruction procedure.*

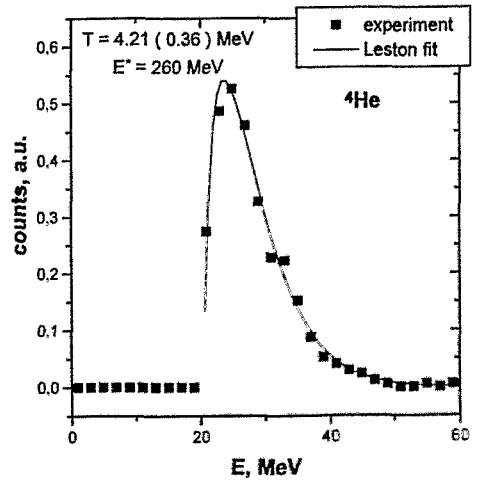

Fig. 2 *Fit of a Maxwell distribution to the pre-scission alpha spectrum from the reaction $^{14}N(53\ AMeV) + ^{232}Th$.*

Some pre-equilibrium contribution seems to extend up to very backward directions. Calculations using the CASCADE code [3] have been started to consider this contribution in the further analysis.

References

[1] H.-G. Ortlepp et al., Nucl. Inst. a. Meth. in Phys. Res. A 403(1998) 65
[2] D.V. Kamanin et al., Preprint FZR-197, to be published in Nucl. Inst. a. Meth. in Phys. Res. A
[3] Y. Schutz et al., Report GANIL P 97 15 (1997)

The Two-Sn Mode in Cold Fission of Cm and Cf Isotopes [B]

Yu.V. Pyatkov[1], A.A. Alexandrov[1], I.A. Alexandrova[1], V.V. Pashkevich[2], Yu.E. Penionzhkevich[2], V.G. Tishchenko[2], A.V. Unzhakova[2], V.A. Maslov[2], I.P. Tsurin[2], H.-G. Ortlepp, P. Gippner, C.-M. Herbach, K.-D. Schilling, W. Wagner, B.I. Fursov[3] and V.F. Mitrofanov[3].

In ref. [1] the manifestation of clustering is investigated by a comparative analysis of cold fission in ^{252}Cf(sf) measured at the FOBOS detector [2] in Dubna, and in ^{249}Cf(n_{th},f) measured at the time-of-flight spectrometer at the reactor of the Moscow Engineering Physics Institute [3]. Cold fission was separated in [1] by cuts in the excitation energy at the scission point which is defined as $E^* = Q_p$ - TKE, where Q_p is the energy release of the reaction and TKE the total kinetic energy of the fragments.

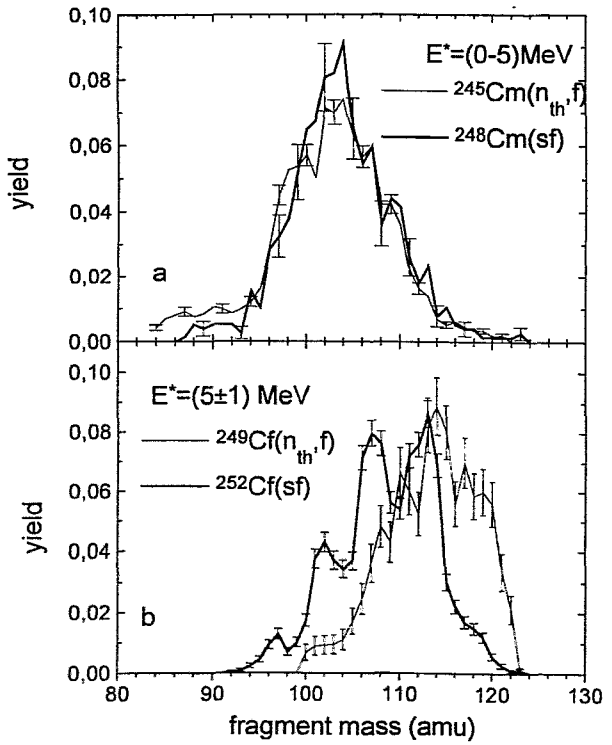

Fig. 1 *Fission fragment mass spectra obtained for the selected excitation energy bins.*

Differences in the mass distributions (fig. 1, bottom) are interpreted on the base of potential energy surface (PES) calculations. A valley representing an overlapping two-Sn configuration influences the induced fission, but not the spontaneous one. It is present in the calculated PES of both ^{250}Cf and ^{252}Cf, but not in the recently calculated PES of ^{246}Cm. Therefore, a comparison of spontaneous and induced fission of Cm isotopes should be of great interest, and further measurements have been performed for ^{245}Cm(n_{th},f) (10^6 fission events) and ^{248}Cm(sf) (5×10^3 events) at the same facilities. In contrast to the Cf case, both Cm measurements show practically identical mass distributions in the cold fission region (fig. 1, top). Because of a too small nucleon content of the Cm isotopes the more overlapping two-Sn configuration cannot create an own valley like in Cf. Consquently, no shift between the two Cm fragment mass spectra is observed.

[1] *Moscow Engineering Physics Institute, 115409, Moscow, Russia*
[2] *Joint Institute for Nuclear Research, 141980, Dubna, Russia*
[3] *Institute for Physics and Power Engineering, 249020, Obninsk, Kaluga Region, Russia*

References

[1] Yu.V. Pyatkov et al., Nucl. Phys. A 624 (1997) 140
[2] H.-G. Ortlepp et al., Nucl. Inst. a. Meth. in Phys. Res. A 403 (1998) 65
[3] A.A. Alexandrov et al., Nucl. Inst. a. Meth. in Phys. Res. A 303 (1991) 323

Comparison of Experimental pp Correlations in Central Ni+Ni Collisions with Results of Transport Models [B,G]

R. Kotte, W. Neubert, C. Plettner and D. Wohlfarth
FOPI collaboration

Small-angle correlations of proton pairs in central collisions of Ni+Ni at 1.93 A·GeV have been investigated with the Helitron/Plastic Wall detector combination of the 4π detector system FOPI at GSI Darmstadt. The deduced space-time extent of the proton emitting source is reported in ref. [1]. Two-proton correlation functions as function of the relative momentum q exhibit a local maximum at $q \simeq 20$ MeV/c. Here we report on a comparison of the momentum dependence of this maximum with corresponding results of transport models.

The full dots in Fig. 1 represent the experimental data for central collisions comprising about 8% of the total cross section. The corresponding correlation functions are defolded with the experimental relative-momentum resolution. Dashed and dotted curves give the results of the pp correlation program of H.W. Barz [2] when using as input the seven-dimensional phase space distributions $f(\mathbf{p}, \mathbf{r}, t)$ of the BUU and IQMD transport models, respectively. An impact parameter of $b = 2$ fm has been used in both models. The results of the calculations have been filtered through the detector acceptance. For the present BUU simulations the medium stiff equation of state (EoS) has been used. Note, that the correlation peak increases (decreases) only slightly (typically less than 3%) if the stiffness of the EoS is changed to soft (hard). The IQMD model (version IQMD-HM with hard EoS and momentum dependent interaction) gives very similar results.

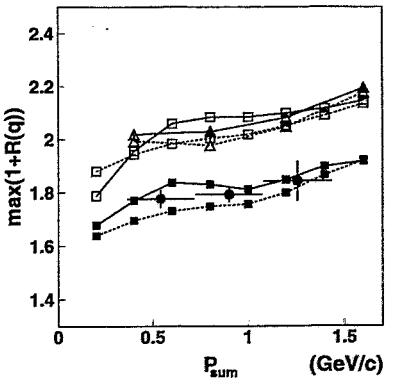

Fig. 1 *The maximum of the experimental relative-momentum correlation function vs. the sum momentum of proton pairs in central Ni+Ni collisions at 1.93 A·GeV (full dots) in comparison with the corresponding results of IQMD (dotted curve) and BUU (dashed and full curves for breakup densities of 0.02 fm^{-3} and 0.01 fm^{-3}, respectively) transport models.*

Both simulations overpredict the peak of the two-proton correlation function. Since not only small relative momenta but also small time differences of the proton pairs influence the correlation peak we suppose that the inadequate description of the experimental data may arise from too compact phase space distributions (also in time) delivered by the transport codes. Indeed, if one reduces in the BUU model the breakup density in the surrounding of the nucleons by a factor of two (from the standard value of 0.02 fm^{-3} to 0.01 fm^{-3}, full curve), the correlation function maximum decreases by more than 10% and even matches well the (slightly increasing with momentum) experimental data. Note, that the average of the corresponding emission time distribution increases only by about 4 fm/c.

However, what cannot be reproduced at all by the transport models is the change [1] of the correlation function maximum if directional cuts are applied to the angle between the difference and the sum of the pair momenta. The difference of longitudinal and transverse correlation functions can easily be substantiated (even with magnitudes of more than 10%) for BUU simulations of central Ni+Ni reactions at 100 A·MeV beam energy, but it is found to vanish almost completely at 400 A·MeV. Thus, it seems questionable whether transport models are able to describe correctly pp correlations at SIS energies.

References

[1] R. Kotte et al., FOPI collaboration, Z. Phys. A 359 (1997) 47
[2] H.W. Barz, pp correlation code, unpublished

Are Light Charged Particles Produced in Central Au + Au Collisions Completely Equilibrated? [B,G]

W. Neubert, R. Kotte, C. Plettner and D. Wohlfarth

Usually, event samples selected by central collision criteria are assumed to be an equilibrated single source which can be characterized by a common temperature. It was noted in ref. [1] that fragment emission in central collisions is incompatible with an equilibrated decay but proceeds via both preequilibrium and equilibrium mechanisms. Recently, this concept was proved in ref. [2] indicating a cooling between successive emission steps. The basic idea of this approach is a comparison of the relative isotopic yields of high energetic particles emitted early in the decay to the relative isotopic abundance of lower energy particles emitted later after the system has cooled. As proposed by Albergo [3] the double yield ratios (R_1,R_2) are related to the temperature by the expression

$$T_{H-He} = \frac{b}{\ln\left(a \cdot (R_1/R_2)\right)}$$

Here we consider the energy dependent yield (Y) ratios R_1= Y(d, E_{k0})/Y(t, E_{k0}) and R_2= Y$(^3He, E_{k0})$/Y$(^4He, E_{k0})$ in which E_{k0}=$E_{cm,i}$ - V_i (i=d, t, ^3He, ^4He) is the particle energy in the c.m.-system prior to Coulomb acceleration (with V_i as Coulomb barrier). The constants b=14.32 and a=1.59 are evaluated from the corresponding binding energies, masses and spin factors.

Kinetic energy spectra of these isotopes produced in central collisions [4] were reanalysed by this method. We evaluated yields in successive steps of E_{k0} to build energy dependent isotopic ratios. The results presented in fig.1 show an uniform trend for the incident energies 100, 150 and 250 AMeV: the higher the particle energy the larger the temperature. This observation suggests that preequilibrium emission contributes to central event samples.

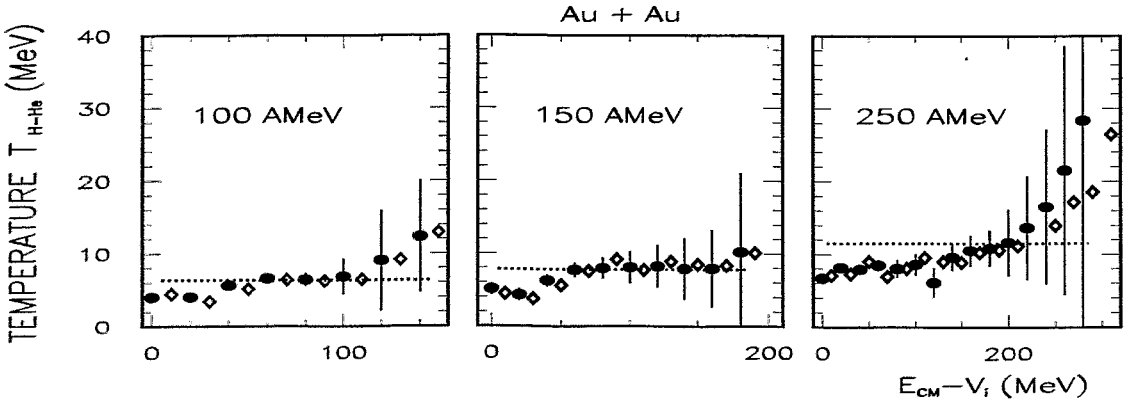

Fig. 1 *Temperature vs. particle energy. The Coulomb barriers V_i are assumed to amount 10 MeV and 20 MeV for Hydrogen and Helium isotopes, respectively. Black points: corrected for V_i, rhombs: without V_i, dotted horizontal lines: average temperature from energy integrated isotopic yields.*

References

[1] D. R. Bowman et al., Phys. Rev. C 52 (1995) 818
[2] H. Xi et al., preprint MSUCL-1073 (May 1997)
[3] S. Albergo et al., Il Nuovo Cimento 89 (1985) 1
[4] G. Poggi et al., FOPI collaboration, Nucl.Phys. A 324 (1993) 177

Fragment Production in 1 GeV Proton Interaction with Carbon [W]

L. N. ANDRONENKO[1],M. N. ANDRONENKO[1],A. A. KOTOV[1],W. NEUBERT, D. M. SELIVERSTOV[1] AND L. A. VAISHNENE[1]

The reaction products emitted from a self-supporting carbon target (800 $\mu g \cdot cm^{-2}$) irradiated by protons ($\simeq 3 \cdot 10^{10} s^{-1}$) from the Gatchina synchrocyclotron were registered by two TOF spectrometers arranged at $\Theta_{lab} = 30^o$ and 126^o with respect to the beam axis. Each arm consists of two transmission PPACs and a twin Bragg IC [1] which allows a reliable detection of all fragments with Z≥2. The measured kinetic energy, energy loss, range and time-of-flight allowed off-line isotope separation of these fragments. Monitoring by the reaction $p+^{27}Al \rightarrow {}^{7}Be+x$ of known formation cross section [2] allowed to convert the measured yields into absolute cross sections. The differential energy spectra (see, e.g. fig.1) of each resolved isotope were fitted by a modified Maxwellian distribution as proposed in ref.[3]. The obtained slope parameters T (apparent temperature) and the relative velocity β of the moving source are compiled in table 1. The transformation of the kinetic energy spectra with these parameters into the c.m. frame suggests the emission from an equilibrated source. But the temperature of ^{3}He is appreciable higher compared with that of ^{4}He, a phenomenon observed in various reactions.

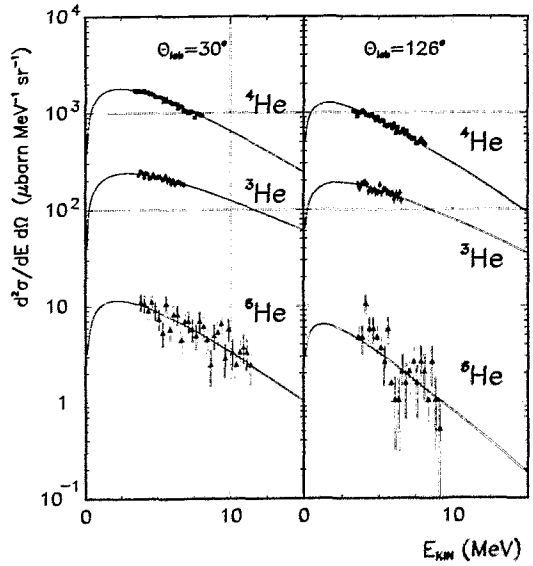

Fig.1 *Differential kinetic energy spectra*

Table 1 *Fragment cross sections and fit parameters of E_{kin} spectra (the errors given in parentheses consider only statistical uncertainties)*

isotope	σ (mbarn)	T (MeV)	$\beta * 10^{-3}$ (units of c)
^{3}He	27.791 (0.559)	6.78 (0.14)	6.7 (0.3)
^{4}He	149.030 (0.600)	5.79 (0.52)	7.6 (0.2)
^{6}He	0.711 (0.038)	6.38 (0.15)	9.2 (0.4)
^{6}Li	9.609 (0.063)	7.11 (0.10)	7.6 (0.2)
^{7}Li	10.371 (0.067)	8.36 (0.10)	8.2 (0.2)
^{7}Be	5.722 (0.070)	11.13 (0.10)	12.5 (0.3)
^{9}Be	3.284 (0.130)	12.68 (0.21)	11.8 (0.3)
$^{10,11}B$	8.201 (0.173)	17.93 (0.14)	11.5 (0.3)

[1] *St.Petersburg Nuclear Physics Institute, 188350 Gatchina, Russia*

References

[1] L. N. Andronenko et al., Nucl. Instr. Meth. A 312 (1992) 467
[2] E. S. Izosimova et al., preprint N^o 87, Khlopin Radium Institute, Leningrad 1978.
[3] G. D. Westfall et al., Phys. Rev. C 17 (1978) 1368

Composite Particles Produced by Coalescence in Central Au + Au Collisions [B,G]

W. NEUBERT, A. S. BOTVINA[1], R. KOTTE, C. PLETTNER AND D. WOHLFARTH

Coalescence is an additional mechanism by which composite fragments are formed in an expanding system. In ref. [1] it was shown that density effects are less important in this process. Therefore, we consider here only the momentum-space coalescence model, i.e. all nucleons having relative momenta smaller than the coalescence momentum $\mathbf{p_c}$ form an appropriate composite particle. The formation probability of a composite fragment is given by an integral over the particle densities in momentum space related to their one-particle distribution functions. This process implemented in the code SMMFC uses an parametrization based on obsolete data [2] and the compilation in ref. [3] concerns only medium-weight systems. There is need to check the applicability of these parameters to the system Au+Au. Since ^3He may be produced favourably by coalescence we investigated the ratio $^3He/^4He$. The calculations were performed with the code SMMFC using the parameter set of ref. [5]. The comparison of calculations and data shown in

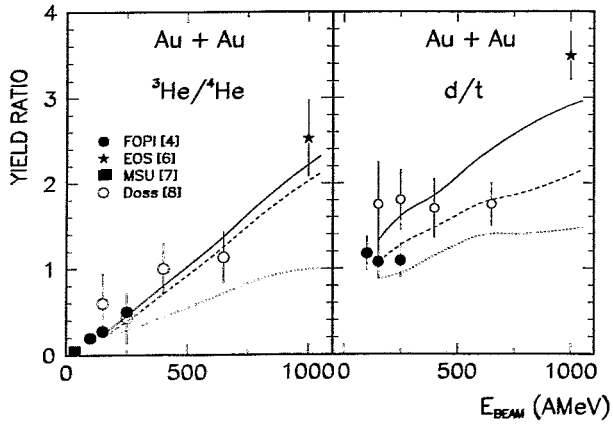

fig. 1 allows the following conclusions: (1) a thermal production mechanism without coalescence underestimates the yield ratios, (2) the coalescence parameters given in the figure caption reproduce the data sufficiently within the whole range of incident energies. Our results confirm the observation of ref. [3] where the coalescence parameters are found to be nearly independent of the incident energy but do decrease with increasing mass of the colliding nuclei. Our coalescence parameters obtained for the Au+Au system agree with systematics.

Fig. 1 *Left panel:* $^3He/^4He$ *ratio vs. beam energy, solid line:* $p_c(^3He)$*=110 MeV/c,* $p_c(^4He)$*=95 MeV/c, dashed line:* $p_c(^3He)$*=110 MeV/c,* $p_c(^4He)$*=100 MeV/c. Right panel: d/t ratio vs. beam energy, solid line:* $p_c(d)$*=90 MeV/c,* $p_c(t)$*= 110 MeV/c, dashed line:* $p_c(d)$*=82 MeV/c,* $p_c(t)$*=115 MeV/c. The dotted lines show the thermal production ratios alone.*

[1] *Hahn-Meitner-Institut Berlin GmbH, Glienicker Str. 100, 14109 Berlin*

References

[1] S.Wang et al., Phys. Rev. Lett. 74 (1995) 2646
[2] V. D. Toneev and K. K. Gudima, Nucl. Phys. A 400 (1983) 173c
[3] S. Das Gupta and A. Z. Mekjian, Phys. Rep. 72 (1981) 131
[4] G. Poggi et al., FOPI collaboration, Nucl.Phys. A 324 (1993) 177
[5] W. Neubert et al., Proc.. Int. Workshop Heavy Ion Physics at Low, Intermediate and Relativistic Energies using 4π Detectors, Poiana Brasov, Romania, Oct 1996, p. 176
[6] M. A. Lisa et al., ibidem, p. 194
[7] M. J. Huang et al., Phys. Rev. Lett. 78 (1997) 1648
[8] K. G. R. Doss et al., Phys. Rev. C 37 (1988) 163

Biomedical Research

Since several years the Institute of Nuclear and Hadron Physics has investigated the possibilities for a transfer of nuclear physics technology to biomedical research. Special aim was put on positron emission tomography (PET) especially when used simultaneously to the tumor therapy with heavy ions. In the future biomedical research with radiation from the new ELBE facility will play an increasing role.

The heavy ion cancer therapy facility at GSI Darmstadt, which has been installed in a collaboration between the GSI Darmstadt, the University Hospital Heidelberg, the DKFZ Heidelberg and the FZ Rossendorf, has been completed in 1997, and the first treatments of tumour patients with beams of ^{12}C have been performed in December 1997. The primary aim of these treatments was to prove the clinical feasibility and reliability of this technically and logistically highly sophisticated facility. Two patients suffering from tumours of the skull base received ^{12}C radiotherapy in combination with high precision photon therapy. The Rossendorf contribution to this project - the positron emission tomography system BASTEI (Beta Activity measurements at the Therapy with Energetic Ions) consists of an in-beam PET-scanner, an extensive software package for controlling the device and handling tomographic data, and a Monte Carlo simulation code predicting from the treatment plan the spatial distribution of β^+-activity that is generated within the irradiated volume via fragmentation reactions between projectiles and atomic nuclei of the tissue. The predicted distributions are compared with those which are measured by PET during the therapeutic irradiations. This allows the accuracy of the irradiation to be evaluated after each therapy fraction.

In general biomedical research using PET will gain considerably from an improvement of the intrinsic spacial resolution of the detectors. The increasing availability of the new high light-yield scintillator LSO (Luthetium Orthosilicate) opens promising perspectives in this respect. LSO will probably replace the current detector material for PET - BGO - within the next years. However, there remains a considerable amount of work to do in order to optimize the processing technology of this new scintillator. Investigations in this field are performed in a collaboration with the University of Warsaw and the Soltan Institute for Nuclear Studies in Otwock-Swierk, Poland.

In a cooperation between the Clinic of Nuclear Medicine of the University Hospital in Dresden and our institute a work in the context of photon activation tomour therapy has been initiated: The role of bremsstrahlung photons following β-decay for the induction of Auger electron emission from certain target atoms has been studied.

Technical Preparations of the Positron Emission Tomograph for the Monitoring of Patient Treatments with Heavy Ion Beams [B]

W. ENGHARDT, H. BRAND[1], B.G. HASCH, R. HINZ, K. LAUCKNER, J. PAWELKE, K. POPPENSIEKER[1], G. RIBITZKI[1], D. SCHARDT[1] AND M. SOBIELLA

In 1997 the installation of the experimental heavy ion tumour therapy facility at GSI Darmstadt has been completed and the clinical operation has been started in December. Simultaneously our positron emission tomograph BASTEI (**Beta** **A**ctivity Mea**S**urements at the **T**herapy with **E**nergetic **I**ons) [1] was prepared for its clinical operation by several technical modifications (cf. cover picture):

A housing of the detector heads and the whole gantry, which fulfils the aesthetic requirements of medical equipment, has been mounted. It has been designed and constructed in the detector laboratory of the institute and was manufactured by Modellbau Dresden GmbH. The step motor control for a precise positioning of the positron camera has been redesigned to reach a user-friendly and safe operation. The basic functionality of the tomograph (start and stop of data acquisition, on-line visualizing of the count rates) has been integrated into the therapy control system, providing access to the device for the therapy operator during patient irradiations. A VME-module has been developed and integrated into the data acquisition system of the tomograph (Real Time Sorter) for connecting this with the beam delivery control unit and for receiving the current values of energy, focus and intensity of the therapy beam. Storing this information together with the list mode annihilation data allows the time dependence of the beam parameters to be recovered after the irradiation. This is an essential condition for a realistic prediction of the spatial distribution of the β^+-activity from the treatment plans for each dose fraction [2].

A large number of software components has been written performing the acquisition, manipulation, inspection and presentation of PET-data, the quick reconstruction by backprojection into a three dimensional image space as well as the weekly and daily checks of the hardware functionality and stability of the tomograph.

Extensively tested versions of the tomographic reconstruction code [3] and the Monte Carlo programme predicting the β^+-activity distributions from the treatment planning [2] have been implemented on a Silicon Graphics PowerChallenge Workstation. The four processor architecture of that computer enables to run several tasks in parallel, ensuring acceptable reaction times during the therapy.

[1] *Gesellschaft für Schwerionenforschung Darmstadt*

References

[1] W. Enghardt et al., IEEE Medical Imaging Conference, Nov. 13-15, 1997, Albuquerque, USA, Conference Records (in press)

[2] B.G. Hasch et al., this Annual Report

[3] K. Lauckner et al., this Annual Report

The First In-Situ PET Monitoring of Tumour Therapy with ^{12}C-Beams [B]

W. Enghardt, J. Debus[1], T. Haberer[2], B.G. Hasch, R. Hinz, O. Jäkel[3], K. Lauckner, M. Krämer[2] and J. Pawelke

At the new experimental heavy ion therapy facility at the GSI Darmstadt the first two patients have been treated with ^{12}C-beams from Dec. 13-17, 1997. The new facility combines several unique features: The intensity controlled rasterscan technique [1], which allows to confine a distribution of biologically most efficient stopping ions exactly to the target volume by magnetically scanning a focused ion beam of variable energy, and a positron emission tomograph [2] for in-situ measuring the spatial distribution which is produced via fragmentation reactions between the incident particles and the atomic nuclei of the tissue [3]. The primary aim of the first patient treatments was to prove the clinical feasibility and reliability of the treatment system, i.e. the chain starting with the diagnostic data, the treatment planning procedure resulting in control data being executed by the therapy unit and checked using the positron emission tomograph, the patient monitors and the quality assurance program. Thus, a female and a male patient both suffering from a craniocervical chordoma growing in close vicinity of the brain stem and the ocular nerve received a ^{12}C-irradiation in combination with a conformal radiotherapy with bremsstrahlung photons, i.e. five and four daily dose fractions, respectively, out of the totally 30 were applied using ^{12}C-beams. The total dose per fraction was subdivided into two irradiation fields each delivering a physical target dose of 0.5 Gy. The almost opposing ^{12}C-fields entered the patients' heads from the left and the right hand side (cf. [4]). All the 18 irradiations have been monitored by means of PET. The PET-measurements represent only a negligible amount of the time in the treatment schedule: After immobilizing the patient and verifing the position the positron camera was moved to its measuring position. Before switching on the beam the PET list mode data acquisition was started by the therapy operator. The measurement was stopped and the positron camera was removed to its park position shortly before the patient was remobilized. Typical count rates of about 200 cps were observed. The list mode data were transferred to the Silicon Graphics PowerChallenge workstation at FZ Rossendorf running the iterative tomographic reconstruction code [5]; the results became available at GSI after about one hour. According to the rather low dose applied per fraction, the β^+-activity distributions had to be reconstructed from only about 40.000 true coincidences for each irradiation leading to a high noise in the reconstructed images. In order to obtain tomographic data in a form which should enable the clinician to distinguish real details from artefactual and noise structures the texture dependent non linear filter algorithm of [6] has been extended to three dimensions and applied to the data. The superposition of the filtered PET-images onto X-ray computed tomograms (cf. [4]) allows a comparison of the different fractions. Visual inspection of that images did not reveal any significant deviations from fraction to fraction and indicated that sensitive structures could be separated from the target volume.

[1] *Universität Heidelberg*
[2] *Gesellschaft für Schwerionenforschung Darmstadt*
[3] *Deutsches Krebsforschungszentrum Heidelberg*

References

[1] T. Haberer et al., Nucl. Instrum. Meth. A330 (1993) 296
[2] W. Enghardt et al., IEEE Medical Imaging Conference, Nov. 13-15, 1997, Albuquerque, USA, Conference Records (in press)
[3] J. Pawelke et al., IEEE Trans. Nucl. Sci. 44 (1997) 1492
[4] B.G. Hasch et al., this Annual Report
[5] K. Lauckner et al., this Annual Report
[6] S. Webb et al., Nucl. Instrum. Meth. A269 (1988) 451

PET-Based Treatment Plan Verification in Heavy Ion Therapy at GSI [B]

B.G. HASCH, W. ENGHARDT, R. HINZ, K. LAUCKNER, J. PAWELKE

In-situ treatment plan verification for the heavy ion tumour therapy at GSI makes use of in-beam positron emission tomography (PET) to verify the dose distribution. But the measured PET-pattern does not match directly the dose distribution (Fig. 1). However, the measured β^+-activity can be correlated to the dose by means of model calculations. We have adaped our model [1] developed on the basis of the irradiation of plastic phantoms and phantoms of tissue equivalent materials to the treatment plan verification in the heavy ion tumour therapy. The treatment planning results in an individual data set which controls the beam delivery. For predicting the β^+-activity corresponding to the planned dose distribution this data set and the X-ray computed tomograms are combined with the precalculated β^+-emitter distributions caused by monoenergetic ^{12}C beams in homogeneous standard material (PMMA). The comparison between the model prediction and the measured β^+-activity within the target can help to decide whether there are deviations between the treatment plan and the treatment or not. The patients get the whole treatment dose divided into several daily fractions. The time dependence of the beam intensity differs from fraction to fraction and influences the measured β^+-activity especially if the irradiation stops in between and continues after a certain time. Just for that special case it is necessary and with our model even possible to recalculate the β^+-activity distribution after the irradiation taking into account this time dependence.

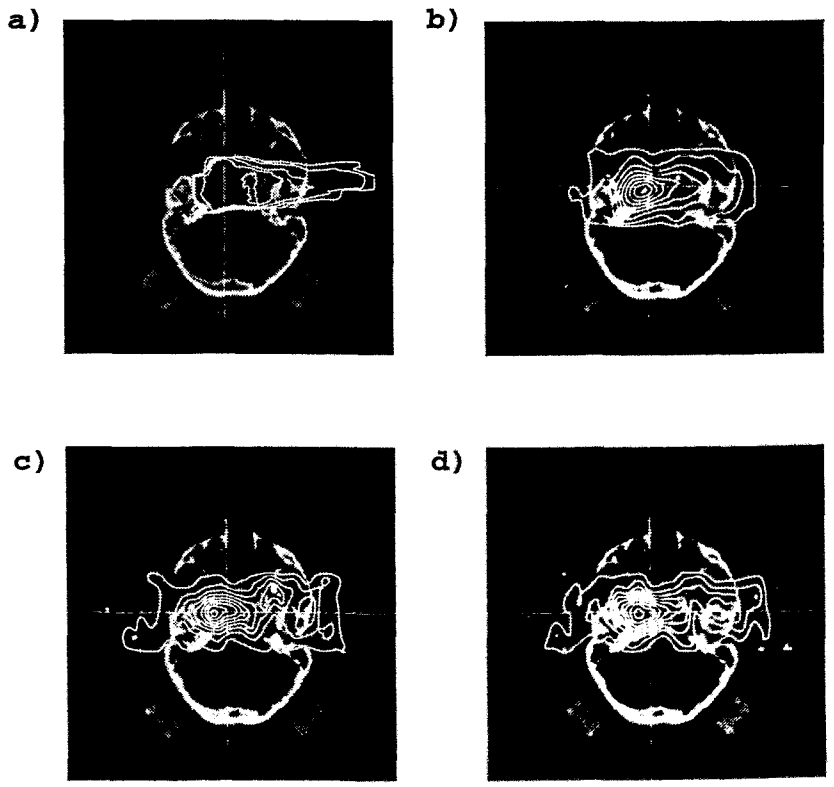

Fig. 1 *X-ray computed tomograms of a patient that has been irradiated with ^{12}C in Dec. 1997. The contour plots superimposed show a) the dose distribution of an irradiation field hitting the patient from the left, b) the precalculated β^+-activity distribution as well as c) and d) the measured β^+-activity distribution for the fraction 1 and 5, respectively. The isodose and isoactivity lines are spaced by 20 % and 10 % of the maximal value.*

References

[1] B.G. Hasch et al., Annual Report 1996, FZR-179 (1997) 87

Performance Study of 3D MLE-Algorithm for Limited Angle PET [B]

K. Lauckner, W. Enghardt and R. Hinz

The MLE-algorithm [1] has been adapted to the limited angle double head positron camera that is installed at the medical beam line at GSI Darmstadt [2]. Unfortunately, it is not possible to measure or calculate the system matrix exactly. In practice this matrix is computed by means of a Monte Carlo procedure that samples the matrix only for the coincidence channels really measured and that takes into account the detector geometry, the detection efficiency, random coincidences and the shift variance of the point spread function. However, each model simplifies the image formation process and includes noise. We demonstrate the performance of the algorithm by the imaging of five point-like sources of ^{22}Na of 2 mm diameter in five independent measurements. The sources have been distributed over a field of view (FOV) as it is typical for tumor therapy (Fig. 1). The mean value of the totally measured counts is about 3.1 million. The reconstruction was performed in an image space of $200 \times 60 \times 50$ voxels (size: 1.6875 mm). The 100. iterative solution is shown in Fig. 1. The characteristics of MLE algorithm have been studied with respect to:

1. Spatial resolution: Table 1 displays the mean value of FWHM determined by a Gaussian fit for each point source extracted from the five measurements. A significant loss of resolution in the z-direction due to the limited angle geometry and a very slight degradation in the x- and y-directions with increasing distance to the centre of FOV of the positron camera are observed.
2. Geometrical fidelity of the position: Table 2 displays the distance between several point sources using the mean values obtained by Gaussian fits. The geometrical fidelity is guaranteed independently of the direction.
3. Recovering the count rate: Table 3 compares the count rates for each of the five points sources obtained from tomographic reconstruction and derived from the source activity. The measured values for sources near to the centre of the FOV are significantly lower ($\sim 10\,\%$). This may be due to an imperfect modelling of the small gaps (width $\sim 2\,$mm) in the detector surfaces which were unavoidable in the construction of the detector heads.

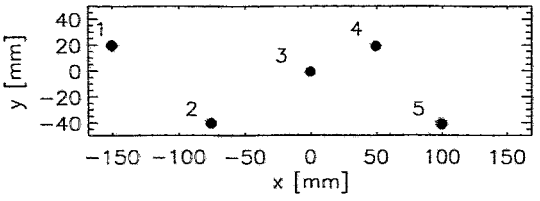

Fig. 1 *100. Iterative solution of 5 point sources*

Table 1 *FWHM of five point sources*

No	x-axis [mm]	y-axis [mm]	z-axis [mm]
P_1	5.00 ± 0.14	5.14 ± 0.23	11.12 ± 1.63
P_2	4.96 ± 0.23	4.96 ± 0.27	9.76 ± 1.20
P_3	4.82 ± 0.09	4.84 ± 0.11	8.16 ± 0.72
P_4	4.94 ± 0.11	4.98 ± 0.09	9.14 ± 0.98
P_5	5.00 ± 0.14	4.98 ± 0.17	10.26 ± 1.01

Table 2 *Geometrical fidelity of the positions*

Distance	Measured distance [mm]	Calculated distance [mm]
$\overline{P_1P_3}$	151.53 ± 0.35	151.33
$\overline{P_1P_2}$	95.97 ± 0.19	96.05
$\overline{P_3P_4}$	53.76 ± 0.23	53.85
$\overline{P_3P_5}$	107.68 ± 0.18	107.70
$\overline{P_2P_5}$	175.12 ± 0.21	175.00

Table 3 *Recovering the count rate*

No	Count rate in ROI	Expected count rate
P_1	$(4.59 \pm 0.11) \cdot 10^7$	$(4.34 \pm 0.17) \cdot 10^7$
P_2	$(4.56 \pm 0.10) \cdot 10^7$	$(4.43 \pm 0.18) \cdot 10^7$
P_3	$(4.04 \pm 0.04) \cdot 10^7$	$(4.44 \pm 0.18) \cdot 10^7$
P_4	$(4.19 \pm 0.08) \cdot 10^7$	$(4.51 \pm 0.18) \cdot 10^7$
P_5	$(4.63 \pm 0.09) \cdot 10^7$	$(4.46 \pm 0.18) \cdot 10^7$

References

[1] L.A. Shepp, Y. Vardi, IEEE Trans. Med. Imaging, MI-5 (1986) 61
[2] K. Lauckner et al., Annual Report 1996, FZR-179 (1997)

Pre-clinical Studies on PET Monitoring of Heavy Ion Therapy at GSI Darmstadt [B]

R. Hinz, W. Enghardt, B. G. Hasch, K. Lauckner, J. Pawelke, M. Sobiella

In preparation for the start of the first medical treatments at the experimental heavy ion therapy facility of GSI Darmstadt effort was put into further development of the PET monitoring procedures. In the following brief survey only the main activities are mentioned.

- An essential aim of PET therapy monitoring is the determination of the range of the primary particles from measured β^+-activity profiles. It was observed that the particle range can be obtained from the estimated parameter set describing the β^+-activity profile. This procedure was applied to measure the ranges of monoenergetic ^{12}C ions in tissue samples (brain, muscle, fat) in order to establish a precise relation between the measured Hounsfield units of this tissue from computed tomography and the range of the ions in tissue as a prerequisite for exact treatment planning.
- The range difference between two adjacent energy values in the energy table of the heavy ion synchrotron (SIS) is one mm in water. Experiments were done to find out the minimal number of particles necessary for generating sufficient β^+-emitters to distinguish two energy steps clearly.
- During the irradiations of six minipigs in September 1997 influences of physiological processes (e.g. blood flow and metabolism) on the dose localisation by PET were studied. In comparison with the animal experiment phantoms made of tissue equivalent materials imitating the lung and neck regions were irradiated. The scattering process of the annihilation γ-quanta in the body was investigated, and the scatter correction of PET image reconstruction was improved.
- The conventional raster scan beginning with the distal dose contour has the drawback that PET is not able to track the beam to the proximal part of the target volume (Fig. 1, left). The contrary raster scan beginning at the proximal part allows the PET monitoring of the move of the distal β^+-activy edge towards the maximal range (Fig. 1, right).

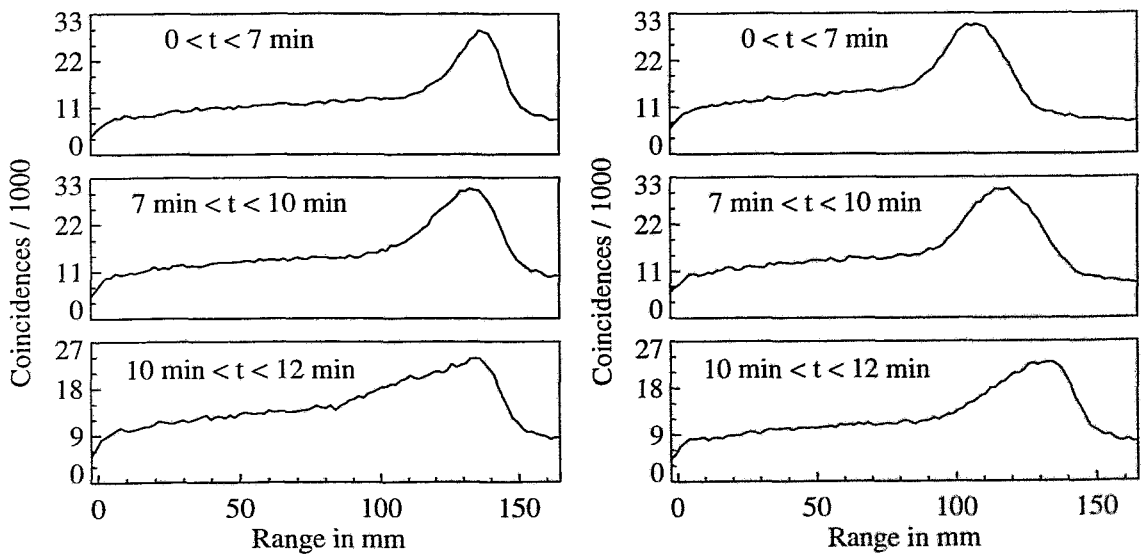

Fig. 1 *The β^+-emitter profiles measured during the irradiation of a 5 Gy dose cube of 4 cm length in a mean depth of 12 cm in a PMMA phantom. Three consecutive time windows from top to bottom. On the left hand side: raster scan in conventional order, i.e. beginning with the highest energy. The decline behind the maximum doesn't move considerably, only the plateau before the peak is widened during the irradiation. On the right: raster scan in reversed order, i.e. beginning with lowest energy. The moving peak indicates the increasing energy of the beam. Consequently, the two bottom plots are almost identical.*

Advantages of LSO Scintillator in High Resolution PET Detectors [B,W]

J. Pawelke, M. Kapusta[1] and M. Moszyński[2]

Most current PET detectors use a design that multiplexes many BGO crystals to few PMTs and is based on sharing scintillation light for position read-out. In order to perform imaging of small animals such as mice and rats, the spatial resolution of these detectors must be improved without deterioration of any other detector property at the same time. Replacing BGO by the new, high light yield scintillator LSO [1] one can expect to be able to reduce the crystal width for higher resolution. We investigated this by direct comparison of scintillator properties of $3\times3\times20$ mm^3 commercially available crystals of LSO (Ramet Ltd., Moscow, Russia) with those of BGO. For this purpose, the light yield, energy resolution, detection efficiency and timing properties have been measured for 511 keV γ-rays of a ^{22}Na source following the methods described in [2,3]. The crystals were prepared by manual polishing of all sides using a 1 μm diamond paste/alcohol mixture. After this, the crystals were wrapped in white teflon tape leaving space for one 3×3 mm^2 side for coupling with a XP2020Q PMT. The results show an approximately four times greater amount of scintillation light collected by the PMT as well as good energy resolution and coincidence timing for LSO in comparison with BGO (table 1). Despite the slightly lower fraction of events which interact photoelectrically, these properties of LSO enable higher spatial resolution, signal-to-noise-ratio and count-rate capability, making this scintillator superior to BGO for PET application.

Furthermore, we investigated the light collection efficiency for LSO crystals as a function of surface finish and crystal size. For this purpose, we directly compared the light yield measured for a crystal with roughened sides with that of the same crystal after polishing for two different crystal sizes (table 2). We repeated these measurements using multiple BGO crystals of varying size cut from adjacent pieces of the same boule, in order to minimize the systematic errors due to sample to sample variations. The reported results for each BGO crystal size are thus an average over five individual crystals (table 2). The light collection is strongly increased due to polishing and is only weakly influenced by geometry. Therefore, the precise crystal size may be chosen for reasons other than light collection efficiency. However, further effort is needed to reduce processing and handling costs of surface finish.

Table 1 *Main crystal parameters*

Scintillator	Light yield [photons/MeV]	Energy resolution (FWHM) [%]	Coincidence time resolution[a] (FWHM) [ns]	Photoelectric fraction[b]
BGO	3767±602	17.0±2.3	7.70±0.60	1.00±0.00
LSO	17010±3553	11.0±0.6	0.59±0.04	0.94±0.01

[a]) 300 keV low energy threshold set [b]) relative values

Table 2 *Geometry and surface treatment dependence of the photoelectron yield [phe/MeV]*

Scintillator	LSO		BGO		
Crystal size [mm^3]	3 × 3 × 20	2 × 2 × 15	3 × 3 × 20	1.7 × 1.7 × 15	1.7 × 1.7 × 10
all sides roughened	1166±227	996±213	319±72	240±98	184±28
all sides polished	3572±576	3529±571	565±64	518±82	441±33

[1] *Institute of Experimental Physics, University of Warsaw, PL-00-681 Warsaw, Poland*
[2] *Soltan Institute for Nuclear Studies, Dept. of Nuclear Electronics, PL-05-400 Otwock-Świerk, Poland*

References

[1] C.L. Melcher and J.S. Schweitzer, IEEE Transact. Nucl. Sci. NS-39 (1992) 502
[2] M. Moszyński et al., IEEE Transact. Nucl. Sci. NS-44 (1997) 1052
[3] M. Kapusta et al.,"Comparison of YAP and BGO for high resolution PET detectors", Nucl. Instrum. Methods (in press)

Investigation of Samples for Photon Activation Therapy

H. LINEMANN[1], R. SCHWENGNER, J. PINKERT[1], G. WUNDERLICH[1],
W. SCHULZE AND U. OEHMICHEN

Auger electrons emitted within a cell nucleus are of high biological effectiveness. In photon activation therapy (PAT) external photons induce the emission of Auger electrons by certain target atoms implanted in a cell nucleus. Focusing the external radiation enables tumour cells to be destroyed without damaging the surrounding tissue.

Our aim was to investigate whether emission of Auger electrons may be induced by bombarding selected target atoms with bremsstrahlung radiation or γ rays following the β decay of radionuclides. Here, the photon energy must exceed the binding energy of a K-electron of the target atom. The target atom should have a large Z to maximise the cross section of photoelectric absorption. A proof of the excitation of the target atoms is possible only by measuring fluorescence X-rays emitted in competition with Auger electrons. The investigated samples consisted of compounds with iodine (KI) or platinum (Cis-Pt) as a target combined with the radionuclides ^{131}I or ^{169}Er, respectively, in solutions. Amounts of 1 ml with an activity of $A \approx 0.5$ MBq in a thin plastic container were placed on a low-energy photon spectrometer. Parts of the measured spectra of the combinations KI - ^{131}I and Pt - ^{131}I are shown in Fig. 1. While the intensities of the $K_{\alpha 1}$, $K_{\alpha 2}$ X-rays of Pt and I are nearly equal in combination with ^{131}I, those of Pt are by a factor of $\approx$ 200 smaller than those of I in combination with ^{169}Er. This difference suggests that the 65.1 and 66.9 keV X-rays of Pt are mainly induced by the 80.2 keV γ ray from ^{131}I decay, whereas the excitation by ^{169}Er, which decays via 49.8 and 50.7 keV γ rays, is very small. Summarising, fluorescence X-rays of the selected target atoms can be induced by radionuclides with γ rays of appropriate energy but scarcely by bremsstrahlung. An increase of the target concentration causes an increase of the X-ray intensity which is proportional up to 50 mg/ml for KI - ^{169}Er but then becomes smaller. A quantitative estimate of the intensity of Auger electrons, which is in the order of 14 % and 4 % of the intensity of the fluorescence X-rays in I and Pt [1], respectively, requires further measurements.

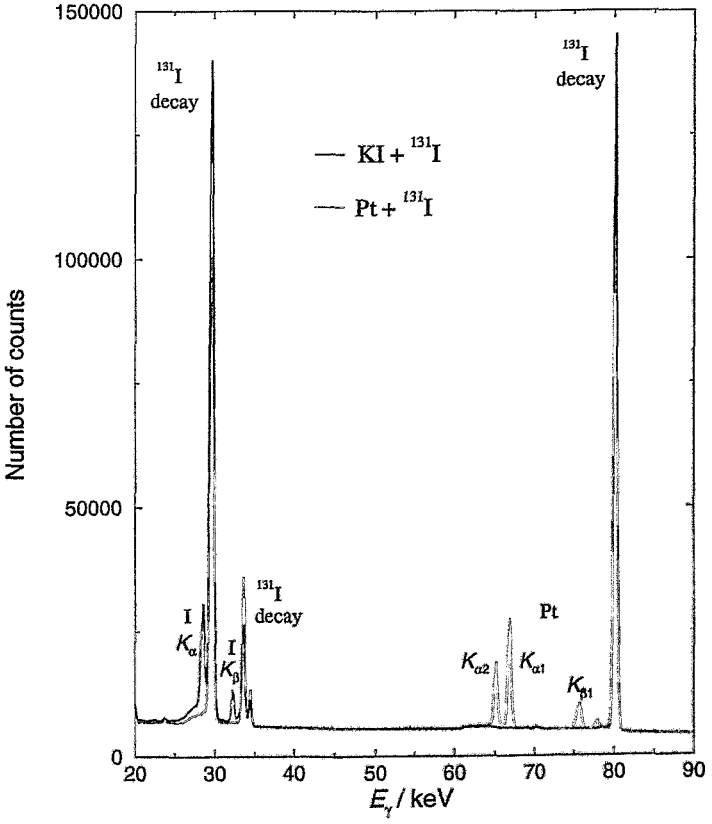

Fig. 1 *Parts of X-ray spectra measured for target materials KI and Pt combined with* ^{131}I.

[1] *Klinik für Nuklearmedizin des Universitätsklinikums der TU Dresden*

References

[1] R. B. Firestone, V. S. Shirley, eds., Table of Isotopes, John Wiley, New York, 1996

PUBLICATIONS AND TALKS

Publications

Fragmentation of the Yrast Band in ^{186}Os at $I^{\pi} = 18^{+}$ and Disappearance of the Collective Minimum;
(Z. Phys. A 356 (1997) 393-397)

Balabanski, D. L., D. Hr. Hristov, R. M. Lieder, T. Rzaca-Urban, W. Gast, G. Hebbinghaus, A. Krämer-Flecken, **H. Schnare**, W. Urban, R. Wyss

Abstract: High-spin states in ^{186}Os have been populated by the ^{186}W(^{4}He,4n)-reaction at 55 MeV. The emitted γ-radiation was detected with the OSIRIS spectrometer. The yrast band, for which the nucleus has a prolate shape, was found to terminate at $I^{\pi} = 18^{+}$. The γ-ray intensity is then distributed between several irregular sequences. Different to other cases of band termination, the minimum in the total routhian surface corresponding to a collective shape is calculated to disappear in this spin region, although the available spin of the valance nucleons is far from being exhausted. A different structure, which is dominated by non-collective states becomes yrast.

Freeze-Out Time in Ultrarelativistic Heavy Ion Collisions from Coulomb Effects in Transverse Pion Spectra
(Phys. Rev. C 56 (1997) 1553)

Barz, H. W., J. P. Bondorf, J. J. Gaardhøje, H. Heiselberg

Abstract: The influence of the nuclear Coulomb field on transverse spectra of π^{+} and π^{-} measured in Pb + Pb reactions at 158 AGeV has been investigated. Pion trajectories are calculated in the field of an expanding fireball. The observed enhancement of the π^{-}/π^{+} ratio at small momenta depends on the temperature and transverse expansion velocity of the source, the rapidity distribution of the net positive charge, and mainly the time of the freeze-out.

Out-of-Plane Emission of Nuclear Matter in Au + Au Collisions at 100 to 800 AMeV
(Nucl. Phys. A 622 (1997) 573-592)

Bastid, N., A. Buta, P. Crochet, P. Dupieux, M. Petrovici, F. Rami, J. P. Alard, V. Amouroux, Z. Basrak, I. Belyaev, D. Best, J. Biegansky, T. Blaich, R. Čaplar, C. Cerruti, N. Cindro, J. P. Coffin, R. Donà, M. Dželalija, E. Erö, Z. G. Fan, P. Fintz, Z. Fodor, L. Fraysse, R. P. Freifelder, A. Gobbi, G. Guillaume, N. Herrmann, K. D. Hildenbrand, S. Hölbling, B. Hong, S. C. Jeong, F. Jundt, J. Keczkemeti, M. Kirejczyk, P. Koncz, Y. Korchagin, **R. Kotte**, M. Krämer, C. Kuhn, A. Lebedev, I. Legrand, Y. Leifels, C. Maazouzi, V. Manko, G. Mgebrishvili, D. Moisa, J. Mösner, W. Neubert, D. Pelte, C. Pinkenburg, P. Pras, W. Reisdorf, J. L. Ritman, C. Roy, A. G. Sadchikov, D. Schüll, Z. Seres, B. Sikora, V. Simion, K. Siwek-Wilczyńska, V. Smolyankin, U. Sodan, K. M. Teh, L. Tizniti, M. Trzaska, M. Vasiliev, P. Wagner, G. S. Wang, J. P. Wessels, T. Wienold, K. Wiśniewski, D. Wohlfarth, A. Zhilin

Abstract: We present new experimental results concerning the azimuthal distribution of proton-likes, light and intermediate mass fragments at midrapidity for Au(100-800 AMeV) + Au collisions measured with the FOPI phase-I detector at GSI in Darmstadt. The azimuthal distributions are investigated as a function of the collision centrality, the incident energy, the fragment charge and transverse momentum. The azimuthal anisotropy is maximum for impact around 7 fm. Intermediate mass fragments present a stronger out-of-plane emission signal than light fragments and a saturation is reached for $Z \geq 4$. The azimuthal anisotropy increases with the fragment transverse momentum and decreases as the incident energy increases. The azimuthal anisotropy of $Z = 2$ particles investigated as a function of the scaled fragment transverse momentum follows an universal curve for bombarding energies between 250-800 AMeV. A signature for a transition from in-plane to out-of-plane emission is evidenced at the lowest beam energies.

K^+-Production in the Reaction $^{58}Ni + ^{58}Ni$ Incident Energies between 1 to 2 AGeV
(Nucl. Phys. A 625 (1997) 307)

Best, D., N. Herrmann, B. Hong, M. Kirejczyk, J. Ritman, K. Wisńiewski, A. Zhilin, A. Gobbi, K. D. Hildenbrand, Y. Leifels, C. Pinkenburg, W. Reisdorf, D. Schüll, U. Sodan, G. S. Wang, T. Wienold, J. P. Alard, V. Amouroux, N. Bastid, I. Belyaev, G. Berek, J. Biegansky, R. Cherbatchev, J. P. Coffin, P. Crochet, P. Dupieux, Z. Fodor, A. Genoux-Lubain, G. Goebels, G. Guillaume, E. Häfele, F. Jundt, J. Kecskemeti, Y. Korchagin, **R. Kotte**, C. Kuhn, A. Lebedev, A. Lebedev, I. Legrand, C. Maazouzi, V. Manko, J. Mösner, S. Mohren, D. Moisa, W. Neubert, D. Pelte, M. Petrovici, P. Pras, F. Rami, C. Roy, Z. Seres, B. Sikora, V. Simion, K. Siwek-Wilczyńska, V. Smolyankin, A. Somov, L. Tizniti, M. Trzaska, M. A. Vasiliev, P. Wagner, D. Wohlfarth, I. Yushmanov

Abstract: Semi-inclusive triple differential multiplicity distributions of positively charged kaons have been measured over a wide range in rapidity and transverse mass for central collisions of ^{58}Ni with ^{58}Ni nuclei. The transverse mass (m_t) spectra have been studied as a function of rapidity at a beam energy 1.93 AGeV. The m_t distributions of K^+ mesons are well described by a single Boltzmann-type function. The spectral slopes are similar to that of the protons indicating that rescattering plays a significant role in the propagation of the kaon. Multiplicity densities have been obtained as a function of rapidity by extrapolating the Boltzmann-type fits to the measured distributions over the remaining phase space. The total K^+ meson yield has been determined at beam energies of 1.06, 1.45, and 1.93 AGeV, and is presented in comparison to existing data. The low total yield indicates that the K^+ meson can not be explained within a hadro-chemical equilibrium scenario, therefore indicating that the yield does remain sensitive to effects related to its production processes such as the equation of state of nuclear matter and/or modifications to the K^+ dispersion relation.

Evidence for "Magnetic Rotation" in Nuclei: Lifetimes of States in the M1-Bands of ^{198,199}Pb
(Phys. Rev. Lett. 78 (1997) 1868)

Clark, R. M., S. J. Aszatalos, G. Baldsiefen, J. A. Becker, L. Berstein, M. A. Deleplanque, R. M. Diamond, P. Fallon, I. M. Hibbert, H. Hübel, R. Krücken, I. Y. Lee, A. O. Macchiavelli, R. M. MacLeod, G. Schmid, F. S. Stephens, K. Vetter, R. Wadsworth, **S. Frauendorf**

Abstract: Lifetimes of states in four of the $M1$ bands in ^{198,199}Pb have been determined through a Dopplershift attenuation method measurement performed using the GAMMASPHERE array. The deduced $B(M1)$ values, which are a sensitive probe of the underlying mechanism for generating these sequences, show remarkable agreement with tilted axis cranking (TAC) calculations. The results represent clear evidence for a new concept in nuclear excitations: "magnetic rotation."

Azimuthal Anisotropies as Stringent Tests for Nuclear Transport Models
(Nucl. Phys. A 627 (1997) 522-542)

Crochet, P., F. Rami, R. Donà, J. P. Coffin, P. Fintz, G. Guillaume, F. Jundt, C. Kuhn, C. Roy, B. de Schauenburg, L. Tizniti, P. Wagner, J. P. Alard, A. Andronic, Z. Basrak, N. Bastid, I. Belyaev, A. Bendarag, G. Berek, D. Best, J. Biegansky, A. Buta, R. Čaplar, N. Cindro, P. Dupieux, M. Dželalija, Z. G. Fan, Z. Fodor, L. Fraysse, R. P. Freifelder, A. Gobbi, N. Herrmann, K. D. Hildenbrand, B. Hong, S. C. Jeong, J. Kecskemeti, M. Kirejczyk, P. Koncz, M. Korolija, **R. Kotte**, A. Lebedev, Y. Leifels, V. Manko, D. Moisa, J. Mösner, W. Neubert, D. Pelte, M. Petrovici, C. Pinkenburg, W. Reisdorf, J. L. Ritman, A. G. Sadchikov, D. Schüll, Z. Seres, B. Sikora, V. Simion, K. Siwek-Wilczyńska, U. Sodan, K. M. Teh, M. Trzaska, G. S. Wang, J. P. Wessels, T. Wienold, K. Wisńiewski, D. Wohlfarth, A. Zhilin, C. Hartnack

emitted in Au + Au collisions at 600 AMeV have been measured using the FOPI facility at GSI-Darmstadt. Data show a strong increase of the in-plane azimuthal anisotropy ratio with the charge of the detected fragment. Intermediate mass fragments are found to exhibit a strong momentum-space alignment with respect of the reaction plane. The experimental results are presented as a function of the polar center-of-mass angle and over a broad range of impact parameters. They are compared to the predictions of the Isospin Quantum Molecular Dynamics model using three different parametrisations of the equation of state. We show that such highly accurate data provide stringent test for microscopic transport models and can potentially constrain separately the stiffness of the nuclear equation of state and the momentum dependence of the nuclear interaction.

Onset of Nuclear Matter Expansion in Au + Au Collisions
(Nucl. Phys. A 624 (1997) 755)

Crochet, P., F. Rami, A. Gobbi, R. Donà, J. P. Coffin, P. Fintz, G. Guillaume, F. Jundt, C. Kuhn, C. Roy, B. de Schauenburg, L. Tizniti, P. Wagner, J. P. Alard, V. Amouroux, A. Andronic, Z. Basrak, N. Bastid, I. Belyaev, D. Best, J. Biegansky, A. Buta, R. Čaplar, N. Cindro, P. Dupieux, M. Dželalija, Z. G. Fan, Z. Fodor, L. Fraysse, R. P. Freifelder, N. Herrmann, K. D. Hildenbrand, B. Hong, S. C. Jeong, J. Kecskemeti, M. Kirejczyk, P. Koncz, M. Korolija, **R. Kotte**, A. Lebedev, Y. Leifels, V. Manko, D. Moisa, J. Mösner, W. Neubert, D. Pelte, M. Petrovici, C. Pinkenburg, P. Pras, V. Ramillien, W. Reisdorf, J. L. Ritman, A. G. Sadchikov, D. Schüll, Z. Seres, B. Sikora, V. Simion, K. Siwek-Wilczyńska, U. Sodan, K. M. Teh, M. Trzaska, M. Vasiliev, G. S. Wang, J. P. Wessels, T. Wienold, K. Wisniewski, D. Wohlfarth, A. Zhilin

Abstract: Using the FOPI detector at GSI Darmstadt, excitation functions of collective flow components were measured for the Au + Au system, in the reaction plane and out of this plane, at seven incident energies ranging from 100 AMeV to 800 AMeV. The threshold energies, corresponding to the onset of sideward-flow (balance energy) and squeeze-out effect (transition energy), are extracted from extrapolations of these excitation functions toward lower beam energies for charged products with $Z \geq 2$. The transitions energy is found to be larger than the balance energy. The impact parameter dependence of both balance and transition energies, when extrapolated to central collisions, suggests comparable although slightly higher values than the threshold energy for the radial flow. The relevant parameter seems to be energy deposited into the system in order to overcome the attractive nuclear forces.

Development of Segmented Ge Detectors for Future γ-Ray Arrays
(Prog. Part. Nucl. Phys. 38 (1997) 29-37)

Eberth, J., H. G. Thomas, D. Weisshaar, F. Becker, B. Fiedler, S. Skoda, P. von Brentano, C. Gund, L. Palafox P. Reiter, D. Schwalm, D. Habs, T. Servene, **R. Schwengner**, H. Schnare, W. Schulze, H. Prade, G. Winter, A. Jungclaus, C. Lingk, C. Teich, K. P. Lieb and the EUROBALL Collaboration)

Abstract: The EUROBALL Cluster detector is composed of seven encapsulated Ge detectors in a common cryostat with a total volume of 2000 ccm of HP Germanium. The development and the performance of the Cluster detector is summarized. Up to six Cluster detectors were used in pre-EUROBALL experiments at the S-DALINAC Darmstadt, at the tandem-postaccelerator facility of the MPI-K Heidelberg and the UNILAC at GSI. Examples of these experiments – the excitation of dipole modes with (γ, γ')-reactions and the first coincidence spectroscopy of the N=Z-nucleus ^{68}Se with a CIUSTER Cube – are discussed. The development of segmented encapsulated Ge detectors for a MINIBALL at the radioactive beam facility REX-ISOLDE has been launched. The status of the project is presented.

Tilted Rotation of Triaxial Nuclei
(Nucl. Phys. A 617 (1997) 131-147)

Frauendorf, S., J. Meng

Abstract: The Tilted Axis Cranking theory is applied to the model of two particles coupled to a triaxial rotor. Comparing with the exact quantal solutions, the interpretation and quality of the mean field approximation is studied. Conditions are discussed when the axis of rotation lies inside or outside the principal planes of the triaxial density distribution. The planar solutions represent $\Delta I = 1$ bands, whereas the aplanar solutions represent pairs of identical $\Delta I = 1$ bands with the same parity. The two bands differ by the chirality of the principal axes with respect to the angular momentum vector. The transition from planar to chiral solutions is evident in both the quantal and the mean field calculations. Its physical origin is discussed.

Magnetic Dipole Bands in Odd Indium Isotopes Built on the $\pi g_{9/2}^{-1} \otimes \nu h_{11/2}^{2}$ Configuration
(Nucl. Phys. A 621 (1997) 736-744)

Frauendorf, S., J. Reif

Abstract: The structure of the magnetic dipole bands is studied by means of shell-model calculations. The calculations correlate with the data, showing a transition from irregular sequences in the light isotopes to regular bands in the heavy ones. The analysis of the wave functions reveals a more complex mechanism of angular momentum generation than in the Pb isotopes: the shears mechanism of the intruder orbitals and the normal parity neutrons make comparable contributions.

Tilted Rotation of Weakly Deformed and Triaxial Nuclei
(Z. Phys. A 358 (1997) 163-167)

Frauendorf, S.

Abstract: The Tilted Axis Cranking theory is reviewed. It is used to describe the appearance of magnetic rotation in weakly deformed nuclei. The possibility of aplanar solutions and their experimental signature are discussed.

Lineshape, Linewidth and Spectral Density of Parametic X-Radiation at Low Electron Energy in Diamond
(Appl. Phys. Lett. 70 (1997) 267)

Freudenberger, J., H. Genz, V.V. Morokhovskii, V.L. Morokhovskii, U. Nething, A. Richter, J.P.F. Sellschop, R. Zahn

Abstract: Applying an absorber technique, the experimental shape and width of a parametric x-radiation line has been determined. The 9 keV radiation was produced by bombarding a diamond crystal of 55 μm thickness with electrons of 6.8 MeV. The variance of the spectral line distribution was found to depend on the tilt angle of the crystal and to have a magnitude of $\sigma = 51$ eV. Simulations based on a Monte Carlo Method exhibit that the observed variance is mainly influenced by multiple scattering of electrons passing through the crystal (≈ 43 eV) and the finite detector opening (≈ 18 eV), leaving for the intrinsic linewidth a value of the order of 1 eV. The spectral density of the line was found to be $J \approx 10^{-7}$ photons/(electron$\times$sr$\times$eV).

Magnetic Rotation in the ^{105}Sn Nucleus
(Phys. Rev. C 55 (1997) R1)

Gadea, A.,G. de Angelis, C. Fahlander, M. De Poli, E. Farnea, Y. Li, D.R. Napoli, Q. Pan, P. Spolaore, D. Bazzacco, S.M. Lenzi, S. Lunardi, C.M. Petrache, F. Brandolini, P. Pavan, C. Rossi Alvarez, M. Sferrazza, P.G. Bizzeti, A.M. Bizzeti Sona, J. Nyberg, M. Lipoglavsek, J. Persson, J. Cederkäll, D. Seweryniak, A. Johnson, H. Grawe, F. Soramel, M. Ogawa, A. Makishima, R. Schubart, **S. Frauendorf**

Abstract: The structure of ^{105}Sn has been investigated through the ^{50}Cr(^{58}Ni,$2pn$) reaction at a beam energy of 210 MeV. In addition to an extension of the spherical level scheme a regular sequence of dipole transitions has been found. The states of the dipole band are suggested to be built on a neutron $h^2_{11/2}$ excitation coupled to proton particle-hole states, which polarize the core to a slightly prolate shape. The experimental results are in agreement with the prediction of tilted axis cranking calculations, which satisfactorily explain the properties of the band.

Correlations between Resonances in a Statistical Scattering Model
(Phys. Rev. E 56 (1997) 2481)

Gorin, T., **F.-M. Dittes**, M. Müller, I. Rotter T.H. Seligman

Abstract: The distortion of the regular motion in a quantum system by its coupling to the continuum of decay channels is investigated. The regular motion is described by means of a Poissonian ensemble. We focus on the case of only a few channels $K < 10$. The coupling to the continuum induces two main effects, due to which the distorted system differs from a chaotic system (described by a Gaussian): (i) The width distribution for large coupling becomes broader than the corresponding χ^2_K distribution in Gaussian orthogonal ensemble case. (ii) Due to the coupling to the continuum, correlations are induced not only between the positions of the resonances but also between positions and widths. These correlations remain even in the strong coupling limit. In order to explain these results, we relate the width of a trapped resonance state to the distance between its neighboring levels and derive an asymptotic expression for the width distribution for the one channel case.

Fine Structure of the $E1$ Response in ^{140}Ce below the Particle Threshold
(Phys. Lett. B 390 (1997) 49-54)

Herzberg, R.-D., P. von Brentano J. Eberth, J. Enders, R. Fischer, N. Huxel, T. Klemme, P. von Neumann-Cosel, N. Nicolay, N. Pietralla, V. Yu. Ponomarev, J. Reif, A. Richter, C. Schlegel, **R. Schwengner**, S. Skoda, H.G. Thomas, I. Wiedenhöver, G. Winter, A. Zilges

Abstract: The $E1$ response of the semi-magic nucleus ^{140}Ce below the particle threshold was measured in a (γ,γ') experiment utilizing the new Euroball Cluster detector at the S-DALINAC. While the energy averaged data are in good agreement with tagged photon results, here they are resolved for the first time into 54 individual transitions. A quasiparticle-phonon model calculation including up to three-phonon configurations compares well to the extracted strength distribution. The interference between one- and two-phonon contributions is essential for a quantitative reproduction.

Abundance of Δ-Resonances in ^{58}Ni + ^{58}Ni Collisions between 1 and 2 AGeV
(Phys. Lett. B 407 (1997) 115)

Hong, B., N. Herrmann, J.L. Ritman, D. Best, A. Gobbi, K.D. Hildenbrand, M. Kirejczyk, Y. Leifels, C. Pinkenburg, W. Reisdorf, D. Schüll, U. Sodan, G.S. Wang, T. Wienold, J.P. Alard, V. Amouroux, N. Bastid, I. Belyaev, G. Berek, J. Biegansky, A. Buta, J.P. Coffin, P. Crochet, R. Donà, P. Dupieux, M. Eskef, P. Fintz, Z. Fodor, L. Fraysse, A. Genoux-Lubain, G. Goebels,

G. Guillaume, E. Häfele, F. Jundt, J. Kecskemeti, M. Korolija, **R. Kotte**, C. Kuhn, A. Lebedev, I. Legrand, C. Maazouzi, V. Manko, J. Mösner, S. Mohren, W. Neubert, D. Pelte, M. Petrovici, P. Pras, F. Rami, C. Roy, Z. Seres, B. Sikora, V. Simion, K. Siwek-Wilczyńska, A. Somov, L. Tizniti, M. Trzaska, M. A. Vasiliev, P. Wagner, D. Wohlfarth, A. Zhilin

Abstract: Charged pion spectra measured in ^{58}Ni-^{58}Ni collisions at 1.06, 1.45 and 1.93 AGeV are interpreted in terms of a thermal model including the decay of Δ resonances. The transverse momentum spectra of pions are well reproduced by adding the pions orinating from the Δ -resonance decay to the component of thermal pions, deduced from the high transverse momentum part of the pion spectra. About 10 and 18% of the nucleons are excited to Δ states at freeze-out for beam energies of 1 and 2 AGeV, respectively.

Breakup Temperature of Target Spectators in ^{197}Au + ^{197}Au Collisions at E/A = 1000 MeV

(Z. Phys. A 359 (1997) 397-406)

Hongfei Xi, T. Odeh, R. Bassini, M. Begemann-Blaich, A. S. Botvina, S. Fritz, S. J. Gaff, C. Groß, G. Immé, I. Iori, U. Kleinevoß, G. J. Kunde, W. D. Kunze, U. Lynen, V. Maddalena, M. Mahi. T. Möhlenkamp, A. Moroni, W. F. J. Müller, C. Nociforo, B. Ocker, F. Petruzzelli, J. Pochodzalla, G. Raciti, G. Riccobene, F. P. Romano, Th. Rubehn, A. Saija, M. Schnittker, A. Schüttauf, C. Schwarz, **W. Seidel**, V. Serfling, C. Sfienti, W. Trautmann, A. Trzcinski, G. Verde, A. Wörner, B. Zwieglinski

Abstract: Breakup temperatures were deduced from double ratios of isotope yields for target spectators produced in the reaction ^{197}Au + ^{197}Au at 1000 MeV per nucleon. Paris of ^{3,4}He and ^{6,7}Li isotopes and pairs of ^{3,4}He and H isotopes(p,d and d,t) yield consistent temperatures after feeding corrections, based on the quantum statistical model, are applied. The temperatures rise with decreasing impact parameter from 4 MeV for peripheral to about 10 MeV for the most central collisions.

The good agreement with the breakup temperatures measured previously for projectile spectators at an incident energy of 600 MeV per nucleon confirms the universality established for the spectator decay at relativistic bombarding energies. The measured temperatures also agree with the breakup tempertures predicted by the statistical multifragmentation model. For these calculations a relation between the initial excitation energy and mass was derived which gives good simultaneous agreement for the fragment charge correlations.

The energy spectra of light charged particles, measured at $\Theta_{lab} = 150°$, exhibit Maxwellian shapes with inverse slope parameters much higher than the breakup temperatures. The statistical multifragmentation model, because Coulomb repulsion and sequential decay processes are included, yields light-particle spectra with inverse slope parameters higher than the breakup temperatures but considerably below the measured values. The systematic behavior of the differences suggests that they are caused by light-charged-particle emission prior to the final breakup stage.

Light Scattering by a Multicomponent Plasma Coupled with Longitudinal-Optical Phonons: Raman Spectra of *p*-Type GaAs:Zn

(Phys. Rev. B 56 (1997) 9524)

Irmer, G., **M. Wenzel**, J. Monecke

Abstract: The LO-phonon–hole-plasmon coupling is investigated for p-type III-V semiconductors. Due to a large carrier damping, only one coupled LO-phonon–plasmon mode (CPPM) appears. Expressions for the theoretical Raman scattering efficiency of a multicomponent plasma are derived in the random phase approximation. They take into account wave-vector-dependent intraband transitions within the heavy- and light-hole bands as well as interband transitions

between them. Finite lifetime effects were included in a generalized Mermin approximation. The theoretical band shapes of the CPPM at different temperatures are compared with Raman measurements of Zn-doped p-type GaAs in the hole concentration range p=10^{17}-10^{20} cm^{-3}. At low temperatures the contribution of the interband transitions cannot be neglected in the frequency range of the CPPM, resulting in a mode broadening. Agreement between the theoretical band shapes and the Raman spectra is obtained without any fit parameter if the hole concentration p and the mobility μ are derived from the measured Hall values p_H and μ_H evaluted on the basis of a two-band model of the conductivity. Raman measurements of the CPPM in Zn-doped p-type GaP show a different temperature dependence which is explained by the different ratio of the light- to the heavy-hole effective mass on the interband transitions.

The Dielectric Function in p-Type III-V Semiconductors
(J. Phys.: Condens. Matter 9 (1997) 5371-5382)

Irmer, G., J. Monecke, **M. Wenzel**

Abstract: The dependences on frequency, wavevector, temperature, and carrier damping of the dielectric functions of p-type semiconductors with zinc-blende or diamond structure are calculated. Analytic expression are derived in the random-phase approximation, and finite lifetime effects are included in a relaxation time approximation. The ranges of dominant intraband and interband transitions are discussed for the example of GaAs. Interband transitions are very significant at low temperatures and small wavevectors. The theoretical results are compared with light scattering experiments on p-GaAs.

Relativistic Description of Exclusive Deuteron Break-Up Reactions
(Phys. Lett. B 404 (1997) 8-14)

Kaptari, L. P., **B. Kämpfer**, S. M. Dorkin, S. S. Semikh

Abstract: The exclusive deuteron break-up reaction is analyzed within a covariant approach based on the Bethe-Salpeter equation with realistic meson-exchange interaction. Relativistic effects in the cross section, tensor analyzing power and polarization transfer are investigated in explicit form. Results of numerial calculation are presented for kinematical conditions in forthcoming $p + D$ reactions at COSY.

Thermal Dilepton and Open Charm Signals Versus Hard Initial Yields in Heavy-Ion Collisions at RHIC and LHC Energies
(Phys. Lett. B 391 (1997) 185-190)

Kämpfer, B., O. P. Pavlenko

Abstract: The hard initial production of open charm and dileptons is compared with possible thermal signals in heavy-ion collisions at RHIC and LHC energies. Our approach is based on the perturbative QCD mini-jet mechanism of quark-gluon matter formation. The thermal dilepton signal is found to rise much stronger as compared to the hard Drell-Yan background with increasing collider energy and clearly dominates at LHC energy. Oppositely, open charm stems from initial hard production. A possible manifestation of gluon shadowing at RHIC and LHC energies is discussed.

Thermal Open Charm Signals Versus Hard Initial Yields in Ultrarelativistic Heavy-Ion Collisions
(J. Phys. G: Nucl. Part. Phys. 23 (1997) 2001-2011)

Kämpfer, B., O. P. Pavlenko, A. Peshier, M. Hentschel, G. Soff

Abstract: Exploiting a unique set of parton distribution functions we estimate hard processes

for open charm, dilepton and mini-jet production. Assuming rapid thermalization within the mini-jet plasma we follow the evolution (expansion and chemical equilibration) of the parton matter and calculate the energy loss of charm quarks in this environment. A substantial part of charm is expected to thermalize. We try to estimate the thermalized open charm component in the final hadron spectra.

The Structure of ^{113}Sn from Proton and Alpha-Particle Induced Reactions
(Z. Phys. A 358 (1997) 303-315)

Käubler, L., Yu. N. Lobach, V. V. Trishin, A. A. Pasternak, M. F. Kudojarov, H. Prade, J. Reif, **R. Schwengner**, G. Winter, J. Blomqvist, J. Döring

Abstract: The results of in-beam investigations of ^{113}Sn using the (p,n), (p,3n) and (α,n) and (α,2n) reactions are summarized. Excited states have been identified until $E_x = 4715\,\mathrm{MeV}$ and $J^\pi = (27/2^-)$. For a large number of levels mean lifetimes τ have been determined with the DSA method. For the $J^\pi = 25/2^+$ state at $E_x = 4059\,\mathrm{MeV}$, $\tau = 1.0(4)\,\mathrm{ns}$ has been measured with the γ-RF method. The experimental results are compared with the predictions of shell-model calculations. Most of the positive-parity states may be considered as one- or three-quasiparticle neutron excitations of the $2d_{5/2}$, $1g_{7/2}$, $3s_{1/2}$, and $2d_{3/2}$ shells, the negative-parity states as the coupling of one $1h_{11/2}$ neutron to the two- or four-quasiparticle neutron excitations in the even-mass ^{112}Sn core. For the $25/2^+$ isomer the three-quasiparticle neutron configuration $\nu(h^2_{11/2}\, g^{-1}_{7/2})$ has been proposed on the basis of a shell-model analysis using the mass-formula formalism. The experimentally observed yrast states in $^{113}_{50}Sn_{63}$ are compared with the coresponding states in the valence mirror nucleus $^{145}_{63}Eu_{82}$ giving remarkable similarities although the parameters for the shell-model calculations differ considerably. The analysis of nearest-neighbour spacing distributions of experimentally obtained $5/2^+$ states in ^{113}Sn does not allow definite conclusions about regularity or chaos.

Proton-Proton Correlations in Central Collisions of Ni + Ni at 1.93 *A*GeV and the Space-Time Extent of the Emission Source
(Z. Phys. A 359 (1997) 47-54)

Kotte, R., J. Biegansky, J. Mösner, W. Neubert, C. Plettner, D. Wohlfarth, J.P. Alard, V. Amouroux, Z. Basrak, N. Bastid, I. Belyaev, G. Berek, D. Best, A. Buta, R. Čaplar, N. Cindro, J.P. Coffin, P. Crochet, R. Donà, P. Dupieux, M. Dželalija, M. Eskef, P. Fintz, Z. Fodor, L. Fraysse, A. Genoux-Lubain, G. Göbels, A. Gobbi, G. Guillaume, E. Häfele, N. Herrmann, K.D. Hildenbrand, S. Hölbling, B. Hong, F. Jundt, J. Kecskemeti, M. Kirejczyk, M. Korolija, C. Kuhn, A. Lebedev, I. Legrand, Y. Leifels, C. Maazouzi, V. Manko, H. Merlitz, S. Mohren, D. Pelte, M. Petrovici, C. Pinkenburg, P. Pras, F. Rami, W. Reisdorf, J.L. Ritman, C. Roy, D. Schüll, Z. Seres, B. Sikora, V. Simion, K. Siwek-Wilczyńska, U. Sodan, A. Somov, L. Tizniti, M. Trzaska, M.A. Vasiliev, P. Wagner, G.S. Wang, T. Wienold, Y. Yatsunenko, A. Zhilin

Abstract: Small-angle correlations of proton pairs produced in central Ni + Ni collisions at a beam energy of 1.93 *A*GeV are investigated with the FOPI detector system at GSI Darmstadt. Simulaneous comparison of longitudinal and transverse correlation functions with the predictions of the Koonin model allows to unravel the space-time ambiguity of the source extension. The determination of the source rest frame is found essential for the identification of this effect. For the present system, the selection of central events comprising about 8% of the total cross section allows for the isolation of a compact source in momentum space which is centered around the c.m. velocity of the colliding nuclei. Taking into account the strong collective expansion of the participant zone, which introduces a reduction of the extracted source radius of more than 30%, r.m.s. radius and emission time parameters of R_{rms}=(4.2±1.2) fm and t_{rms}=(11^{+7}_{-5}) fm/c are extracted, respectively. In contrast, the analysis of the angle-integrated correlation function

mixes the spatial and temporal size of the source and gives an upper limit R_{rms}=(7.0±0.8) fm of the source radius.

Particle-Hole Induced Intruder Bands in ^{117}Sb and ^{119}Sb
(Phys. Rev. C 56 (1997) 760)

LaFosse, D. R., D. B. Fossan, J. R. Hughes, Y. Liang, **H. Schnare**, P. Vaska, M. P. Waring, J.-y. Zhang

Abstract: Collective structures have been investigated via γ-ray studies in ^{117,119}Sb. Previously observed strongly coupled $(\pi g_{9/2})^{-1}$ bands in both nuclei involving 1p-1h proton excitations across the Z=50 gap have been extended, and a alignment of $h_{11/2}$ neutrons identified. New negative-parity strongly coupled bands based on this proton configuration have also been observed in both nuclei. Decoupled bands involving 2p-2h excitations across the gap have been observed in ^{119}Sb, similar to those presented earlier for ^{117}Sb. These bands are interpreted as due to the coupling of a low-K valence proton to the $(\pi g_{7/2}d_{5/2})^2 \otimes (\pi g_{9/2})^{-2}$ deformed state of the respective $_{50}$Sn core nuclei. Anomalies in the expected $h_{11/2}$ neutron crossing of these bands are discussed.

Identification of Excited States in Doubly Odd ^{110}Sb: Smooth Band Termination
(Phys. Rev. C 55 (1997) R2127)

Lane, G. J., D. B. Fossan, I. Thorslund, P. Vaska, R. G. Allatt, E. S. Paul, L. Käubler, **H. Schnare**, I. M. Hibbert, N. O. Brien, R. Wadsworth, W. Andrejtscheff, J. de Graaf, J. Simpson, I. Y. Lee, A. O. Macchiavelli, D. J. Blumenthal, C. N. Davids, C. J. Lister, D. Seweryniak, A. V. Afanasjev, I. Ragnarsson

Abstract: Excited states in ^{110}Sb have been identified for the first time in a series of γ-spectroscopy experiments using both thin and backed targets, including neutron-fold and recoil-mass measurements to provide unambiguous channel identification. The three decoupled intruder bands observed in ^{110}Sb are based upon configurations involving 2p-2h excitations across the Z = 50 shell gap and show the features of smooth band termination. The yrast intruder band, which has been connected to the low-spin levels, is tentatively identified up to its predicted termination at I^{π}=45^{+}. Excellent agreement with configuration-dependent cranked Nilsson-Strutinsky calculations is obtained for the high-spin states near termination.

Study of Neutron-Rich Nuclei Using Deep-Inelastic Reactions
(Phys. Rev. C 56 (1997) 753)

Lee, I. Y., S. Aszatalos, M.-A. Deleplanque, B. Cederwall, R. M. Diamond, P. Fallon, A. O. Macchiavelli, L. Phair, F. S. Stephens, G. J. Wozniak, **S. G. Frauendorf**, J. A. Becker, E. A. Henry, P. F. Hua, D. G. Sarantites, J. X. Saladin, C. H. Yu

Abstract: We have used the ^{48}Ca + ^{176}Yb reaction to study the population of high-spin states in neutron-rich nuclei by deep-inelastic reactions. Using Gammasphere, we observed gamma transitions from nuclei several neutrons richer than the target. Yrast states with spin up to 20 were populated in this reaction. High-spin states in ^{175,177,178}Yb were observed. In this region of reduced pairing, a reference based on experimental data was used to derive experimental Routhians. Systematics of experimental Routhians in neutron-rich Yb nuclei compare well with cranked shell-model calculations.

Pion Production in Mass-Symmetric Heavy-Ion Collisions at 0.8-1.8 AGeV
(Z. Phys. A 357 (1997) 399-409)

Müntz, C., P. Baltes, H. Oeschler, C. Sartorius, C. Sturm, A. Wagner, C. Bormann, D. Brill, Y. Shin, J. Stein, H. Ströbele, W. Ahner, R. Barth, M. Cieślak, M. Debowski, **E. Grosse**, W. Henning, P. Koczoń, M. Mang, D. Miśkowiec, R. Schicker, P. Senger, B. Kohlmeyer, H. Pöppl, F. Pühlhofer, J. Speer, K. Völkel, W. Waluś

Abstract: Double differential cross section of positively charged pions and protons have been measured in nuclear collisions of mass-symmetric systems (Ne + NaF, Ni + Ni, Au + Au, Bi + Pb) at incident energies between 0.8 and 1.8 AGeV as a function of the centrality of the reaction. Using a magnetic spectrometer pions and protons were detected with laboratory angles between 40 and 48 degrees, and with momenta up to about 1400 MeV/c. This setting allows for the study of pions and protons emitted close to midrapidity. The center-of-mass pion spectra deviate from a Boltzmann distribution. The inverse slope parameters of the high-energetic pions are smaller than those of the proton spectra and they exhibit a weaker centrality dependence. A scenario is presented where the shape of the pion spectra reflects the decay kinematics of nucleonic resonances embedded in the thermal and the collective motion of the nucleons in the reaction zone. The number of emitted pions per participating nucleon is higher for light than for heavy mass systems. For a given mass system, the total pion multiplicity increases linearly with the number of participating nucleons, whereas the multiplicity of high-energy pions increases more than linearly. This result is consistent with a scenario where the high-energy pions are produced in multiple energetic baryon-baryon collisions occurring in the high-density phase of the collision.

Fission of Metal Clusters
(Phys. Rep. 285 (1997) 245-320)

Näher, U., S. Børnholm, **S. Frauendorf**, F. Garcias, C. Guet

Abstract: Experimental results on the fission of doubly and other multiply charged metal clusters are reviewed and examined in the light of a simple model, where the fission barrier is approximated as two charged spheres in near-contact, at a mutual distance given by the balance between Coulomb repulsion and attractive polarization effects. The barriers are estimated for different mass and charge splits and are compared with the activation energy for the competing evaporation process. From the model as well as in experiment one finds a strong preference for singly charged trimers (with two electrons) in the fissionchannel, but also fragments with the higher magic electron numbers 8 and 20 may occur with enhanced abundance. In addition, there is a pronounced odd-even effect. In most of the experiments that have been carried out so far, fission occurs as the termination of a chain of evaporations of neutral atoms. This limits the observations to a range where the surface energy dominates over the Coulomb energy of the fission cluster, explaining the tendency for asymmetric fission and justifying the two-sphere barrier approximation. Conditions favoring symmetric fission and other fission modes specific to highly charged metal drops are discussed, and experimental approaches are suggested.

The Nuclear Structure of ^{126}Te Studied with (d,p), (d,^{3}He) and (d,d') Reactions
(Nucl. Phys. A 625 (1997) 598-620)

Ott, J., C. Doll, T von Egidy, R. Georgii, M. Grinberg, W. Schauer, **R. Schwengner**, H.-F. Wirth

Abstract: At the Munich Tandem Accelerator the reactions ^{125}Te(d,p)^{126}Te, ^{126}Te(d,d')^{126}Te and ^{127}I(d,^{3}He)^{126}Te were measured with deuteron energies between 24 and 28 MeV up to excitation energies of about 3.2 MeV. Using γ-lines from previous (n,γ), (n,n'γ) and (γ,γ') experiments, a level scheme of ^{126}Te up to above 3 MeV was established. The results are compared with quasiparticle-phonon model calculations.

Limitations of the Pulse-Shape Technique for Particle Discrimination in Planar Si Detectors
(IEEE Transact. Nucl. Sci. 44 (1997) 1040)

Pausch, G., M. Moszynski, W. Bohne, J. Cederkäll, H. Grawe, W. Klamra, M.-O. Lampert, P. Rohr, R. Schubart, **W. Seidel**, D. Wolski

Abstract: Limitations of the pulse-shape discrimination (PSD) technique – a promising method to identify the charged particles stopped in planar Si-detectors – have been investigated. The particle resolution turned out to be basically determined by resistivity fluctuations in the bulk silicon which cause the charge-collection time to depend on the point of impact. Detector maps showing these fluctuations have been measured and are discussed. Furthermore we present a simple method to test the performance of detectors with respect to PSD. Another limitation of the PSD technique is the finite energy threshold for particle identification. This threshold is caused by an unexpected decrease of the total charge-collection time for ions with a short range, in spite of the fact that the particle tracks are located in a region of very low electric field.

In-Beam PET Imaging for the Control of Heavy-Ion Tumor Therapy
(IEEE Transact. Nucl. Sci. 44 (1997) 4)

Pawelke, J., **W. Enghardt**, Th. Haberer, B. G. Hasch, R. Hinz, M. Krämer, K. Lauckner, M. Sobiella

Abstract: A method for the in-situ control of the heavy-ion tumor therapy by means of positron emission tomography is introduced. This method is founded on the measurement of the dynamic spatial distributions of β^+-emitters generated by nuclear fragmentation during the irradiation and their relation to the dose. In order to study this relationship and to derive the dose distribution from the measured β^+ activity distribution, a framework of model calculations is used. Results of phantom experiments with ^{12}C ion beams will be presented, demonstrating good agreement between experiment and calculation as well as the possibilities and limits of the PET-technique for treatment plan verification and beam monitoring.

Tilted Rotation and Backbending in an Odd-Proton Nucleus
(Phys. Rev. Lett. 79 (1997) 605)

Pearson, C. J., P. M. Walker, C. S. Purry, G. D. Dracoulis, S. Bayer, A. P. Byrne, T. Kibédi, F. G. Kondev, T. Shizuma, R. A. Bark, G. Sletten, **S. Frauendorf**

Abstract: Tilted-axis rotation, arising from Fermi-aligned configurations, has been observed for the first time to cause backbending in an odd-proton nucleus. In ^{181}Re, two t-bands are found to be energetically favored relative to the usual rotation-aligned s-bands, presenting an alternative form of cold nuclear rotation. Interaction between the bands are weak, and unambiguous comparisons with tilted-axis-cranking calculations can be made.

Charged Pion Production in Au on Au Collisions at 1 AGeV
(Z. Phys. A 357 (1997) 215-234)

Pelte, D., E. Häfele, D. Best, G. Goebels, N. Herrmann, C. Pinkenburg, W. Reisdorf, M. Trzaska, J. P. Alard, V. Amouroux, A. Andronic, Z. Basrak, N. Bastid, I. Belyaev, J. Biegansky, A. Buta, R. Čaplar, N. Cindro, J. P. Coffin, P. Crochet, P. Dupieux, M. Dželalija, J. Erö, M. Eskef, P. Fintz, Z. Fodor, A. Genoux-Lubain, A. Gobbi, G. Guillaume, K. D. Hildenbrand, B. Hong, F. Jundt, J. Kecskemeti, M. Kirejczyk, P. Koncz, M. Korolija, Y. Korchagin, **R. Kotte**, C. Kuhn, D. Lambrecht, A. Lebedev, I. Legrand, Y. Leifels, V. Manko, H. Merlitz, J. Mösner, S. Mohren, D. Moisa, W. Neubert, M. Petrovici, P. Pras, F. Rami, V. Ramillien, J. L. Ritman, C. Roy,

D. Schüll, Z. Seres, B. Sikora, V. Simion, K. Siwek-Wilczyńska, V. Smolyankin, U. Sodan, M. Vasiliev, P. Wagner, G. S. Wang, T. Wienold, D. Wohlfarth, A. Zhilin

Abstract: Charged pions are measured with the 4π detector FOPI at GSI using the Au on Au reaction at 1.06 AGeV bombarding energy. The pion multiplicities η_π increase with the number of participants A_{part}. The average pion multiplicities per participant are $\frac{\langle \eta_{\pi^-} \rangle}{\langle A_{part} \rangle} = 0.0308$ and $\frac{\langle \eta_{\pi^+} \rangle}{\langle A_{part} \rangle} = 0.1082$. These values are only half as large as extrapolated from the low-mass systems studied by Harris et al. The ratio $\frac{\eta_{\pi^-}}{\eta_{\pi^+}}$ increases with A_{part} and decreases with the pion kinetic energies. The pion kinetic energy spectra have concave shapes, their parametrization in terms of thermal Boltzmann distributions yields a low ($T_{l,\pi}$) and high ($T_{h,\pi}$) temperature which change with the cm emission angle Θ of the pions. In the angular range $45° < \Theta < 135°$ the low temperature $\langle T_{l,\pi^-} \rangle$ is larger than $\langle T_{l,\pi^+} \rangle$, the high temperatures $\langle T_{h,\pi^-} \rangle$, $\langle T_{h,\pi^+} \rangle$ are, within experimental uncertainties, the same. The inclusive polar angular distributions of pions are anisotropic, $d\sigma/d\Omega$ increases for forward and backward angles. The forward - backward enhancements are independent of the pion kinetic energies or the number of participants. In addition to the preferred forward - backward emission, also the enhanced emission into the transverse direction Θ=90° is observed for pions with high energies or for pions from near-central collisions. These observations and the shape of the rapidity spectra suggest that pions, emitted from the central rapidity region, are partly rescattered by spectator matter. The strength of the rescattering process depends only weakly on the number of participants. The experimental data are compared to the results of *IQMD/GEANT* calculations using momentum dependent NN interactions and a hard equation of state. The calculated pion multiplicities are approximately 50% larger than experimentally determined; the existence of secondary pion sources is reproduced by the calculation, but their predicted strengths are larger than experimentally observed.

Charged Pions from Ni on Ni Collisions between 1 and 2 AGeV
(Z. Phys. A 359 (1997) 55-64)

Pelte, D., M. Eskef, G. Goebels, E. Häfele, N. Herrmann, M. Korolija, H. Merlitz, S. Mohren, M. Trzaska, J. P. Alard, V. Amouroux, A. Andronic, Z. Basrak, N. Bastid, I. Belyaev, D. Best, J. Biegansky, A. Buta, R. Čaplar, N. Cindro, J. P. Coffin, P. Crochet, P. Dupieux, M. Dželalija, E. Erö, P. Fintz, Z. Fodor, A. Genoux-Lubain, A. Gobbi, G. Guillaume, K. D. Hildenbrand, B. Hong, F. Jundt, J. Kecskemeti, M. Kirejczyk, P. Koncz, Y. Korchagin, **R. Kotte**, C. Kuhn, D. Lambrecht, A. Lebedev, I. Legrand, Y. Leifels, V. Manko, J. Mösner, D. Moisa, W. Neubert, M. Petrovici, C. Pinkenburg, P. Pras, F. Rami, V. Ramillien, W. Reisdorf, J. L. Ritman, C. Roy, D. Schüll, Z. Seres, B. Sikora, V. Simion, K. Siwek-Wilczyńska, V. Smolyankin, U. Sodan, M. Vasiliev, P. Wagner, G. S. Wang, T. Wienold, D. Wohlfarth, A. Zhilin

Abstract: Charged pions from Ni + Ni reactions at 1.05, 1.45 and 1.93 AGeV are measured with the *FOPI* detector. The mean $\pi^\pm$ multiplicities per mean number of participants increase with beam energy, in accordance with earlier studies of Ar + KCl and La + La systems. The pion kinetic energy spectra have concave shape and are fitted by the superposition of two Boltzmann distributions with different temperatures. These apparent temperatures depend only weakly on bombarding energy. The pion angular distributions show a forward/backward enhancement at all energies, but not the $\Theta = 90°$ enhancement which was observed in case of the Au + Au system. These features also determine the rapidity distribution which are therefore in disagreement with the hypothesis of one thermal source. The importance of the Coulomb interaction and of the pion rescattering by spectator matter in producing these phenomena is discussed.

Manifestation of Clustering in the ^{252}Cf(sf) and ^{249}Cf(n_{th},f) Reactions
(Nucl. Phys. A 624 (1997) 140-156)

Pyatkov,Yu. V., V. V. Pashkevich, Yu. E. Penionzhkevich, V. G. Tischenko, A. V. Unzhakova, **H.-G. Ortlepp**, P. Gippner, C.-M. Herbach and W. Wagner

Abstract: A comparative analysis of the high-statistics mass-energy distributions of the fission fragments formed in the ^{252}Cf(sf) and ^{249}Cf(n_{th},f) reactions is performed on the basis of the potential energy surface calculations. The available experimental and theoretical results provide evidence for the existence of fission modes due to the clustering of the fissioning nucleus. In ^{252}Cf one of the modes can be treated as a heavy-cluster decay involving the formation of two fragments close to the magic nuclei of Sn. A sharp drop of the proton odd-even effect is observed at an excitation energy above $E^* \approx 40$ MeV at the scission point, which is presumably associated with the complete clusterization of the fissioning nucleus.

Resonant Photon Scattering on the Semi-Magic Nucleus ^{89}Y up to 7 MeV
(Nucl. Phys. A 620 (1997) 1-15)

Reif, J., P. von Brentano, J. Eberth, J. Enders, R.-D. Herzberg, N. Huxel, L. Käubler, P. von Neumann-Cosel, N. Nicolay, N. Pietralla, H. Prade, A. Richter, C. Schlegel, H. Schnare, **R. Schwengner**, T. Servene, S. Skoda, H.G. Thomas, I. Wiedenhöver, G. Winter, A. Zilges

Abstract: The semi-magic nucleus ^{89}Y has been investigated in a (γ,γ') experiment at an end-point energy of the bremsstrahlung of $E_0 = 7$ MeV. The scattered photons have been detected with a EUROBALL Cluster detector. The observed excitations are discussed in the framework of the shell model and a coupling of the unpaired proton to multi-phonon structures in the doubly even neighbors. Transitions above 4.7 MeV are considered to have E1 character. Around 6.3 MeV an unusually large concentration of E1 strength is found. Its origin is likely to correspond to similar structures in the ^{88}Sr and ^{90}Zr isotones which can be interpreted to result from the constructive interference of strong two-phonon amplitudes with weak admixtures from the low-energy tail of the giant dipole resonance.

Central Collisions of Au on Au at 150, 250 and 400 AMeV
(Nucl. Phys. A 612 (1997) 493-556)

Reisdorf, W., D. Best, A. Gobbi, N. Herrmann, K. D. Hildenbrand, B. Hong, S. C. Jeong, Y. Leifels, C. Pinkenburg, J. L. Ritman, D. Schüll, U. Sodan, K. M. Teh, G. S. Wang, J. P. Wessels, T. Wienold, J. P. Alard, V. Amouroux, Z. Basrak, N. Bastid, I. Belyaev, L. Berger, J. Biegansky, M. Bini, S. Boussange, A. Buta, R. Čaplar, N. Cindro, J. P. Coffin, P. Crochet, R. Donà, P. Dupieux, M. Dželalija, J. Erö, M. Eskef, P. Fintz, Z. Fodor, L. Fraysse, A. Genoux-Lubain, G. Göbels, G. Guillaume, Y. Grigorian, E. Häfele, S. Hölbling, A. Houari, M. Ibnouzahir, M. Joriot, J. Kecskemeti, M. Kirejczyk, P. Koncz, Y. Korchagin, M. Korolija, **R. Kotte**, C. Kuhn, D. Lambrecht, A. Lebedev, A. Lebedev, I. Legrand, C. Maazouzi, V. Manko, T. Matulewicz, P. R. Maurenzig, H. Merlitz, G. Mgebrishvili, J. Mösner, S. Mohren, D. Moisa, G. Montarou, I. Montbel, P. Morel, W. Neubert, A. Olmi, G. Pasquali, D. Pelte, M. Petrovici, G. Poggi, P. Pras, F. Rami, V. Ramillien, C. Roy, A. G. Sadchikov, Z. Seres, B. Sikora, V. Simion, K. Siwek-Wilczyńska, V. Smolyankin, N. Taccetti, R. Tezkratt, L. Tizniti, M. Trzaska, M. A. Vasiliev, P. Wagner, K. Wiśniewski, D. Wohlfarth, A. Zhilin

Abstract: Collision of Au on Au at incident energies of 150, 250 and 400 AMeV were studied with the FOPI-facility at GSI Darmstadt. Nuclear charge ($Z \leq 15$) and velocity of the products were detected with full azimuthal acceptance at laboratory angles $1° \leq \Theta_{lab} \leq 30°$. Isotope separated light charged particles were measured with movable multiple telescopes in an angular range of 6-90°. Central collisions representing about 1% of the reaction cross section were selected by requiring high total transverse energy, but vanishing side flow. The velocity space distributions

and yields of the emitted fragments are reported. The data are analyzed in terms of a thermal model including radial flow. A comparison with predictions of the quantum molecular model is presented.

Comment on "On the Relation between Unimolecular Reaction Rates and Overlapping Resonances"
(J. Chem. Phys. Vol. 106 (1997) 11)

Rotter, I.

Abstract: In a quantum mechanical many-body system at high level density different time scales are created by the trapping effect leading to a saturation of the average decay width of the narrow resonances. The trapping effect is a broading of the distribution of the resonance widths, caused by the bifurcation of widths of neighboring resonances, which finally leads to a separation of the times scales. This saturation corresponds to that obtained by Peskin et al. for the decay rate. Thus, decay rate and average decay width behave in the same manner not only at low but also at high level density. The saturation should be proven experimentally by direct time measurements.

Shape of Collective Flow in Highly Central Au (150 AMeV) + Au Collisions
(Z. Phys. A 358 (1997) 73-80)

Roy, C., C. Kuhn, J. P. Coffin, P. Crochet, P. Fintz, G. Guillaume, F. Jundt, C. Maazouzi, F. Rami, L. Tizniti, P. Wagner, J. P. Alard, V. Amouroux, Z. Basrak, N. Bastid, I. Belyaev, D. Best, J. Biegansky, A. Buta, R. Čaplar, N. Cindro, R. Donà, P. Dupieux, M. Dželalija, Z. G. Fan, Z. Fodor, L. Fraysse, A. Gobbi, N. Herrmann, K. D. Hildenbrand, S. Hölbling, B. Hong, S. C. Jeong, J. Kecskemeti, M. Kirejczyk, P. Koncz, Y. Korchagin, **R. Kotte**, A. Lebedev, I. Legrand, Y. Leifels, V. Manko, G. Mgebrishvili, D. Moisa, J. Mösner, W. Neubert, D. Pelte, M. Petrovici, C. Pinkenburg, P. Pras, W. Reisdorf, J. L. Ritman, A. G. Sadchikov, D. Schüll, Z. Seres, B. Sikora, V. Simion, V. Smolyankin, U. Sodan, M. Trzaska, M. Vasiliev, G. S. Wang, J. P. Wessels, T. Wienold, D. Wohlfarth, A. Zhilin, J. Konopka, H. Stöcker

Abstract: Using the FOPI facility at GSI, charged particles ($1 \leq Z \leq 6$) produced in the Au(150 AMeV) + Au reaction have been measured at laboratory angles $1.2° < \Theta_{lab} < 30°$. Highly central collisions have been selected with two criteria, both dealing with the longitudinal and transverse degrees of freedom of the reaction. The relevance of this selection method is supported by QMD calculations which indicate that such criteria are able to select mean impact parameters less than 2 fm. Bias effects introduced by the criteria have been evaluated. The center-of-mass polar angle distributions of low energy clusters emitted in these central collisions, have been extracted: the intensity ratio deduced for a transverse to longitudinal emission is found to be $R=1.4^{+0.2}_{-0.4}$. Model comparisons using QMD are presented. The value of R appears to depend sensitively on the nucleon-nucleon cross section σ_{nn}. Within this model, a value of $\sigma_{nn}=25\pm5$ mb is derived.

Thermodynamic Properties of the $SU(2)_f$ Chiral Quark-Loop Soliton
(Eur. Phys. J. A 1 (1998) 171-186)

Schleif, M., **R. Wünsch**

Abstract: We consider a chiral one-loop hedgehog soliton of the bosonized $SU(2)_f$ Nambu & Jona-Lasinio model which is embedded in a hot medium of constituent quarks. Energy and radius of the soliton are determined in self-consistent mean-field approximation. Quasi-classical corrections to the soliton energy are derived by means of the pushing and cranking approaches. The corresponding inertial parameters are evaluated. It is shown that the inertial mass is equi-

valent to the total internal energy of the soliton. Corrected nucleon and Δ isobar masses are calculated in dependence on temperature and density of the medium. As a result of the self-consistently determined internal structure of the soliton the scaling between constituent quark mass, soliton mass and radius is noticeably disturbed.

Resolution-Enhanced Spectroscopy of ^{81}Y
(Phys. Rev. C 56 (1997) 729)

Schnare, H., G. Winter, L. Käubler, J. Reif, **R. Schwengner**, J. Döring, G.D. Johns, S.L. Tabor, C.J. Gross, Y.A. Akovali, C. Baktash, D.W. Stracener, F.E. Durham, P.F. Hua, M. Korolija, D.R. LaFosse, D.G. Sarantites, I.Y. Lee, A.O. Macchiavelli, W. Rathbun, A. Van der Molen

Abstract: The fusion-evaporation reaction ^{58}Ni(^{32}S,$2\alpha p$) has been used to study the neutron-deficient isotope ^{81}Y. Multiple particle γ-ray coincidences have been detected by the GAMMASPHERE array combined with the MICROBALL charged-particle detector system. Gamma-ray spectra with an improved resolution have been achieved from an event-by-event determination of the nucleus recoil momentum, thus allowing a precise Doppler-shift correction. In this way a resolution enhancement by a factor 2 was obtained for a 1 MeV γ line. During the analysis an $E_\gamma - E_\gamma$ matrix as well as an $E_\gamma - E_\gamma - E_\gamma$ cube have been used to extend the previously known level scheme to higher spin ($I \approx \frac{57}{2}$) and excitation energy ($E_x \approx 17$ MeV). More than 100 new γ rays and 80 new levels have been added to the level scheme and six new bands have been established. The interpretation of these bands in terms of the cranking model and their comparison with similar bands in neighboring nuclei is discussed.

Interfering Doorway States and Giant Resonances.
I. Resonance Spectrum and Multipole Strengths
(Phys. Rev. C 56 (1997) 1031)

Sokolov, V.V., I. Rotter, D.V. Savin, M. Müller

Abstract: A phenomenological schematic model of multipole giant resonances (GR's) is considered which treats the external interaction via common decay channels on the same footing as the coherent part of the internal residual interaction. The damping due to the sea of complicated states is neglected. As a result, the formation of GR is governed by the interplay and competition of two kinds of collectivity, the internal and external one. The mixing of the doorway components of a GR due to the external interaction significantly influences their multipole strengths, widths, and positions in energy. In particular, a narrow resonance state with an appreciable multipole strength is formed when the doorway components strongly overlap.

Interfering Doorway States and Giant Resonances. II. Transition Strengths
(Phys. Rev. C 56 (1997) 1044)

V.V. Sokolov, I. Rotter, D.V. Savin, M. Müller

Abstract: The mixing of the doorway components of a giant resonance (GR) due to the interaction via common decay channels influences significantly the distribution of the multipole strength and the energy spectrum of the decay products of the GR. The concept of the partial widths of a GR becomes ambiguous when the mixing is strong. In this case, the partial widths determined in terms of the K and S matrices must be distinguished. The photoemission turns out to be most sensitive to the overlapping of the doorway states. At high excitation energies, the interference between the doorway states leads to a restructuring towards lower energies and apparent quenching of the dipole strength.

Two-Phonon J=1 States in Even-Mass Te Isotopes with A=122-130
(Nucl. Phys. A 620 (1997) 277-295)

Schwengner, R., G. Winter, W. Schauer, M. Grinberg, F. Becker, P. von Brentano, J. Eberth, J. Enders, T. von Egidy, R.-D. Herzberg, N. Huxel, L. Käubler, P. von Neumann-Cosel, N. Nicolay, J. Ott, N. Pietralla, H. Prade, S. Raman, J. Reif, A. Richter, C. Schlegel, H. Schnare, T. Servene, S. Skoda, T. Steinhardt, C. Stoyanov, H. G. Thomas, I. Wiedenhöver, A. Zilges

Abstract: Excited states of the nuclei ^{122,126,130}Te were populated via the (γ,γ') reaction at endpoint energies of the bremsstrahlung between 4.5 and 5.5 MeV. Gamma rays were detected with a EUROBALL CLUSTER detector and a single HPGe detector. In all investigated nuclei two or three prominent dipole transitions were identified at $E_\gamma \approx 3$ MeV. The corresponding low-lying $J = 1$ states are interpreted as two-phonon excitations. Quasiparticle-phonon-model calculations predict at about 3 MeV one 1^- state arising from the coupling of the first quadrupole and the first octupole phonon, and one 1^+ state arising from the coupling of the first and the second quadrupole phonon, were the latter has isovector character. Such an excitation mode can be considered as an analogue of the scissors mode in vibrational nuclei. The calculated transition strengths are compatible with experimental ones within a factor of about 1.5.

Dipole Excitations in ^{122}Te, ^{126}Te and ^{130}Te
(Z. Phys. A 358 (1997) 197-198)

Schwengner, R., W. Schauer, G. Winter, P. von Brentano, J. Eberth J. Enders, T. von Egidy, M. Grinberg, R.-D. Herzberg, N. Huxel, L. Käubler, P. von Neumann-Cosel, N. Nicolay, J. Ott, N. Pietralla, H. Prade, S. Raman, J. Reif, A. Richter, C. Schlegel, H. Schnare, T. Servene, S. Skoda, C. Stoyanov, H. G. Thomas, I. Wiedenhöver, A. Zilges

Abstract: Excited states of the nuclei ^{122}Te, ^{126}Te and ^{130}Te were populated via the (γ,γ') reaction at endpoint energies of the bremsstrahlung between 4.5 and 5.5 MeV. Gamma rays were detected with a EUROBALL-CLUSTER detector and a single detector. In all nuclei several dipole transitions were identified at energies around 3 MeV. The lowest corresponding $J = 1$ states are interpreted as two-photon excitations. Quasiparticle-phonon-model calculations predict one 1^- state arising from the coupling of the first quadrupole and the first octupole phonon and one 1^+ state arising from the coupling of the first and the isovector second quadrupole phonon at about 3 MeV. The calculated transition strengths are compatible with experimental ones.

Hole Mobilities and the Effective Hall Factor in p-Type GaAs
(J. Appl. Phys. 81 (1997) 7810)

Wenzel, M., G. Irmer, J. Monecke, W. Siegel

Abstract: We prove the effective Hall factor in p-GaAs to be larger than values discussed in the literature up to now. The scattering rates for the relevant scattering mechanism in p-GaAs have been recalculated after critical testing the existing models. These calculations allow to deduce theoretical drift and theoretical Hall mobilities as functions of temperature which can be compared with measured data. Theoretical Hall factors in the heavy and light hole bands and an effective Hall factor result. The calculated room temperature values of the drift mobility and of the effective Hall factor are 118 cm^2/V s and 3.6, respectively. The fitted acoustic deformation potential E_1=7.9 eV and the fitted optical coupling constant D_K=1.24 $\times$ 10^{11} eV/m are close to values published before. It is shown that the measured strong dependence of the Hall mobility on the Hall concentration is not mainly caused by scattering by ionized impurities but by the dependence of the effective Hall factor on the hole concentration.

Electronic Raman Spectra of Shallow Acceptors in p-Type InP
(Solid State Comm. 104 (1997) 371-374)

Wenzel, M., G. Irmer, J. Monecke

Abstract: Electronic Raman scattering is used to study shallow acceptors in Zn-doped and Cd-doped p-type semiconducting InP in the temperature range between 10 K and 160 K. Well-resolved spectra for the Zn-doped samples are obtained. The transition energies are compared with photoluminescence results from the literature and show a satisfying agreement. The acceptor concentrations of the samples investigated range between $2 \cdot 10^{16}\,\mathrm{cm}^{-3}$ and $9 \cdot 10^{17}\,\mathrm{cm}^{-3}$. A linear correlation between the normalized intensity of the electronic spectrum and the acceptor concentration is found.

Acute Response of Pig Skin to Irradiation with ^{12}C Ions or 200 kV X-Rays
(Acta Oncol. 36 (1997) 637)

Zacharias, T., W. Dörr, **W. Enghardt**, Th. Haberer, M. Krämer, R. Kumpf, H. Röthig, M. Scholz, U. Weber, G. Kraft, Th. Herrmann

Abstract: The acute response of pig skin to treatment with graded doses of high energy carbon ions at the Gesellschaft für Schwerionenforschung (GSI, Darmstadt, Germany) was compared to changes after 200 kV X-irradiation. A recently established model for calculation of the biologically effective dose of heavy ions was used to calculate carbon doses that should be isoeffective to the X-ray doses applied. The parameters of the acute epidermal radiation response assessed were macroscopic symptoms and changes in physiological factors like blood flow (flux, concentration of red blood cells), erythema, trans-epidermal water loss, and skin hydration. The parameters analyzed were the maximum and the mean values of each factor during days 24 to 70 post irradiation. Threshold changes used for quantalisation of the data were the median values of each individual parameter, and dose-effect curves were established by probit analysis. With exception of the maximum change in the concentration of red blood cells ($p<0.02$) no significant differences could be found in the response to X-rays or ions, when the ion doses were weighted by the previously estimated RBE values. These results indicate that the model proposed is valid for the calculation of biological effects of ^{12}C-ions for acute normal skin responses, and may at least for epidermis be applied to treatment planning in clinical radiotherapy.

Conference Contributions and Laboratory Reports

Barz, H. W., J.P. Bondorf, J. J. Gaardhøje, H. Heisenberg:
Freeze-Out Time in Ultrarelativistic Heavy Ion Collisions from Coulomb Effects in Transverse Pion Spectra;
FZR-186 (1997)

Barz, H. W., J.P. Bondorf, J. J Gaardhøje and H. Heiselberg:
Coulomb Effects in Relativistic Nuclear Collisions;
preprint NORDITA - 97/87 N; nucl-th/9711064

Barz, H. W., J.P. Bondorf, J. J Gaardhøje, H. Heiselberg:
Study of Freeze-Out Scenario by Means of Pionic Charge Ratio in Ultrarelativistic Heavy-Ion Collisions;
6. Int. Conf. Nucleus-Nucleus Collisions 1997, Gatlinburg, USA, June 2-6, 1997

Barz, H. W., J.P. Bondorf, J. J Gaardhøje:
Coulomb Effekte in transversalen Pionenspektren in ultrarelativistischen Schwerionenreaktionen;
Verhandl. DPG (VI), 32, 45 (1997)

Barz, H. W.:
Freeze-Out Times Extracted from Coulomb Effects;
Workshop "Space-Time 97", Michigan State University, MI, USA, May 28-31, 1997

Bassini, R., M. Begemann-Blaich, S. Fritz, S. J. Gaff, C. Groß, G. Immé, I. Iori, U. Kleinevoß, G. J. Kunde, W. D. Kunze, U. Lynen, M. Mahi, A. Moroni, T. Möhlenkamp, W. F. J. Müller, B. Ocker, T. Odeh, F. Petruzzelli, J. Pochodzalla, G. Riccobene, F. P. Romano, Th. Rubehn, A. Saija, M. Schnittker, A. Schüttauf, C. Schwarz, **W. Seidel**, V. Serfling, C. Sfienti, W. Trautmann, A. Trzcinski, G. Verde, A. Wörner, H. Xi, E. Zude, B. Zwieglinski:
Nuclear Caloric Curve;
3^{rd} INFN-RIKEN Meeting on Perspectives in Heavy-Ions Physics, Padova, Italy, Oct. 13-15, 1997; Proc. pp. 11

Büchner, A., H. Büttig, **F. Gabriel**, P. Gippner, **E. Grosse**, D. Janssen, U. Nething, F. Pobell, H. Prade, R. Schlenk, K,-D. Schilling, W. Seidel, P. vom Stein, J. Voigtländer, M. Wenzel, W. Wendler, A. Wolf, R. Zahn
The Project of a Far-Infrared FEL at the Rossendorf Radiation Source ELBE;
19^{th} Int. FEL Conference, Beijing, Aug. 18-21, 1997; Book of Abstracts p. 181 (Wed P2-6-99)

Dönau, F.:
From Tilded to Principal Axis Cranking – Mixing of Mean Field Solutions;
Int. Conf. Nuclear Structure and Related Topics, Dubna, Sept. 1997

Dönau, F., H.-G. Ortlepp, W. Wagner und C.-M. Herbach:
Kernspaltung in drei große Fragmente – Neue Ergebnisse vom Rossendorfer FOBOS-Detektor im VIK Dubna;
Jahresbericht 1996, Forschungszentrum Rossendorf, 36-42 (1997)

Enghardt, W., J. Debus, T. Haberer, B. G. Hasch, R. Hinz, O. Jäkel, K. Lauckner, J. Pawelke:
Vorklinische Experimente zur PET-Dosislokalisation bei der Schwerionen-Tumortherapie;
Verhandl. DPG (VI), 32, 53 (1997)

Enghardt, W.:
Positron Emission Tomography for Quality Assurance of Heavy Ion Therapy;
ECAT Technical User Meeting, Dresden, Sept. 5-9, 1997; Proc. p. 3-7

Enghardt, W., J. Debus Th. Haberer, B. G. Hasch R. Hinz, O. Jäkel, K. Lauckner, J. Pawelke:
Quality Assurance of Heavy-Ion Therapy by Means of Positron Emission Tomography;
IEEE 1997 Nuclear Science Symposium and Medical Imaging Conference, Albuquerque, USA, Nov. 9-15; Poster

Frauendorf, S., J. Meng:
Chiralität der Rotation dreiaxialer Kerne;
Verhandl. DPG (VI), 32, 16 (1997)

Gorin, T., **F.-M. Dittes**, M. Müller, I. Rotter, T.H. Seligman:
Correlations between Resonances in a Statistical Scattering Model;
FZR-162 (1997)

Hasch, B. G., **W. Enghardt**:
Monte Carlo Simulation der Erzeugung von Positronenemittern bei der Tumorbestrahlung mit schweren Ionen;
Verhandl. DPG (VI), 32, 53 (1997)

Hasch, B. G., **W. Enghardt**, R. Hinz, K. Lauckner, J. Pawelke, M. Sobiella, Th. Haberer, M. Krämer:
In-Beam PET Imaging Heavy-Ion Tumor Therapy;
XV ISIAC Seminar, Budapest, Hungary, July 31 - Aug. 1, 1997

Herbach, C.-M., H.-G. Ortlepp, P. Gippner, D. V. Kamanin, Yu. E. Penionchevich, G. Renz, K.D. Schilling, O.V. Strekalovsky, V.G. Tichtchenko, W. Wagner:
Drei-Fragment-Zerfälle in der Reaction ^{14}N(53 AMeV) + ^{197}Au und ^{232}Th;
Verhandl. DPG (VI), 32, 13 (1997)

Herbach, C.-M., H.-G. Ortlepp, A. A. Aleksandrov, I. A. Aleksandrova, L. Dietterle, V. N. Doronin,P. Gippner, S. A. Ivanovsky, D. V. Kamanin, A. Matthies, Yu. E. Penionzhkevich, Yu. V. Pyatkov, G. Renz, K. D. Schilling, D. I. Shishkin, O. V. Strekalovsky, V. G. Tichtchenko, I. P. Tsurin, C. Umlauf, W. Wagner, M. Wilpert and V. E. Zhuchko:
Collinear Tripartition of Hot Heavy Nuclei below the Multifragmentation Threshold;
214-th National ACS Meeting "Probing Nuclear Matter at Extreme Conditions", Las Vegas, USA, Sep 8-11, 1997

Herbach, C.-M., **H.-G. Ortlepp** and W. Wagner for the FOBOS collaboration:
Decay Study of Hot Nuclei below the Multifragmentation Threshold with the FOBOS Detector at Dubna;
VI International School-Seminar on Heavy Ion Physics, Dubna, Russia, Sept. 22-27, 1997

Herbach, C.-M., **H.-G. Ortlepp**, W. Wagner
Decay Study of Hot Nuclei below the Multifragmentation Threshold with the FOBOS Detector at Dubna;
FZR-198, Nov. 1997

Hinz, R., **W. Enghardt**, B. G. Hasch, K. Lauckner, J. Pawelke, M. Sobiella:
Pre-Clinical Studies on PET Monitoring of Heavy-Ion in Therapy by Means of a Dedicated ECAT EXACT System;
ECAT Technical Users Meeting, Dresden, Sept. 5-9, 1997; pp. 7-25

Hinz, R., **W. Enghardt**, B. G. Hasch, O. Jäkel, K. Lauckner, J. Pawelke, M. Sobiella:
Pre-Clinical Studies on PET Monitoring of Heavy-Ion in Therapy at GSI Darmstadt;
6th Workshop on Heavy-Charged Particles in Biology and Medicine, Baveno, Italy, Sept. 29 - Oct. 1, 1997; GSI-Report 97-09 (1997) H9

Irmer, G., **M. Wenzel**, J. Monecke:
Elektronische Ramanstreuung an flachen Akzeptoren in p-InP;
Herbsttreffen der DGKK, Freiberg, 1997

Kamanin, D.V., **C.-M. Herbach**:
Spektroskopie leichter geladener Teilchen mit der CsI(Tl)-Szintillatorschale des FOBOS-Detektors;
Verhandl. DPG (VI), 32, 22 (1997)

Kämpfer, B., A. Peshier, M. Hentschel, G. Soff, O.P. Pavlenko:
Electromagnetic Signals from Deconfined Matter Resulting from Ultrarelativistic Heavy-Ion Collisions;
Int. Conf. on Nucl. Phys. at the Turn of the Millennium, Wilderness. South Africa, March 10-16, 1996

Kämpfer, B., O.P. Pavlenko:
Estimates of Dilepton Spectra from Open Charm and Bottom Decays in Relativistic Heavy-Ion Collisions;
FZR-188 (1997)

Kämpfer, B., O.P. Pavlenko, A. Peshier, M. Hentschel, G. Soff:
Thermal open Charm Signals Versus Hard Initial Yields in Ultrarelativistic Heavy-Ion Collisions;
FZR-189 (1997)

Kaptari, L.P., **B. Kämpfer**, S. M. Dorkin, S. S. Semikh:
Elastic Proton-Deuteron Backward Scattering: Relativistic Effects and Polarization Observables;
FZR-194 (1997)

Lauckner, K., **W. Enghardt**, R. Hinz, J. Pawelke:
Fully 3D Iterative Reconstruction Algorithmus adapted to an ECAT EXACT System with Limited Angle Geometry;
ECAT Technical Users Meeting, Dresden, Sep. 5-9, 1997; p. 5

Kotte, R., J. Bigansky, J. Mösner, W. Neubert, C. Plettner, D. Wohlfarth et al. (FOPI Collaboration):
Proton-Proton Correlations in Central Collisions of Ni + Ni at 1.93 AGeV and the Space-Time Extent of the Emission Source;
FZR-164 (1997)

Kotte, R., W. Neubert, C. Plettner, D. Wohlfarth:
Proton-Proton-Korrelationen bei zentralen Stößen von 2A·GeV Ni + Ni und die Raum-Zeit-Ausdehnung der Emissionsquelle;
Verhandl. DPG (VI), 32, 83 (1997)

Mohren, S. T., J. Kecskemeti, Y. Leifels, Z. Seres, G. Berek, M. Eskef, Z. Fodor, A. Gobbi, N. Herrmann M. Korolija, **R. Kotte**, H. Merlitz, J. Mösner, W. Neubert, D. Pelte, D. Schüll, M. Stockmeier, D. Wohlfarth:
^{40}Ar + ^{40}Ca at 400 AMeV Beam Energy;
GSI 97-1, 51 (1997)

Neubert, W., A. Botvina, J. Biegansky, **R. Kotte**, D. Wohlfarth:
Vorgleichgewichtsemission und Thermalisierung in zentralen Au + Au Stößen im Energiebereich von 150 AMeV bis 1.05 AGeV;
Verhandl. DPG (VI), 32, 14 (1997)

Ortlepp H.-G., W. Wagner, C.-M. Herbach, A. A. Aleksandrov, I. A. Aleksandrova, M. Andrassy, A. Budzanowski, B. Czech, M. Danzinger, L. Dietterle, V. N. Doronin, S. Dshemuchadse, A. S. Fomichev, W. D. Fromm, M. Gebhardt, P. Gippner, K. Heidel, Sh. Heinitz, H. Homeyer, S. A. Ivanovsky, D. V. Kamanin, I. V. Kolesov, A. Matthies, D. May, S. I. Merzlyakov, W. von Oertzen, Yu. Ts. Oganessian, G. Pausch, Yu. E. Penionzhkevich, Yu. V. Pyatkov, R. V. Radnev, G. Renz, L. A. Rubinskaya, I. D. Sandrev, K.-D. Schilling, W. Seidel, D. I. Shishkin, A. P. Sirotin, H. Sodan, O. V. Strekalovsky, V. G. Tishchenko, V. V. Trofimov, I. P. Tsurin, C. Umlauf, D. V. Vakatov, V. M. Vasko, V. A. Vitenko, E. Will, M. Wilpert, R. Yanez, V. E. Zhuchko, P. Ziem, L. Zrodlowski:
The 4π - Fragment - Spectrometer FOBO;
FZR-181 May 1997

Pawelke, J., **W. Enghardt**, B. G. Hasch, R. Hinz, K. Lauckner, M. Sobiella:
Positron Emission Tomography for Quality Assurance of Heavy-Ion Therapy;
6th Workshop on Heavy-Charged Particles in Biology and Medicine, Baveno, Italy, Sept. 29 - Oct. 1, 1997; GSI-Report 97-09 (1997) H5

Pfitzner, A., W. Cassing:
Dynamics of Density Fluctuations;
8th International Conference on Nuclear Reaction Mechanisms; Proc. p. 407

Schneider, Ch., Th. Kirchner, **H. Müller**, Ch. Schneidereit:
Untersuchung der Reaction $p + {}^{12}C \rightarrow K^+ + X$ mit der Methode der Missing-Mass am ANKE-Spektrometer;
Verhandl. DPG (VI), 32, 70 (1997)

Schwengner, R., G. Winter, J. Reif, H. Schnare, T. Servene, **H. Prade**, M. Wilhelm, S. Kasemann, E. Radermacher, P. von Brentano:
Hochspinzustände im N=48 Kern ^{87}Y;
Verhandl. DPG (VI), 32, 36 (1997)

Servene T., J. Reif, H. Schnare, **R. Schwengner**, G. Winter, T. Härtlein, C. Ender, P. Reiter, S. Skoda, H.-G. Thomas, J. Eberth:
Untersuchung der magnetischen Dipolbande in ^{79}Br mit EUROBALL Cluster Detektoren;
Verhandl. DPG (VI), 32, 36 (1997)

Shklyar, V. V., **B. Kämpfer**, B. L. Reznik, A. I. Titov:
Bremsstrahlung in Intermediate-Energy Nucleon Reactions within an Effective One-Boson Exchange Model;
FZR-191 (1997)

Schleif, M., **R. Wünsch**:
Schwerpunktskorrekturen zur Energie des $SU(2)_f$ NJL-Solitons im Medium;
Verhandl. DPG (VI), 32 71 (1997)

Schleif, M., **R. Wünsch** und T. Meissner:
Self-Consistent Pushing and Cranking Corrections to the Meson Fields of the Chiral Quark-Loop Soliton;
FZR 173 (1997)

Schleif, M., **R. Wünsch**:
The Chiral Quark-Loop Soliton in a Hot Gas of Constituent Quarks;
FZR 182 (1997)

Titov, A. I. **B. Kämpfer**, V. V. Shklyar:
Polarization observables in the reaction $NN \rightarrow NN\phi$;
FZR 202 (1997)

Wenzel, M., G. Irmer, J. Monecke:
Elektronische Ramanstreuung an p-InP;
Frühjahrstagung des Arbeitskreises Festkörperphysik der DPG, Münster 1997

Yanez, R., H.-G. Ortlepp, **C.-M. Herbach**, T. Möhlenkamp:
Theoretical Model Simulations of the FOBOS Experiments;
Verhandl. DPG (VI), 32, 76 (1997)

Lectures and Seminars

Barz, H. W.:
Coulomb Effects in Relativistic Heavy-Ion Reactions;
Niels Bohr Institute, Copenhagen, Denmark, Oct. 29, 1997

Dönau, F.:
On the Spin Orientation in Rotating Nuclei;
University Strasbourg, France, March 1997

Dönau, F.:
Generatorkoordinaten-Methode im Fock-Raum;
IKH/FZ Rossendorf, May 1997

Dönau, F.:
Signature Splitting Effects as a Transition from Tilded to Principal Axis Cranking;
Joint Institute of Heavy Ion Research, Oak Ridge, USA, Aug. 1997

Dönau, F.:
Magnetische Rotation;
Lecture, DPG Physikschule "Elementare Kernanregungen", Bad Honnef, Oct. 1997

Dönau, F.:
Berechnung der Signatur-Aufspaltung mit Vielteilchenfunktionen;
IKH/FZ Rossendorf, Dec. 1997

Dönau, F.:
Struktur des Atomkerns;
Course, TU Dresden, SS 1997

Dohrmann, F.:
Untersuchung der elastischen Proton-Proton-Streuung im Bereich hadronischer Resonanzen;
IKH/FZ Rossendorf, May 1997

Dohrmann, F.:
Bericht über die Few-Body XV Konferenz in Groningen, July 22-26,1997;
IKH/FZ Rossendorf, Sep. 1997

Dohrmann, F.:
Bericht über den Workshop "Soft Photons";
IKH/FZ Rossendorf, Dec. 1997

Enghardt, W.:
Simultan-Kontrolle der Tumorbehandlung mit Strahlen schwerer Ionen durch Positronen-Emissions-Tomographie;
Klinik und Poliklinik für Strahlentherapie der Medizinischen Fakultät "Carl Gustav Carus" der TU Dresden, Jan. 14, 1997

Enghardt, W.:
Positron Emission Tomography for Quality Assurance of Heavy-Ion Tumor Therapy;
ECAT Technical Users Meeting, Dresden, Sept. 5-9, 1997

Enghardt, W.:
The Application of PET to Quality Assurance of Heavy-Ion Tumor Therapy;
Annual Meeting of the European Hadron Therapy Group Innsbruck, Oct. 8-11, 1997

Frauendorf, S.:
Chiral Rotation;
Planary talk, Annual Meeting of the German Physical Society, Göttingen, March 1997

Frauendorf, S.:
Spontaneous Breaking of Isospin Symmetry;
Workshop on Radioactive Beams, GSI Darmstadt, May 26, 1997

Frauendorf, S.:
Tilted Cranking;
Gordon Research Conference on Nuclear Chemistry, New London USA, June 15-20, 1997

Frauendorf, S.:
Magnetism and Currents in Clusters and Nuclei;
Int. Symp. on Atomic Nuclei and Metallic Clusters – Finite Many-Fermion Systems, Prague, Czech Rep., Sept. 1-5, 1997

Frauendorf, S.:
Symmetries of the Rotating Mean Field;
Symposium on New Spectroscopy and Nuclear Structure 1997, dedicated to Aage Bohr and Ben Mottelson, Copenhagen, Denmark, Sept. 16-20, 1997

Frauendorf, S.:
Chiral Rotation;
Nuclear Physics Forum, Nuclear Science Division Colloquium, Lawrence Berkeley Laboratory, Berkeley, USA, February 20, 1997

Frauendorf, S.:
Mesoscopic Systems: Nuclei, Clusters and Others;
Colloquium at the Dept. of Physics, University of Notre Dame, USA, March 24, 1997

Frauendorf, S.:
Magnetic Rotation;
TU Dresden, April 12, 1997

Frauendorf, S.:
Cluster Magnetism and Nuclear Rotation;
Nuclear Physics Forum, Nuclear Science Division Colloquium, Lawrence Berkeley Laboratory, Berkeley, USA, Aug. 24, 1997

Frauendorf, S.:
Symmetries of the Rotating Mean Feld;
IKH/FZ Rossendorf, Sep. 1997

Grosse, E.,
Elektromagnetische Strahlung an ELBE;
FEL-Nutzertreffen (Metall- und Halbleiterphysik) im FZR, Dec. 10, 1997

Grosse, E.,
Elektromagnetische Strahlung an ELBE;
FEL-Nutzertreffen (Chemie, Biologie, Medizin) im FZR, Dec. 11, 1997

Herbach, C.-M., für die FOBOS-Kolloboration
Dreifragmentzerfall schwerer Kerne unterhalb der Schwelle zur Multifragmentation;
GSI Darmstadt, Nov. 26, 1997

Herbach, C.-M.:
Spaltung schwerer Kerne in drei Fragmente mit annähernd gleicher Masse;
Institutsseminar, TU Dresden, Dec. 1997

Hinz, R.:
Technisch-physikalische Beiträge zur Einführung des in-situ Monitorings mittels Positronen-Emissions-Tomographie in die klinische Praxis der Schwerionen-Tumortherapie;
Doktorandenseminar am Institut für Biomedizinische Technik, Fakultät Elektrotechnik, TU Dresden, May 14, 1997

Kämpfer, B.:
Quantenfeldtheorie;
Course, TU Dresden, WS 1997/98

Kämpfer, B.:
Symmetrien und Erhaltungssätze;
Course, TU Dresden, SS 1997

Kämpfer, B.:
Elektromagnetische Signale von Deconfinement-Materie;
Arbeitstreffen "Kernphysik", Schleching, March 1997

Kämpfer, B.:
Thermal Open Charm Signals Versus Hard Initial Yields in Relativistic Heavy-Ion Collisions;
Int. Conf. "Strange Quark Matter 97", Santorini, Greece, April 1997

Kämpfer, B.:
Dielectrons from Open Charm and Bottom Decay;
RHIC-Workshop, Brookhaven, USA, July 1997

Kämpfer, B.:
Bremsstrahlung in Nukleon-Nukleon-Stößen;
Hadronseminar, TU Dresden, Nov. 1997

Kämpfer, B.:
Teilchenerzeugung in Schwerionenreaktionen;
Theorie-Kolloquium, TU Dresden, Nov. 1997

Kämpfer, B.:
Bericht über Workshop SSoft Photons";
IKH/FZ Rossendorf, Dec. 1997

Kirchner, T.:
Transmutationen;
IKH/FZ Rossendorf, Jan. 1997

Kotte R.:
Proton-Proton Correlations in Central Collisions of Ni + Ni at 1.93 AGeV and the Space-Time Extent of the Emission Source;
Laboratoire de Physique Corpusculaire, Université Blaise Pascal, Clermont-Ferrand, France, Jan. 1997

Kotte, R.:
pp-Korrelationen in zentralen Schwerionenstößen von Ni + Ni bei 2 AGeV;
IKH/FZ Rossendorf, March 1997

Kotte, R.:
Abschätzungen von Strangeness-Erzeugungsraten in pA-Reaktionen bei 3 GeV im FOPI-Detektorsystem;
IKH/FZ Rossendorf, Sep. 1997

Kotte R.:
Strangeness Production in pA Collisions at SIS Energies;
FOPI Collaboration Meeting, Clermont-Ferrand, France, Oct. 1997

Lauckner, K.:
Algebraische Rekonstruktionsverfahren für einen Emissions-Tomographen zur Qualitätssicherung der Schwerionen-Tumortherapie;
Doktorandenseminar am Institut für Biomedizinische Technik, Fakultät, Elektronik, TU Dresden, May 14, 1997

Neubert, W.:
The ^{3}He/^{4}He Anomaly in Heavy-Ion Reactions – Data and a Possible Explanation;
IV. Workshop on Nonequilibrium Physics at Short Time Scales, Rostock, April 1997

Ortlepp, H.-G.:
Experimente am Spektrometer FOBOS;
IKH/FZ Rossendorf, Nov. 1997

Plettner, C.:
Kaonen-Nachweis mit dem FOPI-Detektor an der GSI;
Hadronenseminar, TU Dresden, Dec. 1997

Prade, H.:
The ELBE Project in the Forschungszentrum Rossendorf;
Gent, Vakroep Subatomare en Stralingsfysikca, Nov. 1997

Pfitzner, A.:
Dynamics of Two-Body Correlations;
Centro Internationale de Ciencias, Cuernavaca, Mexico, March 14, 1997

Pfitzner, A.:
Dynamics of Density Fluctuations;
Invited talk, 8th International Conference on Nuclear Reaction Mechanisms, Varenna, Italy, June 9-14, 1997

Schleif, M.:
Solitonische Feldkonfigurationen des NJL-Modells im Medium;
TU Dresden, May 1997

Seidel, W.:
Überlegungen zu den Undulatoren für ELBE;
FZR, Arbeitstreffen ELBE-Undulatoren, Febr. 1997

Seidel, W.:
Zusammenfassung und Überblick über weltweite Aktivitäten auf dem Gebiet der Anwendung von IR-FEL Strahlung;
FZR-Zentrumsseminar, "Strahlungsquelle ELBE", April 1997

Seidel, W.:
Der ELBE-FEL im Vergleich zu existierenden IR-FEL's;
FEL-Nutzertreffen (Metall- und Halbleiterphysik) im FZR, Dec. 10, 1997

Seidel, W.,
Der ELBE-FEL im Vergleich zu existierenden IR-FEL's;
FEL-Nutzertreffen (Chemie, Biologie, Medizin) im FZR, Dec. 11, 1997

Schneider, Ch.:
ANKE @ COSY: Status and Proposals;
Hadronenseminar, TU Dresden, Nov. 1997

Wenzel, M.:
Erste FEL-Experimente des FZR im Infrarotbereich;
FEL-Nutzertreffen (Metall- und Halbleiterphysik) im FZR, Dec. 10, 1997

Wenzel, M.:
Erste FEL-Experimente des FZR im Infrarotbereich;
FEL-Nutzertreffen (Chemie, Biologie, Medizin) im FZR, Dec. 11, 1997

Wünsch, R.:
Grundlagen des FEL I;
IKH/FZ Rossendorf, Jun. 1997

Wünsch, R.:
Grundlagen des FEL II;
IKH/FZ Rossendorf, Jun. 1997

Wünsch, R.:
Grundlagen des FEL III;
IKH/FZ Rossendorf, Oct. 1997

Wünsch, R.:
Grundlagen des FEL IV;
IKH/FZ Rossendorf, Nov. 1997

Talks of Visitors

Almehed, D., Lund:
A Microscopic Model of Friction in a Complex Quantum Mechanical System;
Jun. 13, 1997

Andrejtscheff, W., Sofia:
Triaxial Shape Asymmetry of Ground States of Even-Even Nuclei with $50 < A < 190$;
Dec. 16, 1997

Backe, H., Mainz:
Erzeugung brillanter Röntgenstrahlung am Mainzer Mikrotron und ihre Nutzung;
May 22, 1997

Bauer, W., Michigan:
Two-Particle Correlations as a Tool to Study Heavy-Ion Collisions;
Jul. 15, 1997

Bjørnholm, S., Copenhagen:
Ähnlichkeiten und Unterschiede zwischen Atomkernen und Metallclustern;
Aug. 29, 1997

Bohn, C., TJL, Newport News VA:
The FEL-Program at the Thomas Jefferson Laboratory (CEBAF);
Oct. 13, 1997

Brenschede, A., Giessen:
Untersuchung der ω-, ϕ-Erzeugung in pp-Stößen;
Oct. 27, 1997

Brinkmann, K.-T., Dresden:
Pionenproduktion in pp-Reaktionen am TOF;
Mar. 24, 1997

Dudek, J., Strasbourg:
Physics of Superdeformed and Hyperdeformed Nuclei;
Jun. 30, 1997

Gallmeister, K., Bielefeld:
Elektrische Abschirmeffekte in kalten QED-Plasmen;
Jun. 13, 1997

Gillitzer, A., Munich:
Antiprotonen und Kaonen aus relativistischen Kern-Kern-Stößen: Sonden aus verdichteter Kernmaterie;
Nov. 27, 1997

Greiner, M., Dresden:
Wavelets: Von der Signalanalyse zur Analyse komplexer Reaktionen;
Jan. 20, 1997

Heinz, U., Regensburg:
Strangeness und chemisches Gleichgewicht in relativistischen Kernen;
Feb. 10, 1997

Kaptari, L.P., Dubna:
Hadron and Electromagnetic Scattering of the Deuteron at Intermediate Energies;
Sep. 30, 1997

Kaptari, L.P., Dubna:
Solution of Bethe-Salpeter Equation;
Oct. 1, 1997

Kaptari, L.P., Dubna:
Selected Processes and Applications;
Oct. 2, 1997

Kotkin, G., V. Serbo, Novosibirsk, Leipzig:
A Possibility to Control the Polarization of High-Energy Photons by Means of a Laser Beam;
Jun. 27, 1997

Lange, S., Dresden:
Datenanalyse mit neuronalen Netzen;
Feb. 19, 1997

Llacer, J., Berkeley:
Maximum Likelihood Estimation in Image Reconstruction;
Oct. 29, 1997

Moszynski, M., Swierk:
Application of Avalanche Photodiodes in Scintillation Detectors;
May 5, 1997

Mühlschlegel, B., Köln:
Alte und neue Probleme der Supraleitung kleiner Systeme;
May 30, 1997

Pavlenko, O.P., Kiev:
Electromagnetic Radiation of Fast Electrons Passing throught Matter: Landau-Pomerantchuk Effect;
Dec. 15, 1997

Rainer, D., Bayreuth:
Triplet-Pairing in Superfluidem ^{3}He;
Apr. 7, 1997

Ring, P., München:
Relativistische Beschreibung der Kernstruktur;
Apr. 14, 1997

Schneidmiller, E.A., Samara:
Analytical and Numerical Methods for the Calculation of LINAC-Based Free-Electron Lasers;
May 13, 1997

Sashkov, S., Dubna:
Möglichkeiten der Infraroten Fourier-Spektroskopie für Lichtanalyse;
Aug. 4, 1997

Strekalovsky, O., Dubna:
New Aspects in the Development of Automation Systems in the Industry
Dec. 1997

Tichtchenko, V., Dubna:
Decay Studies at ^{40}Ar (36 AMeV) + ^{248}Cm and ^{nat}Ag Using the Fragment Spectrometer FOBOS (present status of data analysis);
Oct. 14, 1997

Titov, A. I., Dubna:
Φ Photoproduction and the Strangeness in the Proton;
Oct. 20, 1997
Φ Production in pp Reactions;
Oct. 21, 1997

Vilesov, A., Göttingen:
Molekülspektroskopie im He-Tröpfchen;
May 12, 1997

Wilkin, C., London:
Final State Interactions in Meson Production in Nucleon-Nucleon Scattering;
Jul. 14, 1997

THE INSTITUTE OF NUCLEAR AND HADRON PHYSICS

Personnel of the Institute for Nuclear and Hadron Physics

Director: Prof. E. Grosse[1]

Sientific Personnel

Dr. H.W. Barz
L. Dietterle
Dr. F.M. Dittes
Dr. F. Dönau
Dr. F. Dohrmann
Dr. S. Dshemuchadse
Dr. W. Enghardt
Dr. S. Frauendorf
Dr. P. Gippner
Dr. B. Hasch
Dr. C.-M. Herbach
Dr. B. Kämpfer
Dr. L. Käubler
Dr. Th. Kirchner
Dr. R. Kotte
Dr. P. Michel
Dr. Th. Möhlenkamp
Dr. K. Möller
Dr. H. Müller
Dr. B. Naumann
Dr. L. Naumann
Dr. W. Neubert
Dr. U. Nething
Dr. H.-G. Ortlepp
Dr. G. Pausch
Dr. J. Pawelke
Dr. H. Prade
Prof. I. Rotter[2]
A. Schamlott
Dr. K.D. Schilling
Dr. H. Schnare
Dr. M. Schlett
Dr. C. Schneider
Dr. W. Seidel
Dr. R. Schwengner
Dr. W. Wagner
Dr. M. Wenzel
Dr. G. Winter †
D. Wohlfarth
Dr. R. Wünsch
Dr. R. A. Yanez
Dr. R. Zahn

PhD Students

D. Almehed
Ch. Borcan
K. Gallmeister
T. Gorin[2]
D. Heinrich
R. Hinz
D. Kamanin
E. Kolomeitsev
K. Lauckner
E. Persson[2]
A. Peshier
C. Plettner
M. Schleif
Th. Servene

Technical Personnel

M. Altus
H. Angermann
U. Baumann
J.U. Berlin
M. Boeck
M. Böse
J. Fiedler
R. Förster
M. Freitag
L. Göbel
K. Heidel
K.H. Hermann
J. Hutsch
J. Kerber
E. Kluge
M. Langer
U. Oehmichen
M. Paul
B. Prietzschk
I. Probst
B. Rimarzig
H. Römer
M. Scheinpflug
Chr. Schneidereit
W. Schulze
M. Sobiella
A. Uhlmann
C. Umlauf

[1] and TU Dresden
[1] and MPI for Physics of Complex Systems

Guest Scientists

Andreoiu C.	IPNE Bucharest/Romania
Prof. Andrejtscheff, W.	INR Sofia/Bulgaria
Dr. Andronenko, M.	Nucl. Phys. Inst. Gatchina/Russia
Dr. Andronenko, L.	St. Peterburg/Russia
Prof. Avakian, R.	Physics Institute Yerevan/Armenia
Dr. Bahrt, J.	BESSY Berlin
Chmel, S.	University Bonn
Dr. Franczak, B.	GSI Darmstadt
Prof. Friese, G.	University Munich
Prof. Gillespie, A.	University Dundee/Scotland
Dr. Grinberg, M.	INR Sofia/Bulgaria
Prof. Ivanov, I.	JINR Dubna/Russia
Dr. Kaptari, L.	JINR Dubna/Russia
Kapusta, M.	Soltan Institute for Nucl. Studies, Swierk/Poland
Dr. Kopal, M.	University Prague/Czech. Rep.
Dr. Llacer, J.	University Berkeley/USA
Dr. Lobach, Y.N.	Institute for Nuclear Research Kiev/Ukraine
Prof. Lorikyan, M.P.	Phys. Institute, Yerevan/Armenia
Prof. Moszynski, M.	Soltan Institute for Nucl. Studies, Swierk/Poland
Prof. Mühlschlegel, B.	University Cologne
Prof. Nikogosian, D.	Physics Institute, Yerevan/Armenia
Dr. Pavlenko, O.P.	Institute for Theor. Phys., Kiev/Ukraine
Poux, V.	Institute de Physique Nucl., Orsay/France
Dr. Prange,	BESSY Berlin
Prof. Ring, P.	TU Munich
Dr. Semikh, S.S.	JINR Dubna/Russia
Dr. Shaskov, S.N.	Beloruss. State University/White Russia
Dr. Sheik, J.	Tata Inst. Fundamental Research, Bombay/India
Dr. Steinke, M.	University Bochum
Dr. Strekalovskij, O.V.	JINR Dubna/Russia
Tichtchenko, V.G.	JINR Dubna/Russia
Prof. Titov, A.I.	JINR Dubna/Russia
Dr. Unzhakova, A.V.	JINR Dubna/Russia
Prof. Vilesov, A.	University Göttingen
Prof. von Oertzen, W.	HMI Berlin
Dr. Wolf, G.	KFKI Budapest/Hungary
Dr. Wolski, D.	Soltan Institute for Nucl. Studies, Swierk/Poland
Yurkov, M.	DESY / Automat. Systems Coop., Samara/Russia